

Electronic Supplementary Information (ESI)

Isoacridone dyes with parallel reactivity from both singlet
and triplet excited states for biphotonic catalysis and
upconversion

Björn Pfund[†], Valeriia Hutskalova[†], Christof Sparr,^{*} and Oliver S. Wenger^{*}

Table of contents

1. General information	S3
1.1 Synthetic materials	S3
1.2 Materials for spectroscopic characterization	S4
1.3 Steady-state measurements.....	S4
1.4 Time-resolved absorption and luminescence measurements	S5
2 Synthetic procedures and characterization.....	S6
2.1 Synthesis of 2,6,7-trifluoro-9-mesityl-10-phenylacridin-10-ium-3-olate (PS(I)).....	S6
2.2 Synthesis of 9-(2-chloro-6-iodophenyl)-2,6,7-trifluoro-10-phenylacridin-10- ium-3-olate (PS(II)).....	S7
2.3 Synthesis of 9-(2-chloro-6-iodophenyl)-2,6,7-trifluoro-10-phenylacridin-10- ium-3-olate (PS(III)).....	S12
2.4 Synthesis of 9-(4,6-diiodo-3-methoxy-2-methylphenyl)-2,6,7-trifluoro-10- phenylacridin-10-ium-3-olate (PS(IV)).....	S15
2.5 Synthesis of 1,6-bis((trimethylsilyl)ethynyl)pyrene ((TMS) ₂ pyr) :.....	S20

3	Additional photochemical properties of the isoacridone photosensitizers	S21
3.1	Extinction coefficients of triplet-excited anthracene in THF	S21
3.2	Intersystem crossing quantum yield	S22
3.3	External heavy atom effect	S24
3.4	Photodegradation quantum yields	S27
4	Triplet-triplet energy transfer catalysis	S34
4.1	Birch-type photoreduction of anthracene derivatives	S36
4.2	Sensitization-initiated electron transfer	S42
4.3	Mechanistic investigation of the sensitization-initiated electron transfer ...	S46
5	Sensitized triplet-triplet annihilation upconversion	S54
5.1	Photophysical properties of the annihilator (TMS) ₂ pyr	S54
5.2	Triplet-triplet energy transfer	S56
5.3	Triplet-triplet annihilation (TTA)	S59
5.4	Quadratic excitation power dependency of the upconversion luminescence S61	
5.5	sTTA-UC quantum yields	S63
5.6	Summary of the sTTA-UC properties	S67
6	NMR spectra	S68
7	References	S81

1. General information

1.1 Synthetic materials

All reaction solvents and reagents were obtained from commercial suppliers and used without further purification unless otherwise stated. Solvents for extractions and chromatography were technical grade. Syringes were used to transfer air and moisture sensitive liquids and solutions. Analytical thin layer chromatography (Merck silica gel 60 F254 plates) was utilized for monitoring reactions and visualized by UV light (254 nm and 355 nm). Flash Chromatography was performed with SiliCycle silica gel 60 (230-400 Mesh) or otherwise stated stationary columns. Concentration *in vacuo* was performed by rotary evaporation to ~10 mbar at 40 °C and drying at ~ 10⁻² mbar at room temperature.

¹H-NMR spectra were recorded on Bruker DPX 400 MHz or Bruker DRX 500 MHz spectrometers at 298 K in the indicated deuterated solvent supplied by *Cambridge Isotope Laboratories*. Chemical shifts (δ) are quoted in parts per million (ppm) and referenced to the residual solvent peak (δ = 7.26 ppm for CDCl₃ and 2.50 ppm for (CD₃)₂SO). The multiplicities are reported in Hz as: s = singlet, br = broad singlet, d = doublet, t = triplet, q = quartet, m = multiplet, dm = doublet of multiplets, and ddm = doublet of doublet of multiplets. ¹³C- spectra were recorded with ¹H-decoupling on Bruker DRX 500 MHz spectrometers at 298 K in the indicated deuterated solvent supplied by *Cambridge Isotope Laboratories*. Chemical shifts (δ) are quoted in parts per million (ppm) and referenced to the residual solvent peak (δ = 77.16 ppm for CDCl₃ and 39.52 ppm for (CD₃)₂SO).

Melting points were measured on a Büchi B-565 melting point apparatus and are uncorrected. IR spectroscopy was measured on an ATR Varian Scimitar 800 FT-IR spectrometer and reported in cm⁻¹. The intensities of the bands are reported as: w = weak, m = medium, s = strong. High-resolution mass spectrometry (HR-ESI) was recorded by Dr. Michael Pfeffer at the University of Basel on a *Bruker MaXis 4G QTOF* ESI mass spectrometer.

1.2 Materials for spectroscopic characterization

Unless otherwise indicated, the chemicals used for optical characterization and spectroscopic experiments were obtained commercially in high purity and used as received. Synthetic procedures and characterization for the synthesized compounds are described in Section 2. Dry tetrahydrofuran (THF) from Sigma-Aldrich or ultrapure Millipore MilliQ water (specific resistance, 18.2 M Ω cm) was used as a solvent for the spectroscopic studies. All solutions for optical spectroscopic measurements were purged with argon (5.0, PanGas) for 5 minutes and sealed under argon (1 atm) using septum cap cuvettes.

1.3 Steady-state measurements

Steady-state UV-Vis absorption spectra were obtained using a Cary 5000 spectrometer from Varian, whereas the luminescence spectra were recorded on a Fluorolog-3-22 instrument from Horiba Jobin-Yvon. Prompt emission spectra were recorded using strongly diluted solutions to avoid filter effects. All emission spectra were corrected for the wavelength-dependent sensitivity of the emission spectrometer. The triplet energies of the isoacridone photosensitizers (PS) were estimated from the emission spectra recorded at 77 K using 2-methyltetrahydrofuran as a solvent by identifying the 0-0 phosphorescence transition. The luminescence quantum yields of the sensitizers were determined 6 times at different concentrations (optical density at the excitation wavelength between 0.02 to 0.1) using an integration sphere from Horiba Jobin-Yvon. For the measurements of the upconversion power dependencies, the upconversion quantum yields, and the photostabilities, the Fluorolog-3-22 spectrometer was equipped with a 532 nm cw laser with an optical output of up to 500 mW from Roithner Lasertechnik as an external light source with precisely adjustable radiative power and high output stability (< 1%) and a beam diameter of 3 mm².

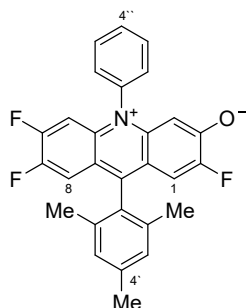
1.4 Time-resolved absorption and luminescence measurements

The luminescence lifetimes of the sensitizers and the used annihilator were measured on a LifeSpec II spectrometer from Edinburgh Instruments using the time-correlated single photon counting (TCSPC) technique and picosecond pulsed diode lasers. Singlet-excited state lifetimes of the sensitizers and of the annihilator were recorded under highly diluted conditions where the optical density did not exceed 0.1 at the excitation wavelength.

For transient UV-Vis absorption and delayed emission spectroscopy, an LP920-KS setup from Edinburgh Instruments was used. For excitation at 532 nm, a frequency-doubled Nd:YAG laser (Q-smart 450 with a repetition rate of 10 Hz, and a pulse width of ca. 10 ns) was employed. For excitation between 420 and 530 nm, a frequency-tripled Nd:YAG laser (Quantel Brilliant, ca. 10 ns pulse width and a repetition rate of 10 Hz) equipped with an optical parametric oscillator (OPO) from Opotek was used. To improve the excitation homogeneity in the detection volume, a beam expander (GBE02-A from Thorlabs) was employed for both pulse beams. The kinetic decay traces at a single wavelength were detected using a photomultiplier tube, whereas the transient UV-Vis absorption and delayed emission spectra were detected using an iCCD camera from Andor. If not specifically indicated, all spectroscopic measurements were carried out at 20 °C.

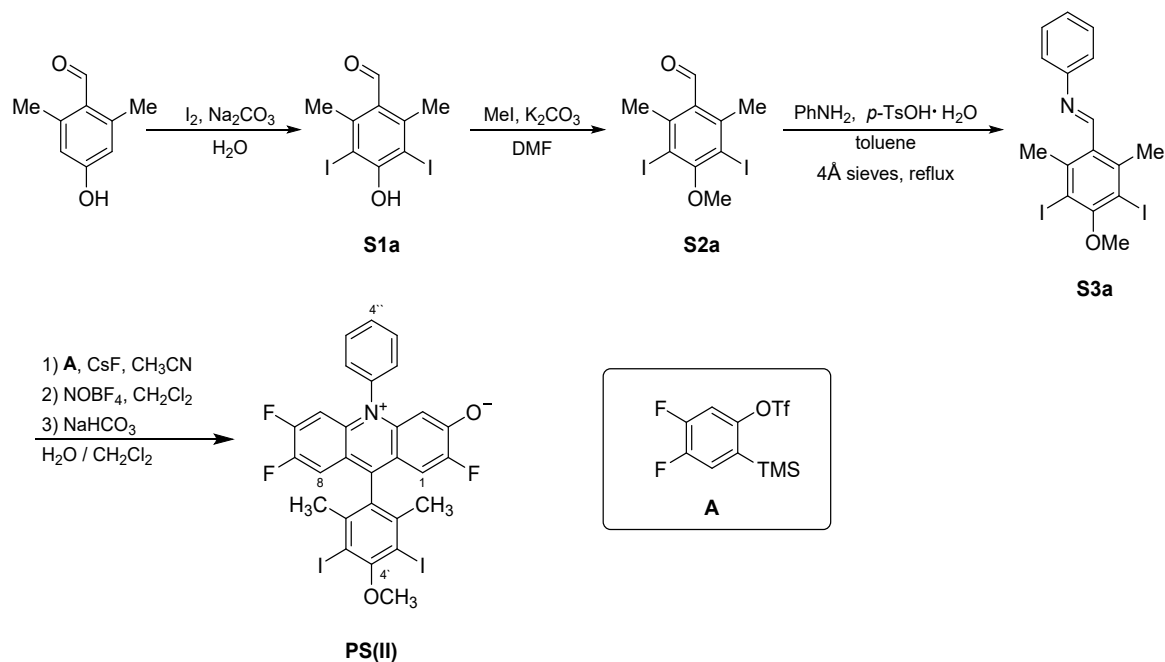
2 Synthetic procedures and characterization

2.1 Synthesis of 2,6,7-trifluoro-9-mesityl-10-phenylacridin-10-ium-3-olate (PS(I)):

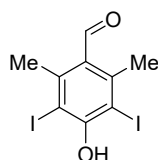


Prepared according to the literature procedure¹ using 2,3,6,7-tetrafluoro-9-mesityl-10-phenylacridin-10-ium tetrafluoroborate (80.0 mg, 150 μmol) to yield the desired product as a red solid (58.0 mg, 131 μmol , 87%). NMR corresponds to reported data.¹

2.2 Synthesis of 9-(2-chloro-6-iodophenyl)-2,6,7-trifluoro-10-phenylacridin-10-ium-3-olate (PS(II))



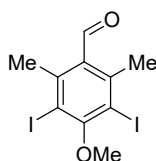
4-Hydroxy-3,5-diiodo-2,6-dimethylbenzaldehyde (S1a):



Prepared according to the modified literature procedure:¹ Iodine (1.46 g, 5.75 mmol, 2.30 eq.) was added to a well-stirred solution of 4-hydroxy-2,6-dimethylbenzaldehyde (375 mg, 2.50 mmol, 1.00 eq.) in water (40 mL) and saturated aqueous Na₂CO₃ (13 mL). The reaction mixture was stirred for 18 hours and then acidified with HCl (1M). The obtained solution was extracted with EtOAc (3×25 mL). The organic layer was then separated, dried over Na₂SO₄ and the solvent was removed. The residue was purified by silica gel column chromatography (cyclohexane/EtOAc, 1:0 to 4:1) to yield the title product as a beige solid (400 mg, 1.00 mmol, 40%, m.p. 160.2 – 161.5 °C): R_f 0.38 (cyclohexane/EtOAc 7:1); ν_{max} (neat): 3151w, 1744w, 1670s, 1533s, 1439w, 1376m, 1274s, 1136s, 1046w, 969w, 908w, 824w; ¹H NMR (500 MHz, CDCl₃): δ =

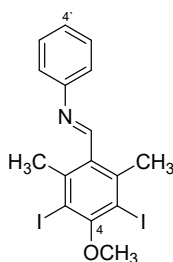
10.32 (1H, s, CHO), 6.47 (1H, s, OH), 2.71 (6H, s, C2-CH₃, C6-CH₃); ¹³C NMR (126 MHz, CDCl₃): δ = 192.4 (CHO), 156.3 (C4), 144.8 (C2, C6), 129.2 (C1), 90.8 (C3, C5), 25.8 (C2-CH₃, C6-CH₃); ESI-MS: m/z calcd. for C₉H₇I₂O₂ 400.8541, found 400.8540 [M].

3,5-Diiodo-4-methoxy-2,6-dimethylbenzaldehyde (S2a):



4-Hydroxy-3,5-diodo-2,6-dimethylbenzaldehyde (190 mg, 470 μmol, 1.00 eq.) was dissolved in DMF (0.8 mL), K₂CO₃ (131 mg, 950 μmol, 2.00 eq.) and MeI (134 mg, 950 μmol, 2.00 eq.) were added. The resulting reaction mixture was stirred for 18 hours and then diluted with EtOAc (20 mL) and water (20 mL). Organic layer was separated, washed with water (2×20 mL), dried over Na₂SO₄. Solvent was removed under reduced pressure to give the desired product as a beige solid (176 mg, 423 μmol, 89%, m. p. 116.1 – 116.3 °C); v_{max} (neat): 2930w, 2848w, 1748w, 1695s, 1532w, 1450w, 1377w, 1292m, 1261w, 1191w, 1156m, 1067m, 940w; ¹H NMR (500 MHz, CDCl₃): δ = 10.35 (1H, s, CHO), 3.89 (3H, s, OCH₃), 2.65 (6H, s, C2-CH₃, C6-CH₃); ¹³C NMR (126 MHz, CDCl₃): δ = 193.7 (CHO), 161.6 (C4), 144.2 (C2, C6), 132.8 (C1), 98.9 (C3, C5), 60.3 (OCH₃), 25.7 (C2-CH₃, C6-CH₃); ESI-MS: m/z calcd. for C₁₀H₁₀I₂NaO₂ 438.8662, found 438.8654 [M+Na⁺].

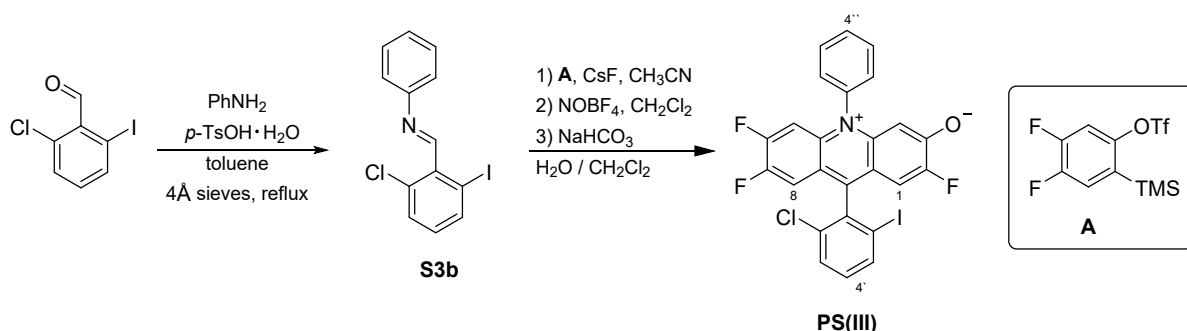
1-(3,5-Diiodo-4-methoxy-2,6-dimethylphenyl)-N-phenylmethanimine (S3a):



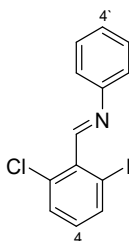
Aniline (29.5 mg, 317 μmol , 1.20 eq.), 3,5-diiodo-4-methoxy-2,6-dimethylbenzaldehyde (110.0 mg, 264 μmol , 1.0 eq.), p-TsOH \cdot H₂O (2.51 mg, 13.2 μmol , 0.05 eq.) were dissolved in 2.5 mL dry toluene. 4 Å molecular sieves were added to the solution. The reaction mixture was refluxed for 18 hours. The volatiles were removed under reduced pressure (5 mbar) and subsequently under high vacuum (<0.1 mbar, 60 °C, to remove excess of aniline) to yield the product as a beige solid (104 mg, 212 μmol , 80%, m.p. 108.1 – 108.4 °C); ν_{max} (neat): 3048w, 2990w, 2954w, 1748w, 1625m, 1590m, 1538w, 1484w, 1449m, 1375w, 1300m, 1161s, 1064s, 940s, 867w, 759m, 693m, 636m; ¹H NMR (500 MHz, CDCl₃) δ = 8.65 (1H, s, CH=N), 7.47 – 7.36 (2H, m, C3'H, C5'H), 7.34 – 7.27 (1H, m, C4'H), 7.24 – 7.14 (2H, m, C2'H, C6'H), 3.87 (3H, s, OCH₃), 2.57 (6H, s, C2-CH₃, C6-CH₃); ¹³C NMR (126 MHz, CDCl₃) δ = 161.3 (CH=N), 159.4 (C4), 151.2 (C1'), 141.7 (C2, C6), 132.8 (C1), 129.3 (C3', C5'), 126.6 (C4'), 120.7 (C2', C6'), 97.1 (C3, C5), 60.3 (OCH₃), 26.5 (C2-CH₃, C6-CH₃); ESI-MS: m/z calcd. for C₁₆H₁₆I₂NO 491.9316, found 491.9324 [M+H⁺].

1453w, 1377w, 1296w, 1179m, 1107w, 1068w, 1027w, 970m, 907m, 876w, 824w, 729m, 642w; ^1H NMR (500 MHz, CDCl_3) δ = 7.80 – 7.74 (2H, m, C3''H, C5''H), 7.74 – 7.68 (1H, m, C4''H), 7.42 – 7.34 (2H, m, C2''H, C6''H), 6.95 (1H, dd, $^3J_{\text{HF}}$ 10.3, $^4J_{\text{HF}}$ 8.3 Hz, C8H), 6.79 – 6.55 (2H, m, C1H, C5H), 5.83 (1H, d, $^3J_{\text{HF}}$ 7.5 Hz, C4H), 4.03 (3H, s, OCH_3), 2.15 (6H, s, C2'- CH_3 , C6'- CH_3); ^{13}C NMR (126 MHz, CDCl_3) δ = 174.05 (d, $^2J_{\text{CF}}$ 19.7 Hz, C3), 160.3 (C4'), 158.1 (d, $^1J_{\text{CF}}$ 269.5 Hz, C2), 154.6 – 152.0 (m, C6), 148.6 – 146.2 (m, C7), 147.0 – 146.7 (m, C9) 144.9 (C4a), 141.3 (C2', C6'), 137.9 (C1''), 137.3 (d, $^3J_{\text{CF}}$ 9.5 Hz, C10a), 132.0 (C3'', C5''), 131.0 (C4''), 129.5 (C1'), 128.4 (C2'', C6''), 121.9 (d, $^3J_{\text{CF}}$ 11.1 Hz, C9a), 117.0 (d, $^3J_{\text{CF}}$ 6.1 Hz, C8a), 114.2 (d, $^2J_{\text{CF}}$ 18.6 Hz, C8), 108.8 (d, $^2J_{\text{CF}}$ 21.8 Hz, C1), 105.8 (d, $^2J_{\text{CF}}$ 23.4 Hz, C5), 104.77 (d, $^3J_{\text{CF}}$ 5.5 Hz, C4), 97.1 (C3', C5'), 60.7 (OCH_3), 27.1 (C2'- CH_3 , C6'- CH_3); ^{19}F NMR (471 MHz, CDCl_3) δ = -119.47 to -122.59 (m), -123.67 to -127.07 (m), -139.12 to -142.45 (m); ESI-MS: m/z calcd. for $\text{C}_{28}\text{H}_{19}\text{F}_3\text{I}_2\text{NO}_2$ 711.9452, found 711.9456 [$\text{M}+\text{H}^+$].

2.3 Synthesis of 9-(2-chloro-6-iodophenyl)-2,6,7-trifluoro-10-phenylacridin-10-ium-3-olate (PS(III))

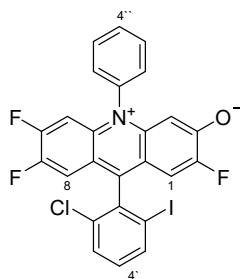


1-(2-Chloro-6-iodophenyl)-N-phenylmethanimine (S3b):



Aniline (52.0 mg, 560 μmol , 1.50 eq.), 2-chloro-6-iodobenzaldehyde (100 mg, 370 μmol , 1.00 eq.), *p*-TsOH·H₂O (3.50 mg, 18.8 μmol , 0.05 eq.) were dissolved in 3.7 mL dry toluene. 4 Å Molecular sieves were added to the obtained solution. The reaction mixture was refluxed for 18 hours. The volatiles were removed under reduced pressure (5 mbar) and subsequently under high vacuum (<0.1 mbar, 60 °C, to remove the excess of aniline) to yield the product as yellow oil (120 mg, 350 μmol , 94%): ν_{max} (neat): 3064w, 3059w, 2884w, 1631m, 1591m, 1558m, 1547m, 1548s, 1423s, 1355w, 1260w, 1201m, 1193m, 1064m, 1024w, 949w, 909w, 879w, 761s; ¹H NMR (500 MHz, CDCl₃) δ = 8.48 (1H, s, CH=N), 7.88 (1H, d, ³J 7.9 Hz, C3H), 7.48 – 7.40 (3H, m, C5H, C3'H, C5'H), 7.32 – 7.27 (3H, m, C2'H, C4'H, C6'H), 7.03 (1H, t, ³J 8.0 Hz, C4H); ¹³C NMR (126 MHz, CDCl₃) δ = 160.2 (CH=N), 150.9 (C1'), 138.7 (C3), 136.8 (C1), 134.1 (C6), 131.4 (C4), 130.2 (C5), 129.2 (C2', C6'), 126.7 (C4'), 120.9 (C3', C5'), 96.9 (C2); ESI-MS: *m/z* calcd. for C₁₃H₁₀ClIN⁺ 341.9541, found 341.9538 [M+H⁺].

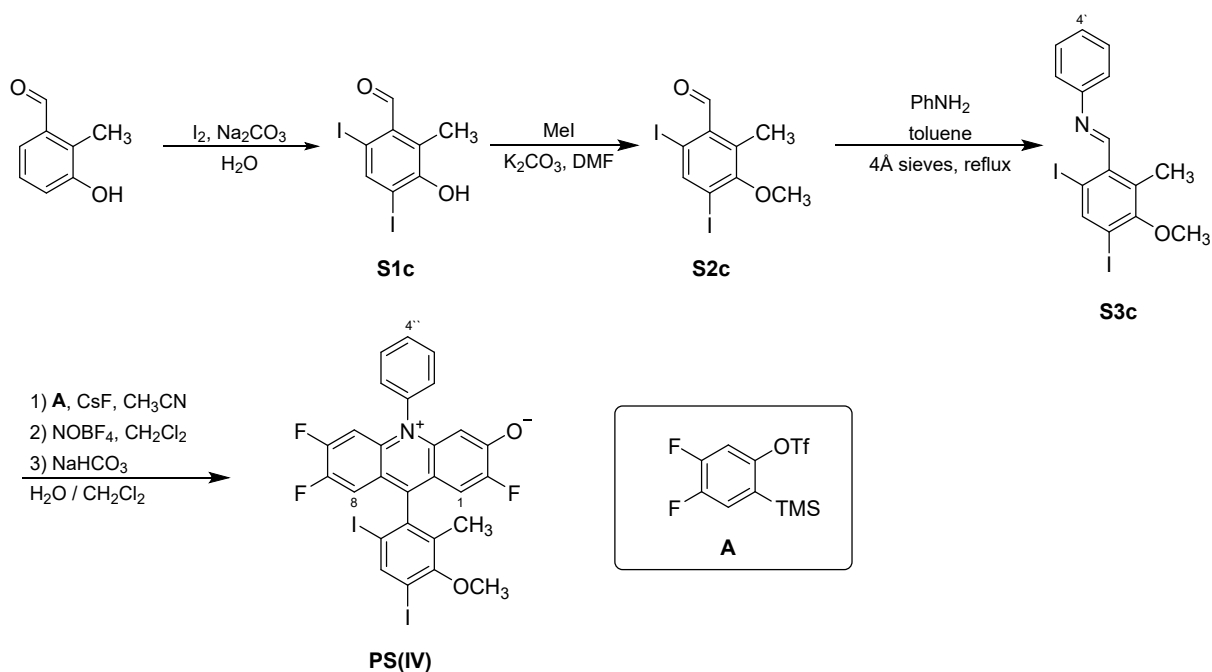
9-(2-Chloro-6-iodophenyl)-2,6,7-trifluoro-10-phenylacridin-10-ium-3-olate (PS(III)):



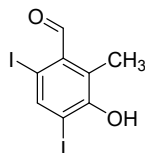
Prepared according to the modified literature procedure:¹ To a mixture of anhydrous CsF (355 mg, 2.34 mmol, 10 eq.) and dry CH₃CN (2.4 mL) under argon were added 1-(2-chloro-6-iodophenyl)-*N*-phenylmethanimine (80.0 mg, 234 μmol, 1.00 eq.) and then 4,5-difluoro-2-(trimethylsilyl)phenyl trifluoromethanesulfonate (430 mg, 1.29 mmol, 5.50 eq.). The reaction mixture was stirred for 18 hours and the solvent was removed under reduced pressure. The residue was dissolved in CH₂Cl₂ (20 mL) and washed with water (30 mL). The aqueous phase was extracted with CH₂Cl₂ (2 × 15 mL), the combined organic layer was dried over Na₂SO₄ and the solvent was removed under reduced pressure. The residue was purified by silica gel column chromatography (cyclohexane / CH₂Cl₂, 100 : 0 to 80 : 20). The obtained acridane intermediate was dissolved in dry CH₂Cl₂ (1.6 mL) and nitrosonium tetrafluoroborate (54.7 mg, 468 μmol, 2.00 eq.) was added. The resulting reaction mixture was stirred for 2 hours at room temperature (the reaction progress was controlled by ¹H NMR), diluted with 15 mL of CH₂Cl₂, washed once with water (20 mL). Saturated aqueous solution of NaHCO₃ (40 mL) was then added to the organic layer and the resulting mixture was vigorously stirred for 18 hours. The organic phase was separated and the extraction with CH₂Cl₂ (2 × 15 mL) was performed. The combined organic layer was dried over Na₂SO₄ and the solvent was removed under reduced pressure. The residue was purified by silica gel column chromatography (CH₂Cl₂ / CH₃OH, 100 : 0 to 9 : 1, R_f 0.86 (CH₂Cl₂: CH₃OH 10:1)) to yield 9-(2-chloro-6-iodophenyl)-2,6,7-trifluoro-10-phenylacridin-10-ium-3-olate as a red solid (37.0 mg, 65.9 μmol, 28% yield over 3 steps, decomp. at 226.4 °C); ν_{max} (neat): 3064w, 2926w, 1581w, 1536s, 1452m, 1422w, 1376w, 1298m, 1182m, 1121m, 1025w, 972m, 908m, 871m, 826w, 782w, 727s, 645m; ¹H NMR (500 MHz,

CDCl₃) δ = 8.05 (1H, dd, ³J 7.9, ⁴J 1.0 Hz, C5'H), 7.81 – 7.74 (2H, m, C3''H, C5''H), 7.74 – 7.67 (2H, m, C3'H, C4''H), 7.45 – 7.36 (2H, m, C2''H, C6''H), 7.31 (1H, t, ³J 7.9 Hz, C4'H), 6.96 (1H, dd, ³J_{HF} 10.3, ⁴J_{HF} 8.2 Hz, C8H), 6.73 – 6.63 (2H, m, C1H, C5H), 5.85 (1H, d, ³J_{HF} = 7.5 Hz, C4H); ¹³C NMR (126 MHz, CDCl₃) δ = 174.1 (d, ²J_{CF} 19.6 Hz, C3), 157.9 (d, ¹J_{CF} 270.5 Hz, C2), 153.1 (dd, ¹J_{CF} 258.0, ²J_{CF} 16.2 Hz, C7), 147.22 (dd, ¹J_{CF} 249.5, ²J_{CF} 14.4 Hz, C6), 146.8 (d, ⁴J_{CF} 12.4 Hz, C9), 145.1 (C4a), 138.5 (C5'), 137.9 (C1''), 137.3 (C1'), 137.1 (d, ³J_{CF} 9.9 Hz, C10a), 133.7 (C2'), 132.4 (C4'), 131.8 (C3''/C5''), 131.7 (C3'/C5'), 130.8 (C4''), 130.2 (C3'), 128.4 (C2''/C6''), 128.3 (C2'/C6'), 121.9 (d, ³J_{CF} 9.0 Hz, C9a), 116.2 (dd, ³J_{CF} 6.7, ⁴J_{CF} 1.7 Hz, C8a), 113.8 (d, ²J_{CF} 19.5 Hz, C8), 108.7 (d, ²J_{CF} 22.4 Hz, C1), 105.6 (d, ²J_{CF} 23.5 Hz, C5), 104.6 (d, ³J_{CF} 5.1 Hz, C4), 99.1 (C6') ¹⁹F NMR (471 MHz, CDCl₃): δ = –120.68 to –120.80 (m), –125.05 to –125.50 (m), –140.46 to –140.72 (m); ESI-MS: m/z calcd. for C₂₅H₁₃ClF₃INO 561.9677, found 561.9680 [M+H⁺].

2.4 Synthesis of 9-(4,6-diiodo-3-methoxy-2-methylphenyl)-2,6,7-trifluoro-10-phenylacridin-10-ium-3-olate (PS(IV))



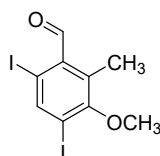
3-Hydroxy-4,6-diiodo-2-methylbenzaldehyde (S1c):



Prepared according to the modified literature procedure:² To a vigorously stirred solution of 3-hydroxy-2-methylbenzaldehyde (200 mg, 1.47 mmol, 1.00 eq.) in water (45 mL) and saturated aqueous sodium carbonate (6.0 mL), iodine (933 mg, 3.68 mmol, 2.50 eq.) was added. The resulting reaction mixture was stirred for 24 h, acidified with 1M HCl and extracted with ethyl acetate (2 × 80 mL). The combined organic phase was dried over Na₂SO₄ and the obtained residue was subjected to silica gel column chromatography (cyclohexane / EtOAc 1 : 0 to 1 : 1) to yield the desired compound 3-hydroxy-4,6-diiodo-2-methylbenzaldehyde as a beige solid (56.0 mg, .144 μmol, 10%); R_f 0.78 (cyclohexane/EtOAc 7 : 2); V_{max} (neat): 3467m, 2925w,

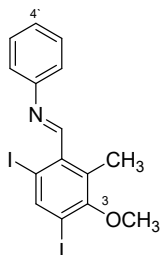
2855w, 2757w, 1690s, 1554m, 1380m, 1298m, 1226m, 1176m, 1077m, 939w, 860w, 715w, 672w, 630s; $^1\text{H NMR}$ (500 MHz, CDCl_3) δ = 10.11 (1H, s, CHO), 8.15 (1H, s, C5H), 5.50 (1H, s, OH), 2.52 (3H, C2-CH₃); $^{13}\text{C NMR}$ (126 MHz, CDCl_3) δ = 197.4 (CHO), 154.4 (C3), 145.3 (C5), 134.9 (C1), 128.1 (C2), 92.7 (C4), 88.9 (C6), 26.9 (CH₃); ESI-MS: m/z calcd. for $\text{C}_8\text{H}_7\text{I}_2\text{O}_2$ 388.8530, found 388.8524 [M+H⁺].

4,6-Diiodo-3-methoxy-2-methylbenzaldehyde (S2c):



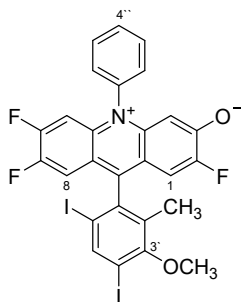
To a stirred solution of 3-hydroxy-4,6-diiodo-2-methylbenzaldehyde (50.0 mg, 129 μmol , 1.00 eq.) and K_2CO_3 (35.7 mg, 258 μmol , 2.00 eq.) in dry DMF (0.21 mL) was added CH_3I (16.1 μL , 258 μmol , 2.00 eq.). The resulting mixture was stirred for 18 hours at room temperature. Then water (25 mL) and EtOAc (25 mL) were added. After the phase separation, the aqueous phase was extracted with EtOAc (2 \times 20 mL). The combined organic fractions were dried over Na_2SO_4 . The solvent was removed to yield the desired product as a beige solid (45.0 mg, 112 μmol , 87%); v_{max} (neat): 2935w, 2847w, 2751w, 1687s, 1541m, 1445s, 1366s, 1237s, 1158w, 1083m, 999s, 911s, 858m, 729w, 637w; $^1\text{H NMR}$ (500 MHz, CDCl_3) δ = 10.09 (1H, s, CHO), 8.30 (1H, s, C5H), 3.75 (3H, OCH₃), 2.52 (3H, s, C2-CH₃); $^{13}\text{C NMR}$ (126 MHz, CDCl_3) δ = 197.4 (CHO), 159.7 (C3), 147.2 (C5), 135.7 (C2), 134.9 (C1), 99.7 (C4), 95.6 (C6), 60.6 (OCH₃), 13.7 (C2-CH₃); ESI-MS: m/z calcd. for $\text{C}_9\text{H}_9\text{I}_2\text{O}_2$ 402.8686, found 402.8690 [M+H⁺].

1-(4,6-Diiodo-3-methoxy-2-methylphenyl)-N-phenylmethanimine (S3c):



Aniline (11.1 mg, 119 μmol , 1.20 eq.), 4,6-diiodo-3-methoxy-2-methylbenzaldehyde (40.0 mg, 99.5 μmol , 1.00 eq.), *p*-TsOH \cdot H₂O (946 μg , 4.98 μmol , 0.05 eq.) were dissolved in 1.0 mL dry toluene. 4 Å Molecular sieves were added to the solution. The reaction mixture was refluxed for 18 hours. The volatiles were removed under reduced pressure (5 mbar) and subsequently under high vacuum (<0.1 mbar, 60 °C, to remove the excess of aniline) to yield the product as a beige solid (43.0 mg, 90.1 μmol , 91%); ν_{max} (neat): 3058w, 2930w, 2857w, 1730w, 1626m, 1590m, 1548w, 1484m, 1446s, 1375s, 1241s, 1152w, 1093w, 1002m, 929w, 862w, 694m, 632s; ¹H NMR (500 MHz, CDCl₃) δ = 8.50 (1H, s, CH=N), 8.23 (1H, s, C5H), 7.47 – 7.37 (2H, m, C3'H, C5'H), 7.33 – 7.20 (3H, m, C2'H, C4'H, C6'H), 3.79 (3H, s, OCH₃), 2.59 (3H, s, C2-CH₃); ¹³C NMR (126 MHz, CDCl₃) δ = 163.9 (CH=N), 159.4 (C3), 151.4 (C1'), 146.0 (C5), 138.8 (C2), 133.9 (C1), 129.4 (C3', C5'), 126.8 (C4'), 121.0 (C2', C6'), 94.9 (C4), 94.0 (C6), 60.6 (OCH₃), 15.1 (C2-CH₃); ESI-MS: *m/z* calcd. for C₁₅H₁₄I₂NO 477.9159, found 477.9166 [M+H⁺].

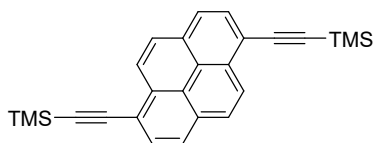
9-(4,6-Diiodo-3-methoxy-2-methylphenyl)-2,6,7-trifluoro-10-phenylacridin-10-ium-3-olate (PS(IV)):



Prepared according to the modified literature procedure:¹ To a mixture of anhydrous CsF (175 mg, 1.15 mmol, 10.0 eq.) and dry CH₃CN (1.2 mL) under argon were added 1-(4,6-diiodo-3-methoxy-2-methylphenyl)-*N*-phenylmethanimine (55.0 mg, 115 μmol, 1.00 eq.) and then 4,5-difluoro-2-(trimethylsilyl)phenyl trifluoromethanesulfonate (211 mg, 633 μmol, 5.50 eq.). The reaction mixture was stirred for 18 hours and the solvent was removed under reduced pressure. The residue was dissolved in CH₂Cl₂ (20 mL) and washed with water (30 mL). The aqueous phase was extracted with CH₂Cl₂ (2 × 15 mL), the combined organic layer was dried over Na₂SO₄ and the solvent was removed under reduced pressure. The residue was purified by silica gel column chromatography (cyclohexane / CH₂Cl₂, 100 : 0 to 80 : 20). The obtained acridane intermediate was dissolved in dry CH₂Cl₂ (1.2 mL) and nitrosonium tetrafluoroborate (26.9 mg, 230 μmol, 2.00 eq.) was added. The resulting reaction mixture was stirred for 2 hours at room temperature (the reaction progress was controlled by ¹H NMR), diluted with 15 mL of CH₂Cl₂, washed once with water (20 mL). Saturated aqueous solution of NaHCO₃ (40 mL) was then added to the organic layer, and the resulting mixture was vigorously stirred for 18 hours. The organic phase was separated and the extraction with CH₂Cl₂ (2 × 15 mL) was performed. The combined organic layer was dried over Na₂SO₄ and the solvent was removed under reduced pressure. The residue was purified by silica gel column chromatography (CH₂Cl₂ / CH₃OH, 100 : 0 to 9 : 1, R_f 0.84 (CH₂Cl₂: CH₃OH 10:1)) to yield 9-(4,6-diiodo-3-methoxy-2-methylphenyl)-2,6,7-

trifluoro-10-phenylacridin-10-ium-3-olate as a red solid (26.0 mg, 37.3 μmol , 32% yield over 3 steps, decomp. at 262.9 $^{\circ}\text{C}$); ν_{max} (neat): 2931w, 1582w, 1539s, 1448w, 1299m, 1201m, 1130w, 1071w, 971w, 910w, 874w, 827w, 730m; ^1H NMR (500 MHz, CDCl_3) δ = 8.40 – 8.37 (1H, m, C5 $^{\prime}$ H), 7.81 – 7.74 (2H, m, C3 $^{\prime\prime}$ H, C5 $^{\prime\prime}$ H), 7.74 – 7.66 (1H, m, C4 $^{\prime\prime}$ H), 7.41 – 7.34 (2H, m, C2 $^{\prime\prime}$ H, C6 $^{\prime\prime}$ H), 6.95 (1H, dd, $^3J_{\text{HF}}$ 10.2, $^4J_{\text{HF}}$ 8.3 Hz, C8H), 6.76 – 6.62 (2H, m, C1H, C5H), 5.84 (1H, d, $^4J_{\text{HF}}$ 7.5 Hz, C4H), 3.90 (3H, s, OCH_3), 2.10 (3H, s, C2 $^{\prime}$ - CH_3); ^{13}C NMR (126 MHz, CDCl_3) δ = 174.1 (d, $^2J_{\text{CF}}$ 19.8 Hz, C3), 159.4 (C3 $^{\prime}$), 158.1 (d, $^1J_{\text{CF}}$ 270.2 Hz, C2), 153.3 (dd, $^1J_{\text{CF}}$ 257.8, $^2J_{\text{CF}}$ 15.3 Hz, C6), 147.8 (d, $^4J_{\text{CF}}$ 8.9 Hz, C9), 147.4 (dd, $^1J_{\text{CF}}$ 249.9, $^2J_{\text{CF}}$ 14.2 Hz, C7), 146.8 (C5 $^{\prime}$) 145.1 (C4a), 139.9 (C1 $^{\prime}$), 138.0 (C1 $^{\prime\prime}$), 137.3 (d, $^3J_{\text{CF}}$ 9.5 Hz, C10a), 132.9 (C2 $^{\prime}$), 132.0 (C3 $^{\prime\prime}$ /C5 $^{\prime\prime}$), 131.85 (C3 $^{\prime\prime}$ /C5 $^{\prime\prime}$), 130.9 (C4 $^{\prime\prime}$), 128.6 (C2 $^{\prime\prime}$ /C6 $^{\prime\prime}$), 128.3 (C2 $^{\prime\prime}$ /C6 $^{\prime\prime}$), 121.7 (dd, $^3J_{\text{CF}}$ 8.4, $^4J_{\text{CF}}$ 2.6 Hz, C9a), 116.34 (d, $^3J_{\text{CF}}$ 4.8 Hz, C8a), 113.9 (d, $^2J_{\text{CF}}$ 19.1 Hz, C8), 108.8 (d, $^2J_{\text{CF}}$ 21.9 Hz, C5), 105.8 (d, $^2J_{\text{CF}}$ 23.4 Hz, C1), 104.8 (d, $^3J_{\text{CF}}$ 5.2 Hz, C4), 95.0 (C6 $^{\prime\prime}$), 93.6 (C4 $^{\prime}$), 61.0 (OCH_3), 15.9 (C2 $^{\prime}$ - CH_3); ^{19}F NMR (471 MHz, CDCl_3) δ = -119.88 to -121.64 (m), -124.08 to -125.69 (m), -139.49 to -140.87 (m); ESI-MS: m/z calcd. for $\text{C}_{27}\text{H}_{17}\text{F}_3\text{I}_2\text{NO}_2$ 697.9295, found 697.9300 [$\text{M}+\text{H}^+$].

2.5 Synthesis of 1,6-bis((trimethylsilyl)ethynyl)pyrene ((TMS)₂pyr):



Prepared according to the modified literature procedure:³ A 20 mL crimp cap vial was charged with 1,6-dibromopyrene (252 mg, 700 μ mol, 1.00 eq.), CuI (9.33 mg, 49.0 μ mol, 0.07 eq.), PPh₃ (12.9 mg, 49.0 μ mol, 0.07 eq.), Pd(PPh₃)₂Cl₂ (34.4 mg, 49.0 μ mol, 0.07 eq.). The mixture was degassed via vacuum/argon cycles (3 times). Then degassed NEt₃ (10 mL) was transferred to the vial. Then ethynyltrimethylsilane (206 mg, 2.10 mmol, 3.00 eq.) was added, and the reaction mixture was refluxed for 18 h. The reaction mixture was then filtered through a thin layer of silica gel (with EtOAc), the solvent was removed under reduced pressure. The crude product was purified by silica gel chromatography (from cyclohexane / CH₂Cl₂ 100 : 0 to 5 : 1), yielding the desired product as a yellow solid (220 mg, 557 μ mol, 80%), NMR is in agreement with the previously reported spectral data.³

3 Additional photochemical properties of the isoacridone photosensitizers

3.1 Extinction coefficients of triplet-excited anthracene in THF

The solvent-dependent molar extinction coefficient of the triplet-excited anthracene ($\Delta\epsilon_{3\text{Ant}}$) at 423 nm in THF was determined by actinometry.^{4, 5}

A reference system of 50 μM $[\text{Ru}(\text{bpy})_3]^{2+}$ in water, undergoing a known change in its molar excitation coefficient at 455 nm upon excitation to its long-lived $^3\text{MLCT}$ excited state ($\Delta\epsilon_{\text{ref}} = -10100 \text{ M}^{-1}\text{cm}^{-1}$),⁶ was compared with the same $[\text{Ru}(\text{bpy})_3]^{2+}$ concentration in THF in the presence of 10 mM anthracene (sample system). We assumed that the triplet-triplet energy transfer (TTET) from $[\text{Ru}(\text{bpy})_3]^{2+}$ to anthracene is quantitative due to the high anthracene concentration and the high driving force of the TTET process of $\sim 0.3 \text{ eV}$.⁷ Transient UV-Vis absorption spectra and single-wavelength kinetics were recorded under identical conditions and are shown in Figure S1. The changes in optical density (ΔOD) at 455 nm (reference system) and 423 nm (sample system) were compared, and the molar extinction coefficient of anthracene in THF ($\Delta\epsilon_{\text{Ant}}$) was calculated using equation S1.

$$\Delta\epsilon_{\text{Ant}} = \Delta\epsilon_{\text{ref}} \times \frac{\Delta\text{OD}_{\text{ref}}}{\Delta\text{OD}} \times \frac{n^2}{n_{\text{ref}}^2} \quad (\text{Equation S1})$$

In equation S1, $\Delta\epsilon_{\text{ref}}$ is the change in molar excitation coefficient of $^3\text{MLCT}$ -excited $[\text{Ru}(\text{bpy})_3]^{2+}$ ($^3[\text{Ru}(\text{bpy})_3]^{2+}$) at 455 nm, ΔOD is the signal intensity of anthracene at 423 nm in THF, $\Delta\text{OD}_{\text{ref}}$ is the change in absorbance due to the formation of $^3[\text{Ru}(\text{bpy})_3]^{2+}$ at 455 nm, and n is the refractive index of water ($n_{\text{ref}} = 1.33$)⁸ and THF ($n = 1.41$)⁸. Three independent determinations were made, resulting in $\Delta\epsilon_{\text{Ant}} = 82'000 \pm 1500 \text{ M}^{-1}\text{cm}^{-1}$ in THF. This result is similar to the literature-known value of $85'700 \pm 3200 \text{ M}^{-1}\text{cm}^{-1}$ in cyclohexane, but markedly different from the value of $53'000 \pm 1900 \text{ M}^{-1}\text{cm}^{-1}$ in benzene.^{4, 5}

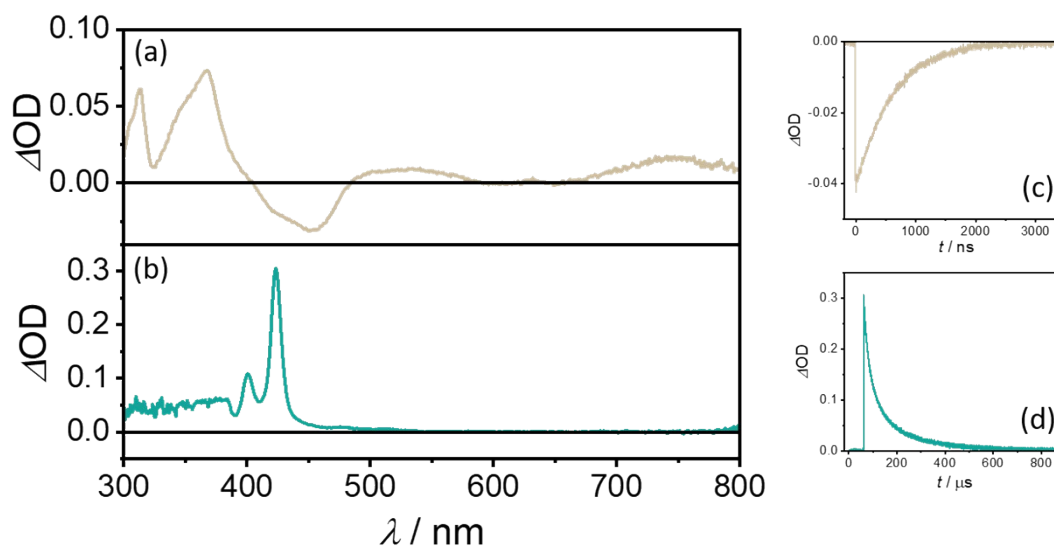


Figure S1: Determination of the molar extinction coefficient of triplet-excited anthracene in THF at 423 nm. Transient UV-Vis absorption spectrum and kinetic trace of a deaerated aqueous solution containing 50 μM $[\text{Ru}(\text{bpy})_3]^{2+}$ (a & c) and a THF solution containing 50 μM $[\text{Ru}(\text{bpy})_3]^{2+}$ and 10 mM anthracene (b & d), were recorded. The transient UV-Vis spectra (a & b) were recorded with a time delay of 5 ns and a time integration of 200 ns, whereas the kinetic traces were detected at 455 nm (c) and 423 nm (d) upon 450 nm pulsed excitation (16 mJ per pulse).

3.2 Intersystem crossing quantum yield

The ISC-QY was determined by relative actinometry. A reference of $[\text{Ru}(\text{bpy})_3]^{2+}$ in water (where ISC of unity is expected)⁹ was compared with a sample solution containing the isoacridone PSs with unknown ISC-QY in the presence of 10 mM anthracene in THF. Both solutions (reference and sample) were adjusted to the same optical density of ~ 0.1 at the excitation wavelength to ensure the same amount of absorbed photons at the excitation wavelength. Time-resolved UV-Vis absorption traces at 455 nm for the reference system and at 423 nm for the sample system were recorded under identical instrument settings. The transient UV-Vis absorption change (ΔOD) at a delay time of 0 ns (immediately after excitation) was used to calculate the ISC-QY.

Since the change in the molar extinction coefficient of the ground-state MLCT bleach at 455 nm of $^3[\text{Ru}(\text{bpy})_3]^{2+}$ ($\Delta\epsilon_{\text{ref}} = -10100 \text{ M}^{-1}\text{cm}^{-1}$)⁶ is known, the concentration of the triplet-excited state of $[\text{Ru}(\text{bpy})_3]^{2+}$ (c_{ref}) was calculated with equation S2.

$$c_{\text{ref}} = c_{\text{photons}} = \frac{\Delta OD_{\text{ref}}}{\Delta\epsilon_{\text{ref}} \times d} \text{ (Equation S2)}$$

Where d is the path length of the optical cuvettes, ΔOD_{ref} the change in optical density at 455 nm, and $\Delta\epsilon_{\text{ref}}$ is the known change in molar extinction coefficient at 455 nm. Due to the quantitative ISC-QY in $[\text{Ru}(\text{bpy})_3]^{2+}$,⁹ this c_{ref} value corresponds to the concentration of absorbed photons (c_{photons}).

To estimate the ISC-QY in the isoacridone dyes, the concentration of the triplet-excited state of the isoacridone PS was determined. As the extinction coefficients of the triplet-excited isoacridone PSs are not known, an additional TTET step to anthracene, featuring a known extinction coefficient ($\Delta\epsilon_{\text{Ant}} = 82'000 \text{ M}^{-1}\text{cm}^{-1}$, see above) in its long-lived triplet-excited state, was considered useful as an additional reaction step. As the TTET is assumed to be quantitative due to its driving-force and the high concentration of anthracene used, the concentration of the triplet-excited state of anthracene ($c_{3\text{Ant}}$) formed after TTET is assumed to be identical to the initially present concentration of triplet-excited isoacridone PSs ($c_{3\text{PS}}$). The concentration of triplet-excited isoacridone PS ($c_{3\text{PS}}$) was determined with equation S3,

$$c_{3\text{PS}} = c_{3\text{Ant}} = \frac{\Delta OD_{\text{Ant}}}{\Delta\epsilon_{\text{Ant}} \times d} \text{ (Equation S3)}$$

where d is the path length of the optical cuvettes (1 cm), ΔOD_{Ant} the change in optical density at 423 nm, and $\Delta\epsilon_{\text{Ant}}$ is the molar extinction coefficient of triplet-excited anthracene at 423 nm.

Using the reference and sample systems, the ISC-QY was calculated with equation S4.

$$ISC - QY = \frac{c_{3Ant}}{c_{ref}} = \frac{\Delta\varepsilon_{ref} \times \Delta OD_{Ant}}{\Delta\varepsilon_{Ant} \times \Delta OD_{ref}} \quad (\text{Equation S4})$$

Where c_{ref} is the concentration of $^3[\text{Ru}(\text{bpy})_3]^{2+}$, corresponding to the concentration of absorbed photons, and c_{3Ant} is the concentration of triplet-excited anthracene (c_{3Ant}), corresponding to the concentration of the triplet-excited isoacridone PS.

Six independent determinations were made for each isoacridone PS and the results are summarized in Table 1 of the main manuscript.

3.3 External heavy atom effect

The external heavy atom effect was investigated as a possibility to increase the ISC-QY of the isoacridone PS(I) in the presence of heavy atom-containing salts or co-solvents. To quantify the ISC-QY, the triplet-excited state of PS(I) was quenched with anthracene (10 mM, where the triplet-excited state of PS(I) is fully quenched), leading to the pronounced triplet-excited anthracene signal at 423 nm (Figure S2a), as described above. The change in optical density caused by the triplet-excited state of anthracene at 423 nm measured without any additive (Table S1, entry 1) was compared to the change in optical density reached at the same wavelength after the addition of an external heavy atom source (Table S1, entry 2-9). As all spectra were recorded under identical conditions, the ISC-QY was calculated using the known ISC-QY of 0.26 for PS(I) in THF (Table S1, entry 1).

Tetra-*n*-butylammonium-bromide ($[\text{N}(\text{Bu})_4] \text{Br}$; Table S1, entry 2) as an external heavy atom source leads to a decrease in ISC-QY, whereas tetra-*n*-butylammonium-iodine ($[\text{N}(\text{Bu})_4] \text{I}$; Table S1, entry 3) induced fast decomposition upon pulsed excitation. Therefore, chlorinated co-solvents such as dichloromethane (CH_2Cl_2 ; Table S1, entry 4) and chloroform (CHCl_3 ; Table S1, entry 5) were tested, but showed no significant ISC-QY enhancement. Consequently, the bromine-containing solvents dibromomethane (CH_2Br_2 ; Table S1, entry 6) and bromoform (CHBr_3 ; Table S1, entry

7) were tested, which also led to fast decomposition upon pulsed excitation. As a last attempt, diiodomethane (CH_2I_2 ; Table S1, entry 8) and iodoform (CHI_3 ; Table S1, entry 9) were tested. Due to the substantial absorption of CHI_3 in the visible spectral range, the ISC-QY enhancement by adding CHI_3 could not be determined in reliable fashion. However, the colorless CH_2I_2 led to a two-fold improvement in ISC-QY (Table S1, entry 7), indicating the usability of the external heavy atom effect for enhanced ISC-QY.

Table S1: Investigation of the increased ISC-QY of PS(I) by using heavy atom containing additives.

entry	additive	concentration / mM	Φ_{ISC}	comment
1	none	n/d	0.26	standard conditions
2	$[\text{N}(\text{Bu})_4]\text{Br}$	100	0.11	decrease in Φ_{ISC}
3	$[\text{N}(\text{Bu})_4] \text{I}$	50	n/d	decomposition
4	CH_2Cl_2	2500	0.29	no significant increase in Φ_{ISC}
5	CHCl_3	2500	0.26	no significant increase in Φ_{ISC}
6	CH_2Br_2	2500	n/d	decomposition
7	CHBr_3	2500	n/d	decomposition
8	CH_2I_2	2500	0.53	strong increase in Φ_{ISC}
9	CHI_3	100	n/d	strong visible absorption at excitation wavelength

To investigate the influence of CH_2I_2 on the ISC-QY of PS(I), kinetic decays at 420 nm (Figure S2a, inset) and transient UV-Vis absorption spectra after a delay time of 100 ns (Figure S2a, main part) were recorded as a function of CH_2I_2 concentration. The ISC-QY was calculated by comparing the change in optical density at 420 nm without CH_2I_2 (black trace in Figure S2a), using the known ISC-QY under these conditions ($\Phi_{\text{ISC}} = 0.26$). The ISC-QY increase of PS(I) is plotted against the CH_2I_2 concentration, resulting in a plateau of around 50% ISC-QY at a CH_2I_2 concentration of 1 M (Figure S2b). However, the two-fold increase in ISC-QY comes with the penalty of a decreased triplet-excited state lifetime of anthracene from 71 μs to 3.6 μs , likely due to faster

reverse intersystem crossing enabled by the heavy atom effect, facilitating the formally spin-forbidden relaxation back to the electronic ground state. Due to this finding, the exploitation of an external heavy atom effect was not pursued in the following studies.

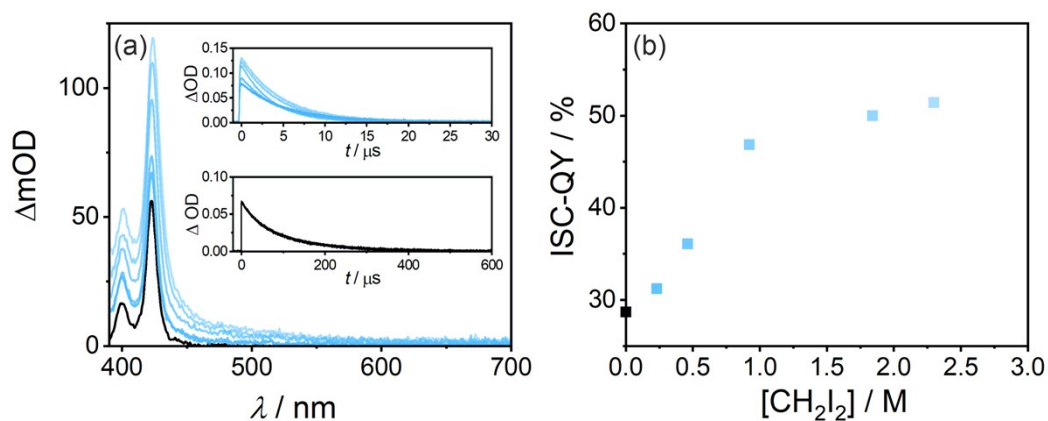


Figure S2: Investigation of the external heavy atom effect. (a) Transient UV-Vis absorption spectra of deaerated THF solutions containing 50 μM PS(I), 10 mM anthracene, and 0 mM (black trace) to 2500 mM (blue traces) CH_2I_2 upon 532 nm pulsed excitation (20 mJ per pulse). All spectra were recorded under identical conditions using a time delay of 100 ns and signal time integration over 200 ns. The insets show the triplet-excited-state decays (recorded under identical conditions) of anthracene at 420 nm with (blue traces) and without the addition of CH_2I_2 (black trace). (b) ISC-QY increase using 0 mM (black data point) up to 2500 mM CH_2I_2 (blue data points) as an external heavy atom source.

3.4 Photodegradation quantum yields

Photorobustness is essential for the reliable use of photosensitizers. Therefore, the photo-degradation quantum yield $\Phi_{degr.}$ of the newly developed PSs was determined using a cw laser, similar as in previous studies (Figures S4-S6).¹⁰⁻¹²

To avoid systematic errors due to possible luminescent photo-degradation products, $\Phi_{degr.}$ was determined at an intensity ratio of $I/I_0 = 0.9$, at which 10% of the initial PS concentration have decomposed. The number of photons emitted by the cw laser were determined with equation S5, where P_{laser} is the power output of the cw laser (100 mW), t is the irradiation time needed to reach $I/I_0 = 0.9$, and E_{photon} is the energy of single photons with a wavelength of 532 nm (3.73×10^{-19} J).

$$\#Photons = \frac{P_{Laser} \times t}{E_{Photon}} \quad (\text{Equation S5})$$

The optical transmittance (T) at the excitation wavelength was used to calculate the effective photon absorption using equation S6, where A is the optical density of the PS solution at 532 nm.

$$T = 10^{-A} \quad (\text{Equation S6})$$

For simplicity, the optical density at 532 nm was considered constant up to the point at which 10% of the PS had decomposed. Using the number of emitted photons ($\#Photons$), the molar concentration of the different PSs (c), and Avogadro's constant (N_A), the photo-degradation quantum yield ($\Phi_{degr.}$) was calculated with equation S7. The resulting values are summarized in Table S2.

$$\Phi_{degr.} = \frac{c \times N_A}{\#Photons \times T} = \frac{c \times N_A}{\frac{P_{Laser} \times t}{E_{Photon}} \times 10^{-A}} \quad (\text{Equation S7})$$

Table S2: Determination of the photo-degradation quantum yields ($\Phi_{\text{degr.}}$).

photosensitizer (PS)	time ($I/I_0=0.9$) / s ^[a]	absorbed photons / μmol ^[b]	initial concentration / μM ^[c]	decomposed PS ($I/I_0=0.9$) / nmol ^[d]	$\Phi_{\text{degr.}}$ / % ^[e]
(I)	216	52	55.7	13.9	0.054
(II)	48	8.2	80.2	20.1	0.23
(III)	19	5.0	51.2	12.8	0.36
(IV)	66	15	46.1	11.5	0.13

^[a] Irradiation time after which 10% of the initial PS is decomposed.

^[b] Molar quantity of absorbed photons within the irradiation time after which 10% of the initial PS are decomposed (column 2).

^[c] Initial concentration of the photosensitizer before irradiation.

^[d] Calculated with $[c_0 - (I/I_0 \times c_0)] \times V$, where V is the sample volume (2.5 mL), c_0 is the initial molar concentration of the isoacridone PS, and I/I_0 (0.9) is the intensity ratio at the point, at which 10% of the initially present photosensitizer has decomposed.

^[e] Photo-degradation quantum yield ($\Phi_{\text{degr.}}$) calculated using Equation S7.

All four photosensitizers show photo-decomposition quantum yields in the range of 0.05% and 0.36%. However, the inherent photostability (Figure S3a) of a given PS is not a good measure of the photostability of the PS under catalytic conditions, because the relevant excited states, from which photo-degradation occurs, are usually quenched rapidly under catalytic conditions (Figure S3b).

Therefore, the photorobustness was measured in a reaction environment that is more directly comparable to a typical reaction mixture as relevant under catalytic conditions. Specifically, 10 mM anthracene as a triplet energy acceptor was added to the PS solution. Since the isoacridone PS exhibit strong singlet emission (not quenched by the triplet acceptor), the same measurement method as for the unquenched photo-degradation measurements could be used (Figure S4). By comparing the photorobustness in the absence (Figure S4, colored traces) and in the presence of the triplet quencher anthracene (Figure S4, brown traces), a substantial increase in photorobustness became evident under TTET conditions.

Over the irradiation time of 60 minutes, no decomposition of the PS could be observed. However, increasing temperature due to the irradiation could have a non-negligible effect on the observed decomposition. To estimate the lower limit of the degradation quantum yield under the applied conditions, we assumed a maximum decomposition of 5 % during the experimental time of 60 minutes (3600 s) for all isoacridone PS. With this assumption, the decomposition quantum yield was estimated similarly to the unquenched decomposition quantum yield, summarized in Table S3. The degradation quantum yields under operating conditions for all isoacridone PS are very low with values around 0.001%, compared to inherent decomposition quantum yields between 0.05% and 0.36 %.

Table S3: Photo-degradation quantum yields under triplet-triplet energy transfer conditions ($\Phi_{\text{degr, TTET}}$).

photosensitizer (PS)	time / s ^[a]	absorbed photons / μmol ^[b]	initial concentration / μM ^[c]	TTET decomposed PS / nmol ^[d]	$\Phi_{\text{degr, TTET}}$ / % ^[e]
(I)	3600	867	55.7	6.97	0.0016
(II)	3600	618	80.2	10.0	0.0015
(III)	3600	602	51.2	6.40	0.0009
(IV)	3600	804	46.1	5.76	0.0012

^[a] Irradiation time, after which 5% of the initial PSs are decomposed.

^[b] Molar quantity of absorbed photons within the 60 minutes irradiation time (see text for details).

^[c] Initial concentration of the photosensitizer before irradiation.

^[d] Calculated with $[c_0 - (I/I_0 \times c_0)] \times V$, where the V is the sample volume (2.5 mL), c_0 is the initial molar concentration of the isoacridone photosensitizer, and I/I_0 (0.95) is the intensity ratio at the irradiation time, after which approximately 5% of the initially present photosensitizer were decomposed.

^[e] Photo-degradation quantum yield according to equation S7.

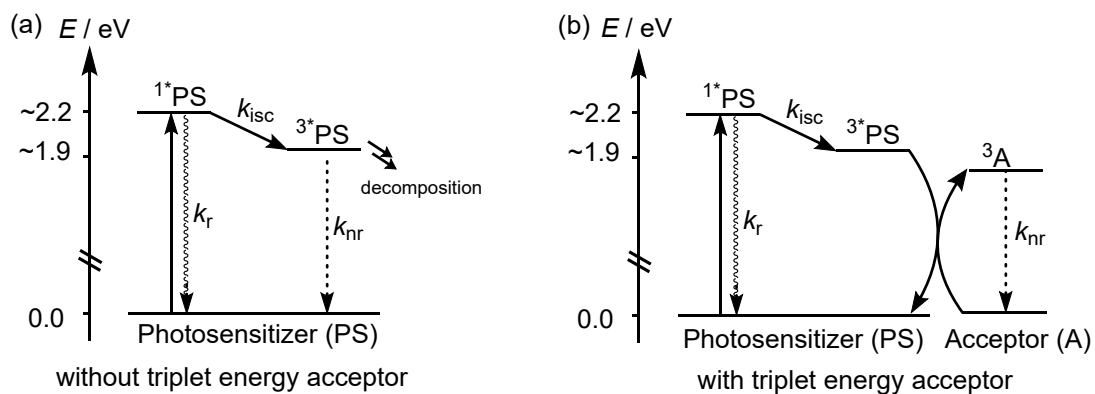


Figure S3 : Simplified energy diagrams with relative energies of the lowest singlet and triplet-excited states of the isoacridone PSs. Panel (a) illustrates the photo-degradation from the lowest triplet-excited state, whereas (b) illustrates the increased photostability when quenching of the triplet-excited state by triplet-triplet energy transfer occurs. The underlying assumption in both diagrams and in the determination of the individual rate constant is that there is no direct nonradiative relaxation from the S_1 state to the S_0 ground state.

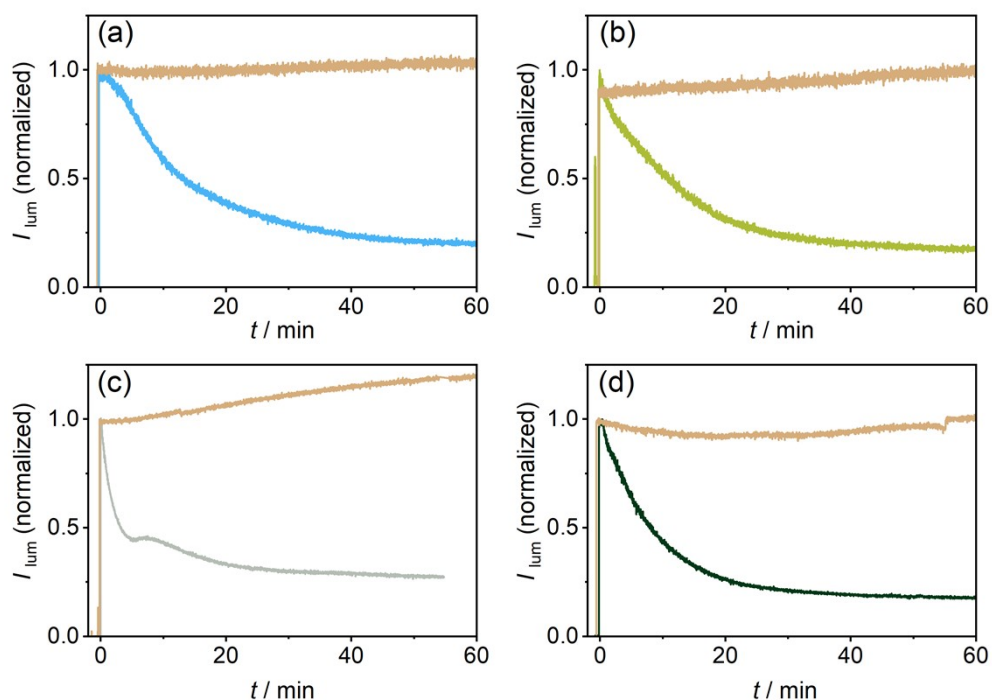


Figure S4: Photostability upon irradiation with a 532 nm cw laser (100 mW) in argon-saturated THF solution at room temperature. Normalized fluorescence intensities emitted by solutions containing 55 μM PS(I) panel (a), 80 μM PS(II) panel (b), 51 μM PS(III) panel (c) and 46 μM PS(IV) panel (d) in the presence of 10 mM anthracene (brown traces) and in the absence of anthracene. All time traces recorded in the absence of anthracene show a pronounced decrease in fluorescence intensity at 600 nm as a function of irradiation time.

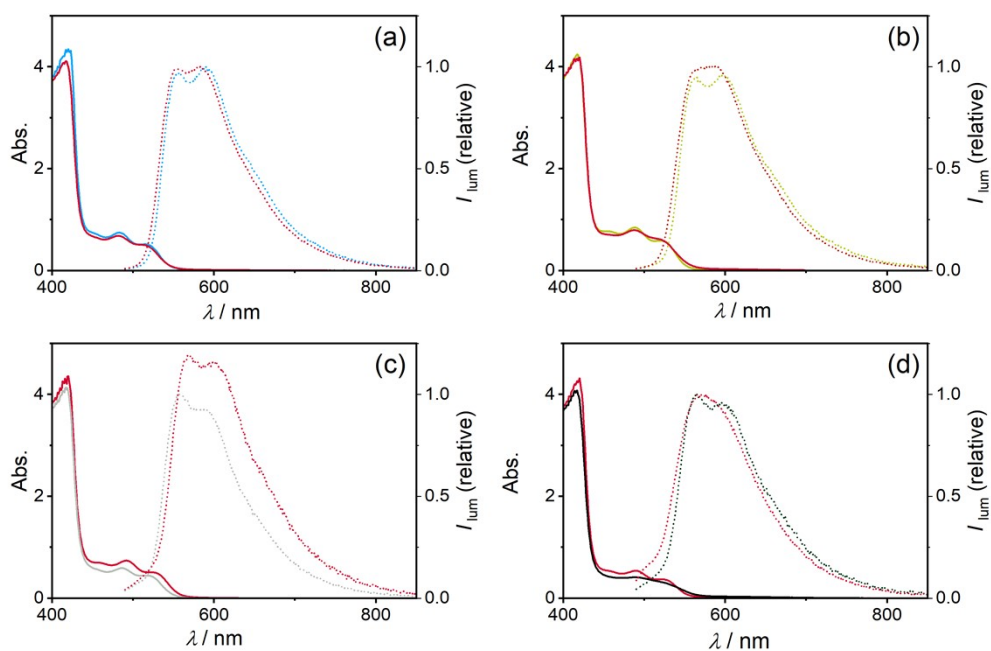


Figure S5: Luminescence (dotted lines) and absorption spectra (solid lines) recorded before and after (red traces) irradiation of 55 μM PS(I) panel (a), 80 μM PS(II) panel (b), 51 μM PS(III) panel (c) and 46 μM PS(IV) panel (d) with a 532 nm cw laser (100 mW). The samples shown here contained 10 mM anthracene in argon-saturated THF solution at room temperature.

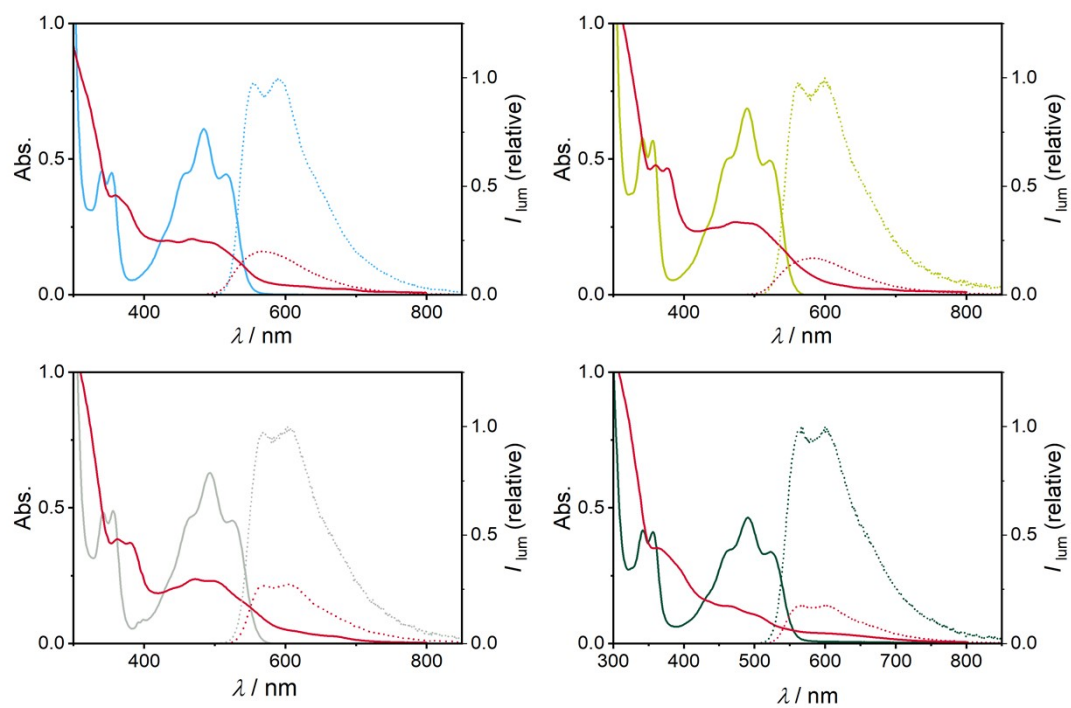
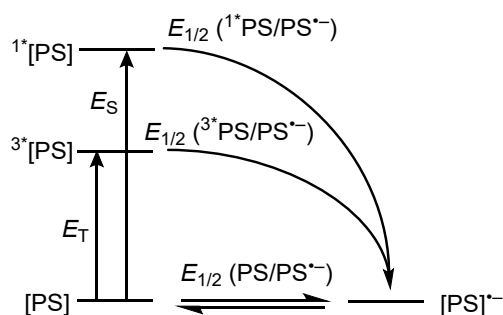


Figure S6: Luminescence (dotted lines) and absorption spectra (solid lines) recorded before and after (red traces) irradiation of 55 μM PS(I) panel (a), 80 μM PS(II) panel (b), 51 μM PS(III) panel (c) and 46 μM PS(IV) panel (d) with a 532 nm cw laser (100 mW). The samples shown here did not contain any anthracene in argon-saturated THF solution at room temperature.

4 Triplet-triplet energy transfer catalysis

To assess the photoredox reactivity of the newly developed photosensitizers, the singlet- and triplet-excited state redox potentials were estimated based on the singlet- and triplet-excited state energies and the relevant ground state redox potentials using the Rehm-Weller equation (Table S4).¹³ Based on the excited-state redox potentials and the triplet energies, suitable photochemical reactions were then selected, for which the expectable reaction mechanism involves both an electron and an energy transfer step.

Table S4: Reductive cycle of the investigated photosensitizers (PS), based on the voltammograms shown in Figure S7, including the energies of their photoactive singlet- and triplet-excited states, derived from the spectroscopic studies discussed in the main manuscript. All potentials are reported in V vs SCE.



PS	E_S [a]	E_T	$E_{1/2}$ (PS/PS $^{\bullet-}$) / V vs SCE [d]	$E_{1/2}$ (1^* PS/PS $^{\bullet-}$) / V vs SCE [e]	$E_{1/2}$ (3^* PS/PS $^{\bullet-}$) / V vs SCE [e]
(I)	2.33	1.88 [c]	-1.20	1.13	0.77
(II)	2.28	1.88 [c]	-1.10	1.18	0.80
(III)	2.29	1.88 [b]	-1.10	1.19	0.80
(IV)	2.30	1.88 [b]	-1.15	1.15	0.75

[a] Determination at the intersection of the fluorescence and the UV-Vis absorption spectra.

[b] Energy of the triplet-excited state was estimated based on the 0-0 transition of the phosphorescence spectra at 77 K.

[c] Energy of the triplet-excited state was equated to the triplet energies of PS(III) and PS (IV), because all investigated isoacridone PS show comparable excited state properties (see main part).

[d] Measured in 0.1 M *n*-Bu₄NPF₆ in degassed and dry MeCN against SCE.

[e] Excited state potentials were estimated using the Rehm-Weller equation.¹³

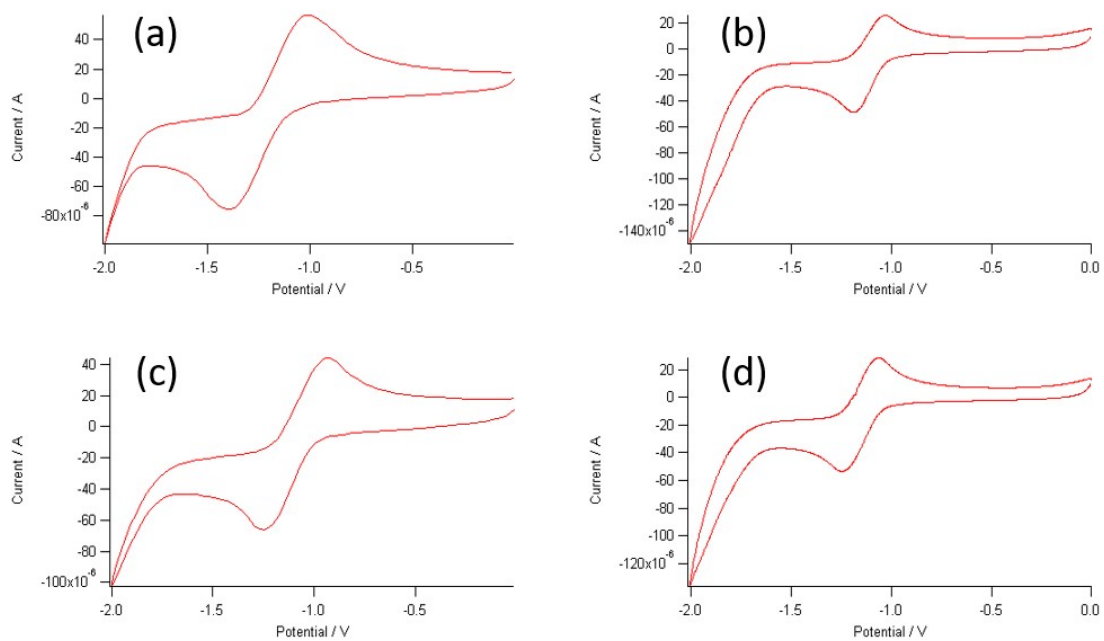


Figure S7: Cyclic voltammograms of PS(I) panel (a), PS(II) panel (b), PS(III) panel (c), and PS(IV) panel (d) measured in the presence of 0.1 M $n\text{-Bu}_4\text{NPF}_6$ in deaerated MeCN at 20 °C.

4.1 Birch-type photoreduction of anthracene derivatives

To explore the reactivity of the electronically excited isoacridone photosensitizers, the Birch-type photoreduction of anthracene derivatives was tested. In the previously postulated mechanism (Figure S8),¹⁴ the triplet-excited photosensitizers (^3PS) undergo a triplet-triplet energy transfer (TTET, pink circle), forming the triplet-excited state of anthracene derivatives (b). In a parallel process taking place in the presence of excess sacrificial electron donor (diisopropylethylamine, DIPEA), one-electron reduced photosensitizer ($\text{PS}^{\cdot-}$) is formed via reductive excited state quenching. Subsequent single electron transfer (SET, purple circle) from the reduced isoacridone species ($\text{PS}^{\cdot-}$) to the triplet-excited anthracene, leads to the radical monoanion forms of the individual anthracene derivatives (c). Hydrogen atom transfer (HAT, black circle), for example from the one-electron oxidized form of DIPEA, (d)) and subsequent proton transfer (for example with DIPEA^+ as acid, but involving $\text{CH}_3\text{NH}_3\text{Cl}$ as a mediator), can then lead to the doubly reduced final product (e).¹⁴ A detailed mechanistic investigation of the dual reactivity of ^1PS and ^3PS is discussed in Section 4.3.

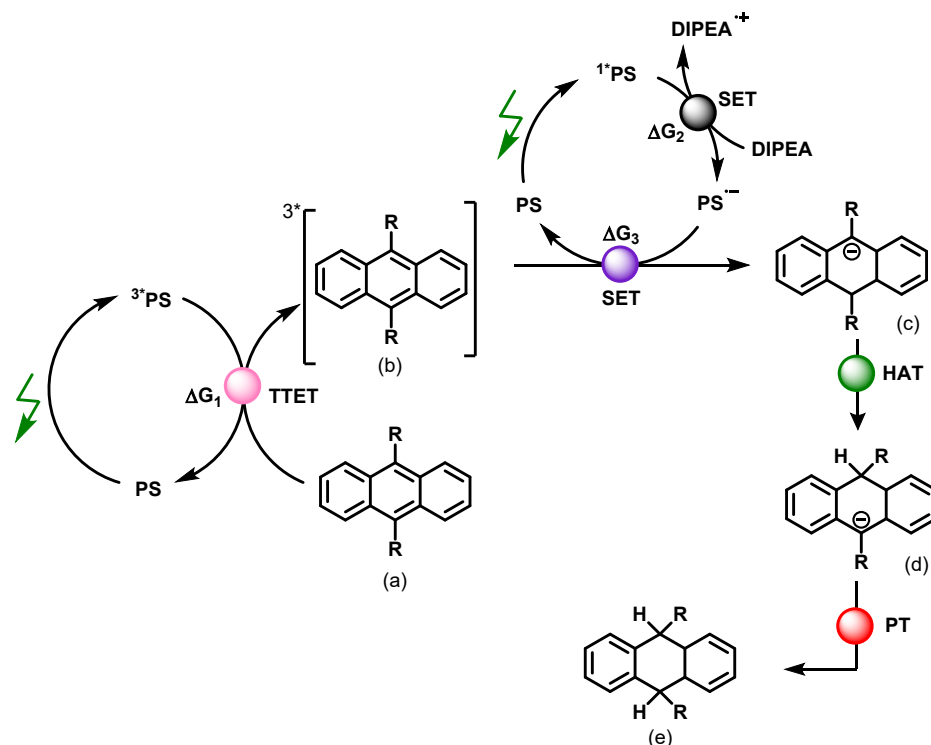


Figure S8: Postulated mechanism adapted from ref. ¹⁴, involving TTET, SET, HAT, and PT as key steps. TTET = triplet-triplet energy transfer; SET = single-electron transfer; HAT = hydrogen atom transfer; PT = proton transfer.

General procedure A for reaction optimization:

Performed according to the modified literature procedure:¹⁴ DMF (0.35 mL) was added to a mixture of anthracene (6.24 mg, 35.0 μ mol), the photocatalyst, DIPEA, and an additive in a 4-mL screw top vial equipped with a stirring bar. The vial was placed under an argon atmosphere, cooled to -78°C , degassed by evacuation (5 min), backfilled with argon, and warmed to room temperature. This procedure was repeated three times and the reaction mixture was then irradiated with blue LED (SynLED photoreactor) for 18 hours. Then the resulting mixture was diluted with water (10 mL) and extracted with EtOAc (3×10 mL). The combined organic phases were washed with brine (3×15 mL), dried over Na_2SO_4 , and the solvent was removed under reduced pressure. NMR standard (1,2,4,5-tetramethylbenzene) was added to the residue and the reaction outcome was analyzed by ^1H NMR spectroscopy.

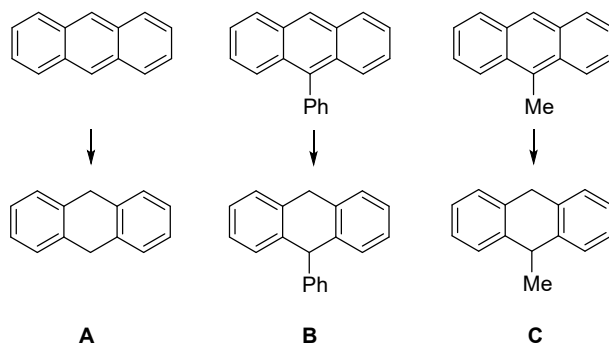
Table S5: Reaction conditions screening for the Birch-type photoreduction of arenes.

Entry ^[a]	PC	Additive	PC (mol%)	DIPEA (eq.)	CH ₃ NH ₃ Cl (eq.)	Conversion ^[b]	Conversion ^[c] (with dimer)	Yield ^[d] (NMR)	SM : dimer : P ^[e]
Variations of the of PC loadings									
1	(I)		1	2	2	16%	74%	11%	1 : 1.1 : 0.6
2	(I)		2	2	2	34%	57%	28%	1 : 0.3 : 0.8
3	(I)		5	2	2	35%	62%	19%	1 : 0.3 : 0.9
4	(I)		10	2	2	49%	72%	33%	1 : 0.4 : 1.8
5	(I)		13	2	2	30%	50%	18%	1 : 0.2 : 0.6
Variations of DIPEA quantity									
6	(I)		2	2	2	34%	57%	28%	1 : 0.3 : 0.8
7	(I)		2	4	2	24%	85%	16%	1 : 2.0 : 1.6
8	(I)		2	6	2	62%	91%	36%	1 : 1.6 : 6.8
9	(I)		2	8	2	50%	67%	30%	1 : 0.3 : 1.5
10	(I)		2	10	2	24%	92%	18%	1 : 4.4 : 3.2
11	(I)		2	15	2	50%	100%	35%	0 : 1.0 : 2.0
Variations of CH₃NH₃Cl quantity									
12	(I)		2	2	1	18%	62%	11%	1 : 0.6 : 0.5
13	(I)		2	2	2	34%	57%	28%	1 : 0.3 : 0.8
14	(I)		2	2	4	10%	70%	7%	1 : 1.0 : 0.4
15	(I)		2	2	10	20%	81%	14%	1 : 1.7 : 1.0
Variations of two parameters									
16	(I)		4	4	2	39%	89%	34%	1 : 2.2 : 3.5
17	(I)		5	8	2	35%	87%	31%	1 : 2.1 : 2.8
18	(I)		5	10	2	38%	94%	29%	1 : 5.0 : 6.7
19	(I)		8	8	2	37%	90%	33%	1 : 2.7 : 3.7
20	(I)		5	8	4	47%	100%	26%	0 : 1.0 : 1.8
Impact of additives									
21	(I)	<i>i</i> PrSiSH (0.4 eq.)	2	6	2	16%	85%	6%	1 : 2.3 : 1.0
22	(I)	<i>i</i> PrSiSH (0.8 eq.)	2	6	2	16%	72%	9%	1 : 1.0 : 0.6
Application of Ir-based photocatalysts									
23	[Ir]		2	6	2	100%	100%	49%	0 : 0 : 1

^[a] Reactions were performed on 35.0 μmol scale in DMF (0.35 mL), 18 h, Ar; ^[b] Conversion of the anthracene substrate to the product **A** was determined by ¹H NMR analysis: $n(\mathbf{A}) / ((n(\mathbf{A}) + 2 \cdot n(\text{dimer}) + n(\text{anthracene})))$; ^[c] Conversion of the anthracene substrate to the main product **A** and the dimer side-product (9,9',10,10'-tetrahydro-9,9'-bianthracene) was determined by ¹H NMR analysis: $(n(\mathbf{A}) + 2 \cdot n(\text{dimer})) / ((n(\mathbf{A}) + 2 \cdot n(\text{dimer}) + n(\text{anthracene})))$; ^[d] The reaction yield was determined by quantitative ¹H NMR analysis by adding durene (1,2,4,5-benzene) as a standard to the crude material after the isolation procedure; ^[e] The ratio between remaining starting material (SM)

after the reaction (anthracene), the dimer side product, and the target product (**A**) was obtained via ^1H NMR analysis. $[\text{Ir}] = [\text{Ir}(\text{dF}(\text{CF}_3)\text{ppy})_2(\text{dtbpy})]\text{PF}_6$

General procedure B for the Birch-type photoreduction and the exploration of its substrate scope:



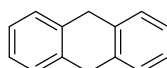
DMF (0.80 mL) was added to a mixture of the respective arene substrate (80.0 μmol , 1.00 eq.), the photocatalyst (2.0 mol%), DIPEA (62.3 mg, 480 μmol , 6.00 eq.), and $\text{CH}_3\text{NH}_3\text{Cl}$ (11.0 mg, 160 μmol , 2.00 eq.) in a 4-mL screw top vial equipped with a stirring bar. The vial was placed under an argon atmosphere, cooled to -78°C , degassed by evacuation (5 min), backfilled with argon, and warmed to room temperature. This procedure was repeated three times and the reaction mixture was then irradiated with blue LED (SynLED photoreactor) for 18 hours. Then the resulting mixture was diluted with water (20 mL) and extracted with EtOAc (3×15 mL). The combined organic layer was washed with brine (3×15 mL), dried over Na_2SO_4 , and the solvent was removed under reduced pressure. The residue was purified by the silica gel column (*n*-hexane / CH_2Cl_2 from 100 : 0 to 70 : 30).

Table S6: Comparison of different photocatalysts for Birch-type reduction.

Entry ^[a]	Substrate	PC	Conversion	Isolated yield	Conversion (with dimer)
1	9-phenylanthracene	(III)	70%	61%	
2	9-phenylanthracene	(I)	94%	90%	
3	9-phenylanthracene	[Ir]	75%	50%	
4	9-methylanthracene	(III)	71%	66%	
5	9-methylanthracene	(I)	96%	57%	
6	9-methylanthracene	[Ir]	100%	53%	
7	anthracene	(III)	22%	24%	70%
8	anthracene	(I)	37%	35%	91%
9	anthracene	[Ir]	100%	49%	100%

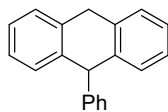
^[a] Reactions were performed on 80.0 μmol scale in DMF (0.80 mL), 18 h, Ar; [Ir] = $[\text{Ir}(\text{dF}(\text{CF}_3)\text{ppy})_2(\text{dtbpy})]\text{PF}_6$

9,10-Dihydroanthracene (A):



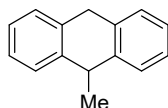
Prepared according to the general procedure **B** using anthracene (14.3 mg, 80.0 μmol) to give the title compound as a white solid (entry 7 – 3.40 mg, 18.9 μmol , 24%; entry 8 – 5.00 mg, 27.7 μmol , 35%; entry 9 – 7.00 mg, 38.8 μmol , 49%). NMR corresponds to reported data:¹⁴ ^1H NMR (400 MHz, CDCl_3) δ = 7.34 – 7.27 (4H, m), 7.24 – 7.15 (4H, m), 3.94 (4H, s).

9-Phenyl-9,10-dihydroanthracene (B):



Prepared according to the general procedure **B** using 9-phenylanthracene (20.3 mg, 80.0 μmol) to give the title compound as a beige solid (entry 1 – 12.5 mg, 48.9 μmol , 61%; entry 2 – 18.5 mg, 72.2 μmol , 90%; entry 3 – 10.2 mg, 39.8 μmol , 50%). NMR corresponds to reported data:¹⁴ ^1H NMR (400 MHz, CDCl_3) δ = 7.35 – 7.27 (4H, m), 7.24 – 7.17 (1H, m), 7.17 – 7.11 (1H, m), 7.10 – 7.04 (2H, m), 5.26 (1H, s), 4.02 (1H, d, 2J 18.4 Hz), 3.90 (1H, d, 3J 18.2 Hz).

9-Methyl-9,10-dihydroanthracene (C):



Prepared according to the general procedure **B** using 9-methylanthracene (15.4 mg, 80.0 μmol) to give the title compound as yellow solid (entry 4 – 10.3 mg, 53.0 μmol , 66%; entry 5 – 8.80 mg, 45.3 μmol , 57%; entry 3 – 8.20 mg, 42.2 μmol , 53%). NMR corresponds to reported data:¹⁴ ^1H NMR (400 MHz, CDCl_3) δ = 7.33 – 7.27 (4H, m), 7.24 – 7.14 (4H, m), 4.13 (1H, d, 2J 18.3 Hz), 4.05 (1H, q, 3J 7.2 Hz), 3.89 (1H, d, 2J 18.2 Hz), 1.43 (3H, d, 3J 7.3 Hz).

4.2 Sensitization-initiated electron transfer

In addition to the Birch-type photoreduction, sensitization-initiated electron transfer (Seni-ET) was previously identified as another promising strategy for challenging multi-photon reductions, which rely on two consecutive light absorption events.¹⁵ Two different mechanisms have been postulated in literature for different catalytic systems (Figure S9).¹⁵⁻¹⁸ In mechanism (a), TTET from a $[\text{Ru}(\text{bpy})_3]^{2+}$ PS to a co-catalyst such as 9,10-diphenylanthracene (DPA) or anthracene occurs in parallel with photoreduction of the PS by excess sacrificial electron donor (D_{sac}). This is followed by SET from the reduced photosensitizer ($\text{PS}^{\cdot-}$) to the triplet-excited co-catalyst, forming the co-catalyst radical anion ($\text{DPA}^{\cdot-}$). Both initial photoinduced steps are discussed in more detail in section 4.3, to show the plausibility of the proposed mechanism.

In mechanism (b), the singlet-excited state of DPA or a related co-catalyst forms via sTTA-UC. The resulting singlet-excited state can be reduced with a suitable electron donor to yield the radical anion form of DPA or a related other co-catalyst.¹⁸ Since the isoacridone PS have a higher triplet energy (1.9 eV) than DPA (1.77 eV)⁸ and anthracene (1.80 eV)⁸, mechanism (b) seems viable in our catalytic systems as well.

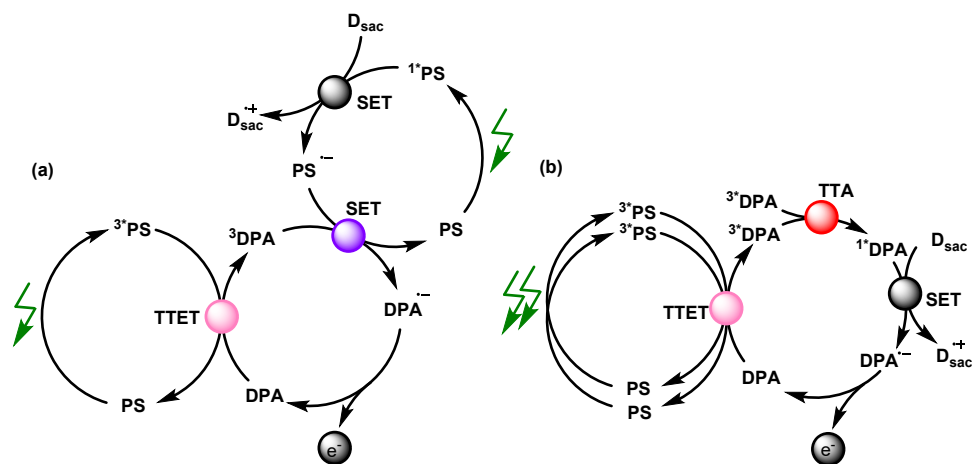
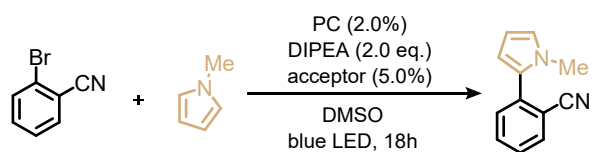


Figure S9: Bi-photonic mechanisms for sensitization-initiated electron transfer (Seni-ET) for different catalytic systems. (a) Mechanism as postulated in refs. ^{14, 16}. (b) Mechanism involving sensitized triplet-triplet energy transfer annihilation upconversion (sTTA-UC) as established in refs. ^{17, 18}. TTET = triplet-triplet energy transfer; SET = single-electron transfer; TTA = triplet-triplet annihilation, D_{sac} = sacrificial electron donor, PS = photosensitizer.

General procedure C for Table S7:

2-Bromobenzonitrile (18.2 mg, 100 μmol , 1.00 eq.), photocatalyst, acceptor were transferred to a 4-mL vial the mixture was degassed via vacuum/argon cycles (3 times). The degassed DMSO (0.50 mL) was added to the vial. Then DIPEA and 1-methyl-1*H*-pyrrole (81.1 mg, 1.00 mmol, 10.0 eq.) were added and the solution was bubbled with argon for 1 minute. The reaction mixture was irradiated with a blue LED (SynLED photoreactor) for 18 hours. The resulting mixture was diluted with water (15 mL) and extracted with EtOAc (3 \times 15 mL). The combined organic layer was washed with brine (3 \times 15 mL), dried over Na_2SO_4 , and the solvent was removed under reduced pressure. NMR standard (1,2,4,5-tetramethylbenzene) was added to the residue and the reaction outcome was analyzed by ^1H NMR spectroscopy. For entries 13 and 17: The residue was purified by preparative TLC (*n*-hexane / EtOAc = 8/1, R_f = 0.50) to yield the desired product as a beige solid (entry 13 – 5.68 mg, 31.2 μmol , 31%; entry 17 – 6.09 mg, 33.4 μmol , 33%). NMR corresponds to the reported data:¹⁵ ^1H NMR (400 MHz, CDCl_3) δ = 7.80 – 7.68 (1H, m), 7.61 (1H, td, 3J 7.7, 4J 1.4 Hz), 7.49 – 7.32 (2H, m), 6.83 – 6.74 (1H, m), 6.41 (1H, dd, 3J 3.7, 4J 1.7 Hz), 6.25 (1H, dd, 3J 3.7, 4J 2.8 Hz), 3.61 (3H, s).

Table S7: Optimization table for sensitization-initiated electron transfer catalysis.



entry	PS	PS / mol%	DIPEA/ eq.	acceptor	Acceptor / mol%	Conv.	Yield (NMR) / (isolated)
Impact of DIPEA							
1	(I)	2	2	anthracene	5	35%	22%
2	(I)	2	4	anthracene	5	42%	28%
3	(I)	2	10	anthracene	5	17%	12%
4	(I)	2	30	anthracene	5	26%	15%
Impact of PC							
1	(I)	2	2	anthracene	5	35%	22%
5	(III)	2	2	anthracene	5	32%	20%
6	(I)	1	2	anthracene	5	38%	33%
7	(I)	4	2	anthracene	5	43%	33%
8	(I)	6	2	anthracene	5	41%	40%
9	(I)	13	2	anthracene	5	37%	30%
Impact of Acceptor							
1	(I)	2	2	anthracene	5	35%	22%
10	(I)	2	2	9-phenyl anthracene	5	34%	34%
11	(I)	2	2	DPA ^[b]	5	36%	33%
12	[Ru] ^[a]	2	2	DPA ^[b]	5	47%	37% / 31%
13	(I)	2	2	DPA ^[b]	10	43%	35%
14	(I)	2	2	DPA ^[b]	20	29%	29%
15	(I)	2	2	(TMS) ₂ pyr ^[c]	5	20%	15%
Change of 2 Parameters							
11	(I)	2	2	DPA ^[b]	5	36%	33%
17	(I)	4	4	DPA ^[b]	5	47%	34% / 33%
18	(I)	4	4	DPA ^[b]	10	n/a	31%

^[a] [Ru(bpy)₃]Cl₂

^[b] 9,10-diphenylanthracene

^[c] 1,6-bis((trimethylsilyl)ethynyl)pyrene

4.3 Mechanistic investigation of the sensitization-initiated electron transfer

The postulated dual reactivity of the singlet excited state (Figure S10, purple segment) and the triplet excited state (Figure S10, orange segment) was investigated. In a first step, the singlet excited state reactivity of $^1\text{PS}(\text{I})$ with DIPEA as the sacrificial electron donor (D_{sac}) was explored (Figure S10, purple part). In a second step, the triplet excited state reactivity of $^3\text{PS}(\text{I})$ was studied (Figure S10, orange part).

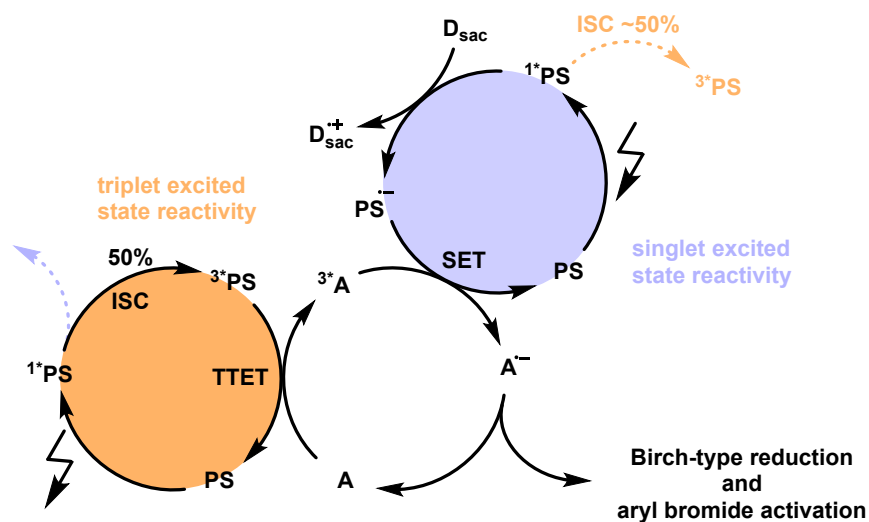


Figure S10: Postulated mechanism for Birch-type arene reduction and aryl bromide activation, identical to Figure 5 in the main manuscript. The orange segment describes the triplet-triplet energy transfer (TTET) reactivity of ^3PS . In contrast, the purple segment describes the single electron transfer (SET, purple part) of ^1PS with DIPEA as a sacrificial electron donor, owing to the more potent oxidizing ability of the singlet excited state with respect to the triplet excited state.

Reactivity from the singlet excited state of PS(I)

The quenching efficiency (η) of the singlet excited state of $^1\text{PS(I)}$ with a redox potential of 1.13 V vs SCE (Table S4) in the presence of 0.5 M DIPEA (nominal concentration under reaction conditions) with an oxidation potential of 0.9 V vs. SCE⁸ was estimated by the singlet excited state emission quenching of $^1\text{PS(I)}$ in the absence (τ_0) and presence ($\tau_{0.5M}$) of 0.5 M DIPEA (Figure S11).

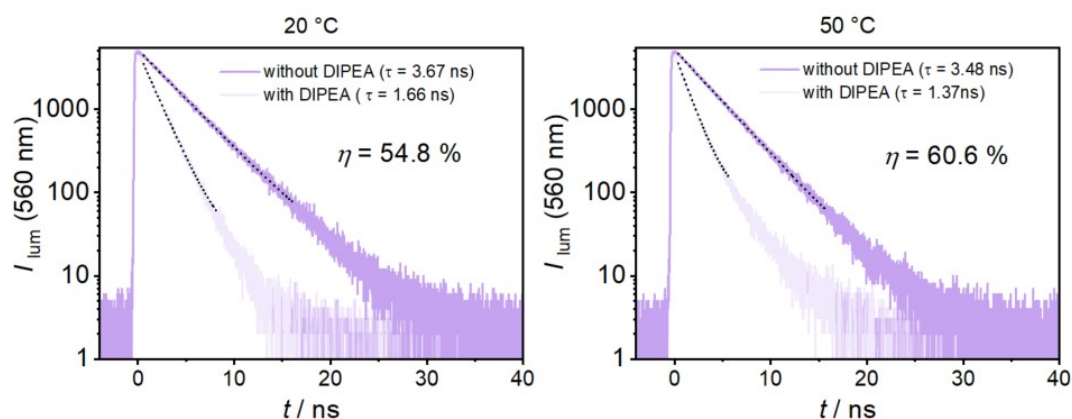


Figure S11: Emission decay rates of PS(I) at 560 nm were measured after 472 nm pulsed excitation of a aerated DMSO solution containing PS(I) ($c = 1 \times 10^{-5}$ M) in the absence (dark purple lines) and presence of DIPEA (nominal concentration of 0.5 M, light purple lines) at 20 °C and 50 °C using TCSPC technique.

The quenching efficiency was calculated using equation S8,

$$\eta = \frac{\tau_0 - \tau_{0.5M}}{\tau_0} \quad (\text{Equation S8})$$

with τ_0 the natural singlet excited state lifetime of $^1\text{PS(I)}$ in DMSO ($\tau_0 = 3.67$ ns), and $\tau_{0.5M}$ the singlet excited state lifetime of $^1\text{PS(I)}$ in DMSO in the presence of a nominal concentration of 0.5 M DIPEA ($\tau_{0.5M} = 1.66$ ns). The resulting 54.8% SET efficiency (Table S8) at 20°C is lower than the expected 84% efficiency calculated with equation S9,

$$\eta = \frac{\tau_0 - \tau}{\tau_0} = \frac{k_q \times [Q]}{\tau_0^{-1} + k_q \times [Q]} \quad (\text{Equation S9})$$

where diffusion-controlled reaction rate constants ($k_q = 2.9 \times 10^9 \text{ M}^{-1} \text{ s}^{-1}$)⁸ in DMSO was assumed due to the high driving force for SET of 0.23 eV ($= -e \times (0.9 \text{ V vs SCE} -$

1.13 V Vs SCE, with e the elementary charge).¹³ Further, the natural excited-state lifetime τ_0 of $^1\text{PS}(\text{I})$ in DMSO ($\tau_0 = 3.67$ ns), and the concentration of the DIPEA ($[\text{Q}]$) as the sacrificial electron donor under reaction conditions (nominal concentration of 0.5 M) was used.

The unexpectedly low SET efficiency is attributed to the limited solubility of DIPEA in DMSO, also visible as small droplets, leading to what looks like an emulsion between DIPEA and DMSO. After rearranging equation S9, the maximum solubility of DIPEA ($[\text{DIPEA}]_{\text{max}}$) was calculated using equation S10,

$$[\text{DIPEA}]_{\text{max}} = \frac{\tau_0 - \tau}{k_q \times \tau_0 \times \tau} \quad (\text{Equation S10})$$

where k_q is the diffusion-controlled reaction rate constant in DMSO ($k_q = 2.9 \times 10^9 \text{ M}^{-1} \text{ s}^{-1}$), τ_0 is the natural excited-state lifetime of $\text{PS}(\text{I})$ (3.67 ns in DMSO), and τ is the excited-state lifetime in the presence of DIPEA, resulting in a maximum solubility of DIPEA of 114 mM in DMSO.

As irradiation of photocatalytic reactions often result in elevated temperatures (leading to enhanced solubility), the same excited state emission quenching was investigated at 50 °C (Figure S11). However, only a minor change in reaction efficiency was observed, with 60.6% at 50 °C compared to 54.8% at 20 °C. Due to the minor temperature differences during photocatalysis (<35 °C), and the small effect on the quenching efficiency, temperature effects were neglected.

SET reactions originating from singlet excited states are known for their limited cage escape quantum yields.¹⁹⁻²² Hence, the cage escape quantum yield for one exemplary reaction system was determined by relative actinometry. Specifically, we used tris(4-chlorophenyl)amine (TAA-Cl) as an electron donor due to the clear absorption band at 700 nm of its one-electron oxidized form and the known change in the absorption coefficient ($\Delta\epsilon$) of $27'000 \text{ M}^{-1} \text{ cm}^{-1}$ at that wavelength.²³ Further, the oxidation potential of $\sim 0.99 \text{ V vs SCE}$ ²³ for TAA-Cl is high enough to react selectively with $^1\text{PS}(\text{I})$ ($E_{1/2}$ ($^1\text{PS}/\text{PS}^{\cdot-}$) 1.13 V vs SCE), but too low to react with $^3\text{PS}(\text{I})$ ($E_{1/2}$ ($^1\text{PS}/\text{PS}^{\cdot-}$) 0.77 V vs

SCE). Hence, the cage escape of the SET reaction originating from $^1\text{PS(I)}$ can be solely observed, without the interference of additional SET from $^3\text{PS(I)}$.

A reference solution of $[\text{Ru}(\text{bpy})_3]^{2+}$ in water (where ISC-QY of unity is expected)⁹ was compared with a sample solution containing PS(I) in the presence of 20 mM TAA-Cl in CH_3CN . Both solutions (reference and sample) were adjusted to the same optical density of ~ 0.2 at the excitation wavelength to ensure the same amount of absorbed photons at the excitation wavelength (Figure S12(a)). Time-resolved UV-Vis absorption traces at 455 nm for the reference system and at 700 nm for the sample system were recorded under identical instrument settings (Figure S12 (b)&(c)). The kinetic transient UV-Vis absorption traces (ΔOD) at a delay time of 10 ns were used to calculate the cage escape quantum yield (Figure S12(c)). However, the quenching efficiency of $^1\text{PS(I)}$ with 20 mM of TAA-Cl is not quantitative (due to limited solubility of TAA-Cl and short singlet excited state lifetime of $^1\text{PS(I)}$). Hence the signal intensity of TAA-Cl $^{*+}$ was corrected with the observed quenching efficiency of $^1\text{PS(I)}$ with TAA-Cl (η_q , similar to Equation S8) for the sample system (Figure S12(d), for details see Figure S12). The cage escape quantum yield (CE-QY) was calculated using equation S11,

$$CE - QY = \frac{c_{TAA-Cl^{*+}}(\text{measured})}{c_{TAA-Cl^{*+}}(\text{theoretical})} = \frac{\Delta\varepsilon_{TAA-Cl^{*+}} \times \Delta\text{OD}_{TAA-Cl^{*+}}}{\Delta\varepsilon_{ref} \times \Delta\text{OD}_{ref} \times \eta_q} \times \frac{\eta_{CH_3CN}}{\eta_{water}} \quad (\text{Equation S11})$$

where $c_{TAA-Cl^{*+}}$ is the concentration of the TAA-Cl $^{*+}$, $\Delta\varepsilon$ is the change in molar absorption coefficient of TAA-Cl $^{*+}$ ($27'000 \text{ M}^{-1} \text{ s}^{-1}$ at 700 nm)²³ and $^3[\text{Ru}(\text{bpy})_3]^{2+}$ ($-10'100 \text{ M}^{-1} \text{ s}^{-1}$ at 455 nm),⁶ ΔOD is the transient UV-Vis absorption change at 700 nm for TAA-Cl $^{*+}$ and at 455 nm for $^3[\text{Ru}(\text{bpy})_3]^{2+}$, η_q is the quenching efficiency of $^1\text{PS(I)}$ with 20 mM of TAA-Cl and η is the refractive index of the used solvents ($\eta_{CH_3CN} = 1.34^8$ and $\eta_{water} = 1.33^8$).

The resulting cage escape quantum yield of 0.75 indicates that 75 % of the SET transfer from DIPEA to $^1\text{PS(I)}$ process leads to a productive pathway, forming the reduced PS(I) $^-$. As a result, the SET with $^1\text{PS(I)}$ and DIPEA has a maximum overall efficiency of 0.41 ($= \eta \times \text{CE-QY} = 0.54 \times 0.75$).

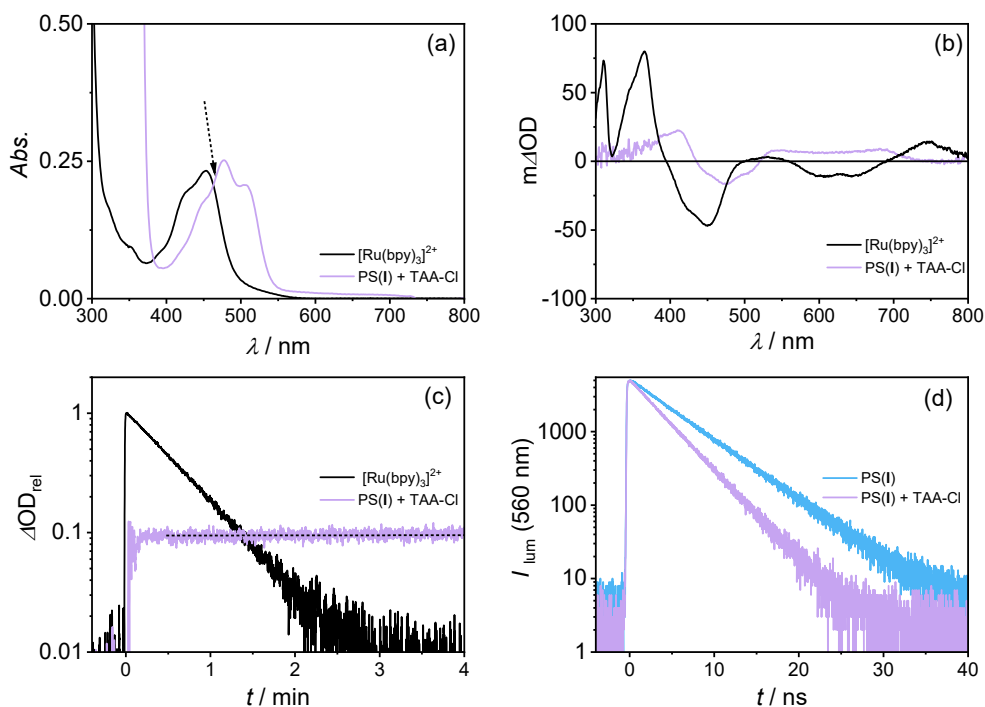


Figure S12: Cage escape quantum yield measurements of PS(I) with tris(4-chlorophenyl)amine (TAA-Cl) using $[\text{Ru}(\text{bpy})_3]^{2+}$ as a reference system. (a) UV-Vis absorption spectra of the sample solution in deaerated CH_3CN containing PS(I) ($c = 1 \times 10^{-5}$ M) and 20 mM TAA-Cl (purple line) and the reference solution in deaerated water containing 20 μM $[\text{Ru}(\text{bpy})_3]^{2+}$ (black line). The arrow indicates the same optical density of both reference and sample solution (where the same amount of photons is absorbed). (b) Transient UV-Vis absorption spectra of the reference (purple line) and sample solution (black line) after 457 nm pulsed excitation (12 mJ per pulse) after a time delay of 20 ns and 200 ns integration time. (c) Relative (normalized) kinetic traces of the transient absorption signal after 457 nm pulsed excitation (12 mJ per pulse) at 455 nm for the reference system (black line) and 700 nm for the sample system. (d) Luminescence lifetime detected at 560 nm upon 472 nm pulsed excitation of 1×10^{-5} M PS(I) in CH_3CN in the presence (purple line) and absence (blue line) of 20 mM TAA-Cl were measured using TCSPC techniques. The quenching efficiency was calculated using $\eta = (\tau_0 - \tau) / \tau_0$ with the natural singlet excited state lifetime ($\tau_0 = 5.23$ ns) and the singlet excited state lifetime in the presence of 10 mM TAA-Cl ($\tau = 3.51$ ns).

Reactivity from the triplet excited state of PS(I)

The triplet excited state of PS(I) with its reduction potential of 0.77 V vs SCE and energy of 1.9 eV can undergo triplet-triplet energy transfer with the energy acceptor. In principle, $^3\text{PS(I)}$ can also undergo SET with DIPEA (effective concentration of 114 mM, see preceding subsection) with its oxidation potential of ~ 0.9 V vs SCE.⁸ Hence, the TTET and SET reaction efficiencies were estimated by taking all relevant decay pathways from the $^3\text{PS(I)}$ into account (SET, TTET, and natural excited state decay). Due to the similar triplet excited state energy of 9,10-diphenylanthracene (1.77 eV; used in one of the photocatalysis experiments) and $(\text{TMS})_2\text{pyr}$ (~ 1.7 eV; used in the upconversion experiment), similar rate constants for TTET to these two compounds were assumed, resulting in an estimated TTET reaction rate constant (k_{TTET}) of $1 \times 10^9 \text{ M}^{-1} \text{ s}^{-1}$ (see Figure S16 for details). With the TTET rate constant and the catalytically relevant concentration of the energy acceptor ($c = 10 \text{ mM}$) the TTET reaction rate (r_{TTET}) of $1.0 \times 10^7 \text{ s}^{-1}$ ($= k_{\text{TTET}} \times c = 1 \times 10^9 \text{ M}^{-1} \text{ s}^{-1} \times 0.01 \text{ M}$) was estimated.

The reaction rate constant for SET of $^3\text{PS(I)}$ with DIPEA was measured using transient UV-Vis absorption spectroscopy, by tracking the decay of the ESA band at 410 nm (see Figure 2) in the presence and absence of DIPEA (Figure S13). Only very minor quenching was observed. In addition to the decreased $^3\text{PS(I)}$ lifetime, a signal intensity decrease was observed when increasing amounts of DIPEA were present. Such an observation often indicates static quenching. In this specific case here, the observed different signal intensities are however most likely due to the faster SET reactivity from the photosensitizer's singlet excited state.

The rate constant for SET from the triplet excited state was extracted from the data in Figure S13 using Stern-Volmer analysis, resulting in an estimated single electron transfer rate constant for $^3\text{PS(I)}$ with DIPEA of $3.4 \times 10^7 \text{ M}^{-1} \text{ s}^{-1}$. With the SET rate constant ($k_{\text{SET}} = 3.4 \times 10^7 \text{ M}^{-1} \text{ s}^{-1}$) and the catalytically relevant concentration of DIPEA ($c = 114 \text{ mM}$), the SET reaction rate (r_{SET}) of $3.9 \times 10^6 \text{ s}^{-1}$ ($= k_{\text{SET}} \times c = 3.4 \times 10^7 \text{ M}^{-1} \text{ s}^{-1} \times 0.114 \text{ M}$) was estimated.

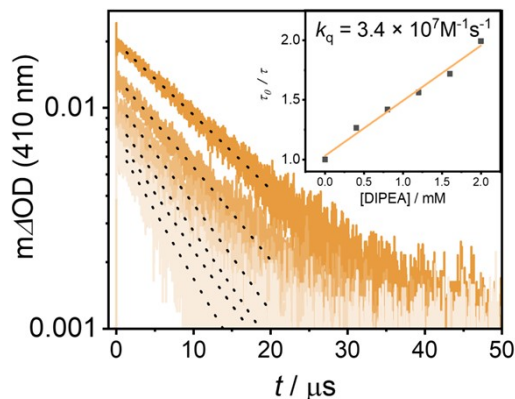


Figure S13: Transient UV-Vis absorption decays at 410 nm after 532 nm pulsed excitation (30 mJ per pulse) of a deaerated THF solution containing PS(I) ($c = 1 \times 10^{-5}$ M) in the absence (dark orange trace) and presence (other traces) of different DIPEA concentrations. Inset shows the Stern Volmer plot, resulting in a reaction rate constant of $3.4 \times 10^7 \text{ M}^{-1} \text{ s}^{-1}$.

With all reaction rates (r) in hand the overall quenching efficiency of TTET (ϕ_{TTET}) and SET (η_{SET}) was calculated using equations S12 and S13,

$$\eta_{\text{TTET}} = \frac{r_{\text{TTET}}}{r_{\text{TTET}} \times r_{\text{SET}} \times r_{\tau}} \quad (\text{Equation S12})$$

$$\eta_{\text{SET}} = \frac{r_{\text{SET}}}{r_{\text{TTET}} \times r_{\text{SET}} \times r_{\tau}} \quad (\text{Equation S13})$$

where r_{TTET} is the TTET reaction rate, r_{SET} it the SET reaction rate, and r_{τ} is the excited state decay rate constant ($= 1/\tau_{\text{T1}} = 2.3 \times 10^4 \text{ s}^{-1}$, where τ_{T1} is the natural triplet excited state lifetime of 43.7 μs).

The resulting overall SET reaction efficiency of 0.28 is significantly smaller compared to the TTET reaction efficiency of 0.72 (Table S8)

In contrast to the singlet excited state reactivity, the cage escape of the triplet reactivity was expected to be close to unity.

Table S8: Summary of excited state lifetimes (τ_0), reaction rate constants k_q , relevant concentrations for catalysis, and reaction efficiencies (η) of the singlet ($^1\text{PS(I)}$) and triplet ($^3\text{PS(I)}$) excited states.

	τ_0 / ns	k_{SET} / $10^7 \text{ M}^{-1} \text{ s}^{-1}$	[DIPEA] / mM	η_{SET} / %	k_{TTET} / $10^7 \text{ M}^{-1} \text{ s}^{-1}$	[Acc] / mM	η_{TTET} / %
$^1\text{PS(I)}$	3.7 [a]	290 [c]	114 [e]	54.8 [f]	n/d	n/d	n/d
$^3\text{PS(I)}$	43'700 [b]	3.4 [d]	114 [e]	28 [f]	100 [g]	10 [h]	72 [i]

[a] Singlet excited state lifetime (τ_0) of PS(I) ($1 \times 10^{-5} \text{ M}$) in DMSO using TCSPC techniques.

[b] Triplet excited state lifetime (τ_0) of PS(I) ($1 \times 10^{-5} \text{ M}$) in THF using transient UV-Vis absorption spectroscopy.

[c] Expected to be the diffusion-limited reaction rate constant in DMSO.⁸

[d] Single electron transfer rate constant (k_{SET}) of PS(I) with DIPEA determined in THF with transient UV-Vis absorption spectroscopy, monitoring the GSA signal at 410 nm.

[e] Calculated solubility of DIPEA in DMSO (for details, see text).

[f] Single electron transfer efficiency for $^1\text{PS(I)}$ and $^3\text{PS(I)}$.

[g] Triplet-triplet energy transfer rate constant (k_{TTET}) of PS(I) with a triplet acceptor molecule determined in THF with transient UV-Vis absorption spectroscopy, monitoring the GSA signal at 410 nm. For details, see Figure S16.

[h] Used concentration of the energy acceptor molecule in the SenI-ET catalysis.

[i] Energy transfer efficiency was calculated using equation S12 for $^3\text{PS(I)}$.

With the different quenching efficiencies in hand, the overall TTET efficiency for the formation of the triplet excited state of DPA was estimated. The analysis of the singlet excited state reactivity showed that $^1\text{PS(I)}$ reacts only with an efficiency of 0.41 ($= \eta \times \text{CE-QY} = 0.54 \times 0.75$) to electron transfer products, with a singlet excited state quenching efficiency of 54%. Consequently, 46% of the initial singlet excited state population can undergo ISC with a ISC-QY between 0.52 and 0.26, resulting in a formation efficiency of the triplet excited state ^3PS between 0.24 and 0.12.

With the TTET efficiency of 72%, the overall reaction efficiency for the formation of the triplet excited state of the anthracene derivatives was calculated to be between 0.17 ($= 0.24 \times 0.72$) and 0.09 ($= 0.12 \times 0.72$).

5 Sensitized triplet-triplet annihilation upconversion

5.1 Photophysical properties of the annihilator (TMS)₂pyr

To lower the triplet energy of pyrene (2.1 eV)⁸ and to increase the triplet-triplet-energy transfer rate from the isoacridone PS to the annihilator, pyrene was functionalized on positions 1 and 7 with two trimethylsilyl (TMS) protected acetylenes (Figure 6b, (TMS)₂pyr). To investigate the effect of this pyrene modification, UV-Vis absorption and emission spectra were recorded (Figure S14) and were compared to unsubstituted pyrene (Table S9).

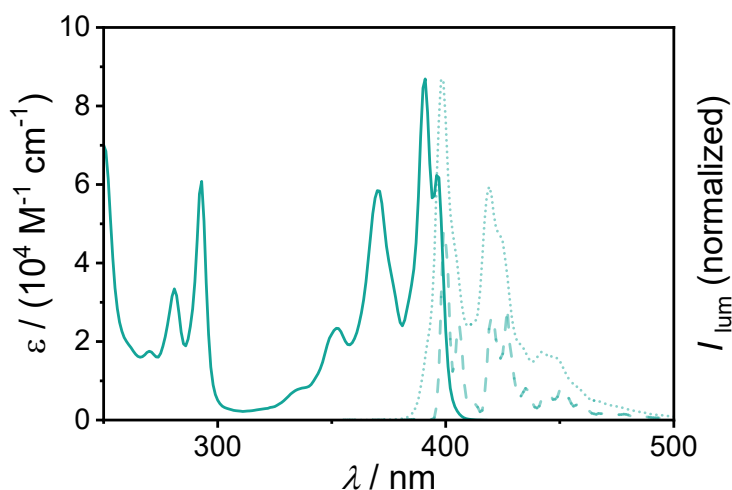


Figure S14: Calibrated absorption (solid lines) and normalized luminescence spectra (dotted lines) in THF containing 1×10^{-5} M (TMS)₂pyr at 20 °C. The low-temperature spectrum (dashed lines) was obtained in frozen 2-methyl-tetrahydrofuran at 77 K. Both emission spectra were recorded upon 370 nm excitation.

(TMS)₂pyr shows a red-shifted absorption band maximum at 390 nm compared to pyrene (335 nm),¹ corresponding to a energy shift of ~0.5 eV. A smaller energy shift of 0.25 eV is determined from the respective emission band maxima, which are at 400 nm for (TMS)₂pyr and at 370 nm for pyrene.¹ By analysing the intersection between absorption and room-temperature emission of (TMS)₂pyr, a singlet-excited state energy (E_{S_1}) of 3.12 eV was estimated. This is 0.48 eV lower compared to unsubstituted pyrene, for which a singlet-excited state energy of 3.6 eV has been reported (Table S7). These differences are in line with those previously reported for

polyaromatic hydrocarbons with TMS or TIPS protected acetylenes.²⁴⁻²⁶ To examine the triplet-excited state of (TMS)₂pyr, an attempt to detect phosphorescence at 77 K in 2-methyltetrahydrofuran was made. The resulting emission spectrum (dashed trace in Figure S14) is largely identical to the fluorescence emission at room temperature (dotted trace in Figure S14). There is no evidence for phosphorescence, and consequently, the T₁ energy cannot be determined in this manner. It seems plausible to assume that the T₁ energy is similarly affected by the acetylene-substitution of pyrene as the S₁ energy, which would imply a triplet energy of ~1.7 eV for (TMS)₂pyr based on an S₁ energy of 2.1 eV for pyrene. Given a triplet energy of 1.9 eV for the isoacridone PS investigated here, this can be expected to result reaction free energy of ca. -0.2 eV for triplet-triplet energy transfer from our photosensitizers to (TMS)₂pyr, which in turn is anticipated to permit for very rapid (and potentially nearly diffusion-controlled) TTET kinetics.

Table S9. Summary of selected photophysical properties of the (TMS)₂pyr annihilator compared to pyrene.

Acceptor	E_{S_1} / eV	τ_{S_1} / ns	Φ_{FL}	E_{T_1} / eV
pyrene ⁸	3.6	190	0.72	2.1
(TMS) ₂ pyr	3.12 ^[a]	2.4 ^[b]	0.90 ^[c]	(1.7) ^[d]

^[a] Estimated from the intersection between absorption and emission spectra, similar to a previous study.²⁷

^[b] Measured using the TCSPC technique in DMF (data are not shown).

^[c] Fluorescence quantum yields (Φ_{FL}) were obtained using an integration sphere.

^[d] No phosphorescence at 77K could be observed; value estimated as described above.

5.2 Triplet-triplet energy transfer

As the triplet-excited state of the isoacridone PS is non-emissive, transient UV-Vis spectroscopy was employed to determine the rate constants for TTET to the (TMS)₂pyr annihilator. Sensitized transient UV-Vis absorption spectra of the triplet-excited state of (TMS)₂pyr (³[(TMS)₂pyr]) were recorded using PS(III) as a photosensitizer. The transient UV-Vis spectrum of ³[(TMS)₂pyr] (Figure S15, red trace) shows broad excited-state absorption (ESA) bands with local maxima at 550 nm and 450 nm. Comparison with the transient UV-Vis spectrum of triplet-excited PS(III) (Figure S15, gray trace) reveals that no isolated transient UV-Vis absorption bands of PS(III) exist, at which the triplet-excited state quenching of PS(III) by (TMS)₂pyr can be monitored cleanly without spectral contributions from ³[(TMS)₂pyr]. Fortunately, the transient absorption difference spectrum of the triplet-excited isoacridone PS shows no spectral change at ~480 nm, whereas ³[(TMS)₂pyr] absorbs prominently at this wavelength (Figure S15, vertical black dashed line). Consequently, at this specific wavelength, the formation of ³[(TMS)₂pyr] can be observed cleanly without significant spectral contribution from the photosensitizer. Because the formation rate of ³[(TMS)₂pyr] and the decay rate of the triplet-excited isoacridone PS are expected to be identical for a single-step triplet-triplet energy transfer process, a Stern-Volmer analysis can be performed by tracing the formation rate of ³[(TMS)₂pyr] as a function of annihilator concentration (Figure S16).

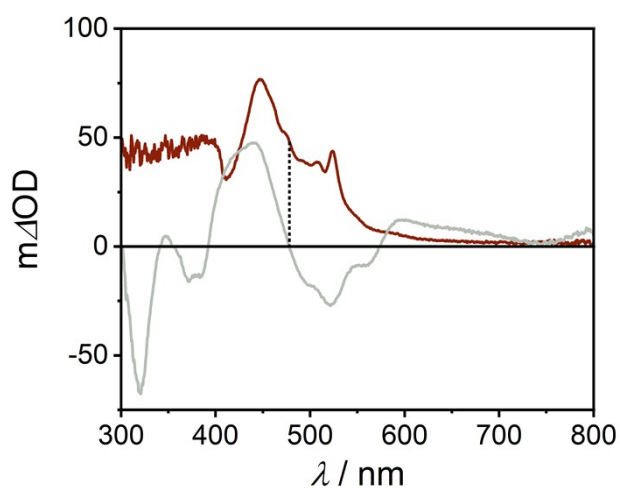


Figure S15. Transient UV-Vis absorption spectra of deaerated THF solutions containing 50 μM PS(III) (grey trace) and 50 μM PS(III) with 2 mM $(\text{TMS})_2\text{pyr}$ (red trace). The transient UV-Vis absorption spectra were recorded after 532 nm pulsed excitation (35 mJ per pulse) and a delay time of 500 ns. The vertical black dotted line marks the point, at which the formation of the triplet-excited $(\text{TMS})_2\text{pyr}$ from triplet-excited PS can be detected cleanly without significant spectral contributions of PS(III).

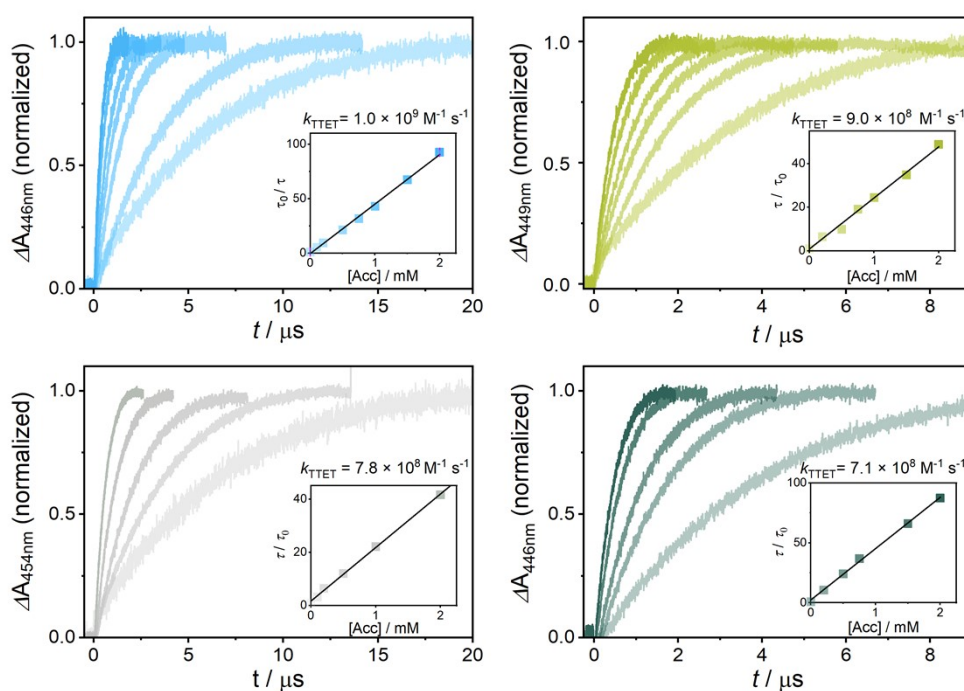


Figure S16. Transient absorption kinetics monitoring the formation of the triplet-excited annihilator $(\text{TMS})_2\text{pyr}$ via energy transfer from triplet-excited PS(I) (a), PS(II) (b), PS(III) (c), and PS(IV) (d) (main plots). The kinetic traces were recorded at wavelengths, at which the spectral contributions of the individual triplet-excited sensitizers were minimal, as discussed above on the specific example of PS(III). All kinetic traces were recorded in a deaerated THF solution at 20 °C containing $2 \times 10^{-5} \text{ M}$ PS and between 0 and 2 mM $(\text{TMS})_2\text{pyr}$. The insets contain the resulting Stern-Volmer plots, based on the unquenched (natural) T_1 excited state lifetimes of isoacridone PS.

5.3 Triplet-triplet annihilation (TTA)

The triplet-excited state of the annihilator (TMS)₂pyr decays in parallel via two different pathways, namely the non-radiative decay back to the ground state (k_T , following first-order reaction kinetics) and triplet-triplet annihilation (TTA, k_{TTA}), following second-order reaction kinetics. To determine the rate constants of both processes, the concentration of $^3[(\text{TMS})_2\text{pyr}]$ was varied by using different excitation powers in a pulsed experiment, and the resulting transient absorption decays (ΔOD) at 450 nm, diagnostic for $^3[(\text{TMS})_2\text{pyr}]$, were fitted using equation S14.²⁸

With the obtained β -value and the concentration of $^3[(\text{TMS})_2\text{pyr}]$, calculated from the change in optical density (ΔOD) and the molar extinction coefficient of $^3[(\text{TMS})_2\text{pyr}]$ at 450 nm ($22'500 \text{ M}^{-1} \text{ cm}^{-1}$, determined similarly as described in section 3.1), the triplet-triplet annihilation rate constant (k_{TTA}) was calculated with equation S15.

$$\Delta OD = \frac{\Delta OD_0 \times (1 - \beta)}{e^{(k_T \times t)} - \beta} \quad (\text{Equation S14})$$

$$\beta = \frac{k_{TTA} \times [^3Ann]_0}{k_{TTA} \times [^3Ann]_0 + k_T} \quad (\text{Equation S15})$$

The triplet-excited state decay of the annihilator, sensitized by PS(I), was analyzed by using different laser pulse energies to vary the initial $^3[(\text{TMS})_2\text{pyr}]$ concentrations (Figure S17). The kinetic parameters obtained from all decay traces were averaged, resulting in a triplet-triplet annihilation rate constant of $(3.6 \pm 0.2) \times 10^9 \text{ M}^{-1} \text{ s}^{-1}$.

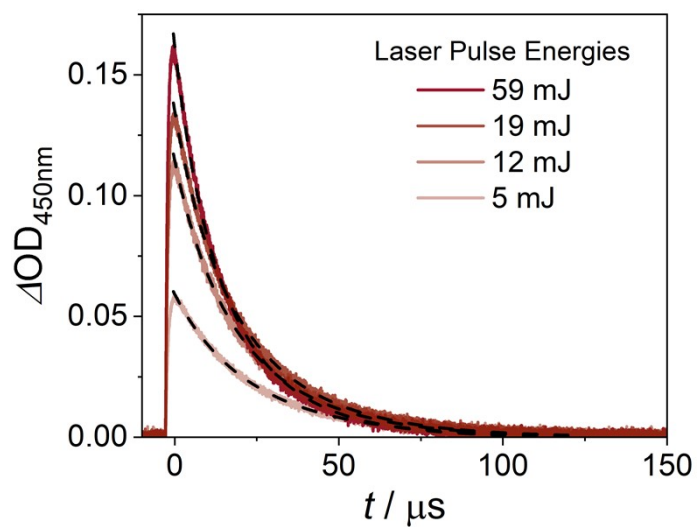


Figure S17. Triplet-excited state decays of $(\text{TMS})_2\text{pyr}$ in argon-saturated THF containing 2×10^{-5} M PS(I) and 2 mM annihilator $(\text{TMS})_2\text{pyr}$ after excitation at 532 nm with pulse energies between 5 and 59 mJ. The experimental transient absorption decay traces at 450 nm (solid colored traces) were fitted with equation S14 (dashed black traces).

5.4 Quadratic excitation power dependency of the upconversion luminescence

To demonstrate the quadratic dependency of the biphotonic sTTA-UC mechanism, a 532 nm cw laser was employed as a light source. Inner filter effects were reduced by aligning the 532 nm cw laser beam such that the edge of the sample cuvette facing the detector was irradiated, in order to minimize the path length of the generated upconversion light towards the detector. This procedure seemed helpful to minimize re-absorption of the upconverted light by the sensitizer/annihilator combination.

The upconversion emission was measured in THF at 20 °C using 20 µM isoacridone PS and 400 µM (TMS)₂pyr annihilator. The excitation power dependencies of the integrated upconverted luminescence (Figure S18, brown traces) were fitted with the power function $f(x) = c + a \cdot x^b$. The resulting exponents (b) obtained for all four isoacridone PSs are summarized in Table S10. All investigated isoacridone PS give an exponent of ~2, confirming the biphotonic nature of the sTTA-UC process.²⁹

To confirm the linear power output of the cw laser source, the prompt fluorescence intensities emitted by the four different photosensitizers were measured as a function of excitation power density. Since the PS fluorescence remains unquenched in the presence of the (TMS)₂pyr annihilator, the same sample solutions (containing 20 µM isoacridone PS and 400 µM (TMS)₂pyr), were used. The excitation power dependency of the integrated PS fluorescence intensities (Figure S18, colored traces) were fitted with the same power function ($f(x) = c + a \cdot x^b$), and the parameters determined from these fits are summarized in Table S10. The resulting exponent of ~1 for all four investigated isoacridone PS confirms the linear output power of the cw laser and the monophotonic nature of the prompt PS fluorescence.

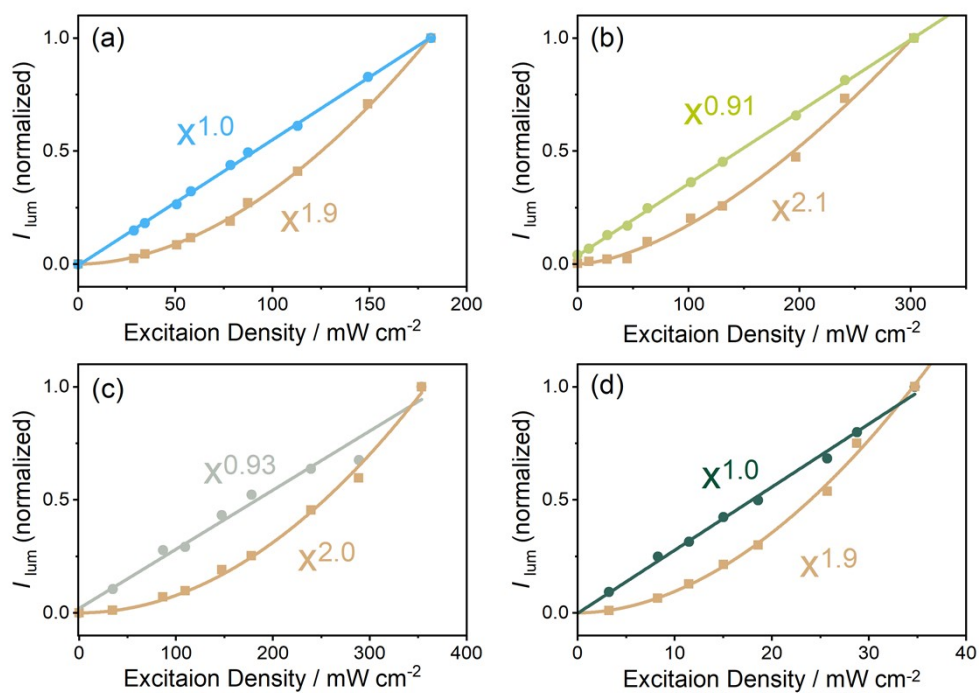


Figure S18. Excitation power dependencies of the upconversion emission (brown traces) and the prompt sensitizer fluorescence (traces in other colors) detected from deaerated THF solutions containing 20 μM PS(I) (a), PS(II) (b), PS(III) (c), or PS(IV) (d) with 400 μM $(\text{TMS})_2\text{pyr}$.

5.5 sTTA-UC quantum yields

The prompt fluorescence of the isoacridone photosensitizers is not quenched by the (TMS)₂pyr annihilator. Consequently, the delayed upconversion emission from the annihilator S₁ state and the prompt S₁ fluorescence emitted by the sensitizer can be observed simultaneously. Because the PS fluorescence quantum yields (Φ_{FL}) are known (see Table 1, main manuscript), the UC quantum yield (Φ_{UC}) is directly accessible by comparing the integrated upconversion emission intensity (I_{UC}) with the integrated prompt fluorescence intensity of the isoacridone photosensitizers (I_{FL}) using equation S16.

$$\Phi_{UC} = \Phi_{FL} \times \frac{I_{UC}}{I_{FL}} \quad (\text{Equation S16})$$

Deaerated THF solutions of the isoacridone photosensitizers (20 μM) containing 400 μM (TMS)₂pyr annihilator were irradiated with a 532 nm cw laser at 20 °C, and the upconversion emission intensity, as well as the prompt fluorescence intensity were measured as a function of excitation power density. The resulting excitation power dependent upconversion luminescence quantum yields are shown in Figure 6 of the main paper. Due to the fast decomposition of the upconversion system containing isoacridone PS(II) at high power densities, the upconversion quantum yield could not be determined for this specific sensitizer / annihilator couple. For the three other upconversion systems comprising the isoacridone PS(I), PS(III), and PS(IV), the upconversion quantum yields were estimated at an excitation power density of 1500 mW cm^{-1} , because higher excitation power densities led to photo-decomposition. The values (Table S10) are reported using the definition of the upconversion quantum yield, according to which a quantum yield of 50 % represents the maximum achievable value, due to the biphotonic nature of the upconversion process. The experimentally determined upconversion quantum yields increase from 0.19% for PS(I) to 0.22% for PS(III) and to 0.38% for PS(IV), following the same trend as the intersystem crossing quantum yields.

When comparing PS(I) with an ISC-QY of 0.26 to PS(III) with an ISC-QY of 0.43, a factor of 1.6 (= 0.43 / 0.26) increase of the UC-QY can be expected under the assumption that intersystem crossing is the most important change when replacing PS(I) by PS(III). However, the upconversion quantum yield increases merely by a factor of 1.2. This discrepancy might have its origin in the somewhat lower photostability of PS(III) in comparison to PS(I). When comparing PS(I) with PS(IV), the upconversion quantum yield improves by a factor of 2 from 0.19% to 0.38%, whereas the ISC-QY increases by the same factor from 0.26 to 0.52, matching the expected increase.

However, the absolute values of the upconversion quantum yields determined for the three investigated photosensitizers seem relatively moderate in comparison to recently explored other upconversion systems using different sensitizers.³⁰⁻³⁴ In an attempt to identify the main loss channels in the overall sTTA-UC process, equation S17 was used to calculate the overall UC-QY (Φ_{UC}).³⁵

$$\Phi_{UC} = \frac{1}{2} \times f \times \Phi_{ISC} \times \Phi_{TTET} \times \Phi_{TTA} \times \Phi_{FL} \quad (\text{Equation S17})$$

In equation S17, f is the spin-statistical probability of 1/9,³⁶ Φ_{ISC} the intersystem crossing efficiency, Φ_{TTET} the triplet-triplet energy transfer efficiency, Φ_{TTA} the triplet-triplet annihilation efficiency, and Φ_{FL} the annihilator fluorescence quantum yield. To simplify the analysis, only the upconversion system with PS(I) is considered in the following.

The $\Phi_{ISC} = 0.26$ of PS(I) and $\Phi_{FL} = 0.9$ values of (TMS)₂pyr were determined as described above. The TTET efficiency (Φ_{TTET}) was estimated based on equation S18, where k_{TTET} is the triplet-triplet energy transfer rate constant ($k_{TTET} = 1 \times 10^9 \text{ M}^{-1} \text{ s}^{-1}$, Table S10), τ_0 is the natural triplet-excited state lifetime of PS(I) of 43.7 μs , and $[A]$ is the concentration of the (TMS)₂pyr annihilator (400 μM) used in the UC system.

$$\Phi_{EnT} = \frac{k_{EnT} \times [A]}{\tau_0^{-1} + (k_{EnT} \times [A])} \quad (\text{Equation S18})$$

The resulting TTET efficiency (Φ_{TTET}) of ~0.95 indicates that TTET from triplet-excited PS(I) to the annihilator is essentially quantitative and does not represent a major loss channel.

To estimate the TTA efficiency, equation S19 was used, where k_{TTA} is the triplet-triplet annihilation rate constant ($k_{TTA} = 3.6 \pm 0.2 \times 10^9 \text{ M}^{-1} \text{ s}^{-1}$), τ_0 is the natural triplet-excited state lifetime of the annihilator, and $[A_T]$ is the concentration of the triplet-excited (TMS)₂pyr.

$$\Phi_{TTA} = \frac{k_{TTA} \times [A_T]}{\tau_0^{-1} + (k_{TTA} \times [A_T])} \quad (\text{Equation S19})$$

The laser-induced TTET experiment in Figure S17 was used to estimate the annihilator triplet-excited state concentration. Based on the experimentally determined triplet-excited state absorption maximum (0.17 OD) at the highest laser energy of 59 mJ per pulse and the determined molar extinction coefficient of 22'500 $\text{M}^{-1}\text{cm}^{-1}$ for triplet-excited annihilator at 450 nm, the triplet-excited state concentration of (TMS)₂pyr was calculated ($[A_T] = 7.6 \text{ }\mu\text{M}$). The natural triplet-excited state lifetime (τ_0) was extracted from the fit parameter k_T (equation S14) of the kinetic traces in Figure S17, by taking the inverse of k_T , resulting in $\tau_0 = 25.5 \text{ }\mu\text{s}$. Based on these values, the triplet-triplet annihilation efficiency was calculated with equation S18, resulting in a Φ_{TTA} value of 0.41. It should be kept in mind that pulsed and continuous-wave excitation conditions differ strongly from one another and can potentially produce very different concentrations of triplet-excited annihilators.³⁴ Therefore, the Φ_{TTA} value of 0.41 determined here represents a crude estimate.

With all factors at hand, the theoretical UC-QY was calculated using equation S17, resulting in a value of 0.51 %, which comes reasonably close to the experimental value of 0.21%.

$$\Phi_{UC} = \frac{1}{2} \times f \times \Phi_{ISC} \times \Phi_{TTET} \times \Phi_{TTA} \times \Phi_{FL} \times 100\%$$

$$\Phi_{UC} = \frac{1}{2} \times \frac{1}{9} \times 0.26 \times 0.95 \times 0.41 \times 0.9 \times 100\%$$

$$= 0.51\%$$

In this analysis, the TTA efficiency is one of the main limiting factors of the overall upconversion performance. To improve the upconversion efficiency, a change of the annihilator may be beneficial.

5.6 Summary of the sTTA-UC properties

Table S10: Summary of selected upconversion-relevant properties of the investigated photosensitizers.

PS	$\Phi_{\text{ISC}}^{[\text{a}]}$	$k_{\text{TTET}}^{[\text{b}]}$ / $10^8 \text{ M}^{-1} \text{ s}^{-1}$	$x^b(\text{Em})^{[\text{c}]}$	$x^b(\text{UC})^{[\text{d}]}$	UC-QY ^[e]
(I)	0.26	10	1.0	1.9	0.19
(II)	0.30	9.0	0.91	2.1	n/a
(III)	0.43	7.8	0.93	2.0	0.22
(IV)	0.52	7.1	1.0	1.9	0.38

^[a] Intersystem crossing quantum yields (Φ_{ISC}).

^[b] Triplet-triplet energy transfer rate constant (k_{TTET}) determined with transient absorption spectroscopy, monitoring the growing signal of the triplet-excited state of the annihilator (TMS)₂pyr (Figure S16).

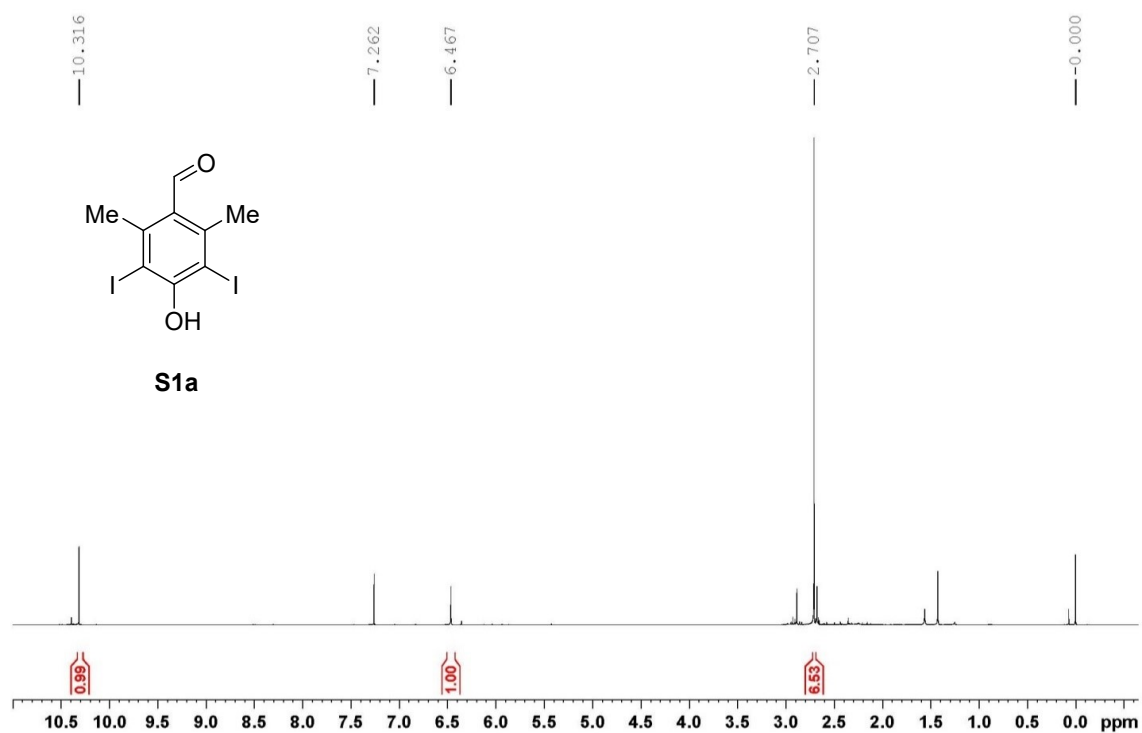
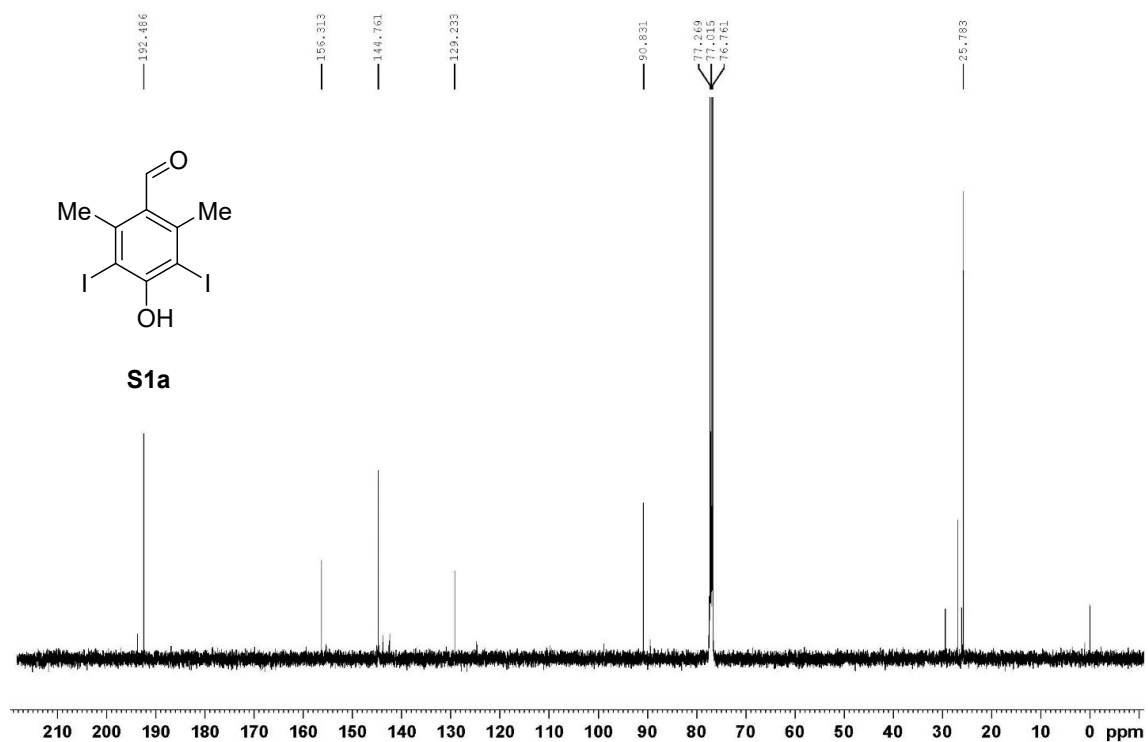
^[c] Excitation power dependence of the prompt photosensitizer fluorescence intensity upon 532 nm cw laser irradiation, fitted to a power function $f(x) = c + a \cdot x^b$.

^[d] Excitation power dependence of the upconversion emission intensity upon 532 nm cw laser irradiation, fitted to a power function $f(x) = c + a \cdot x^b$.

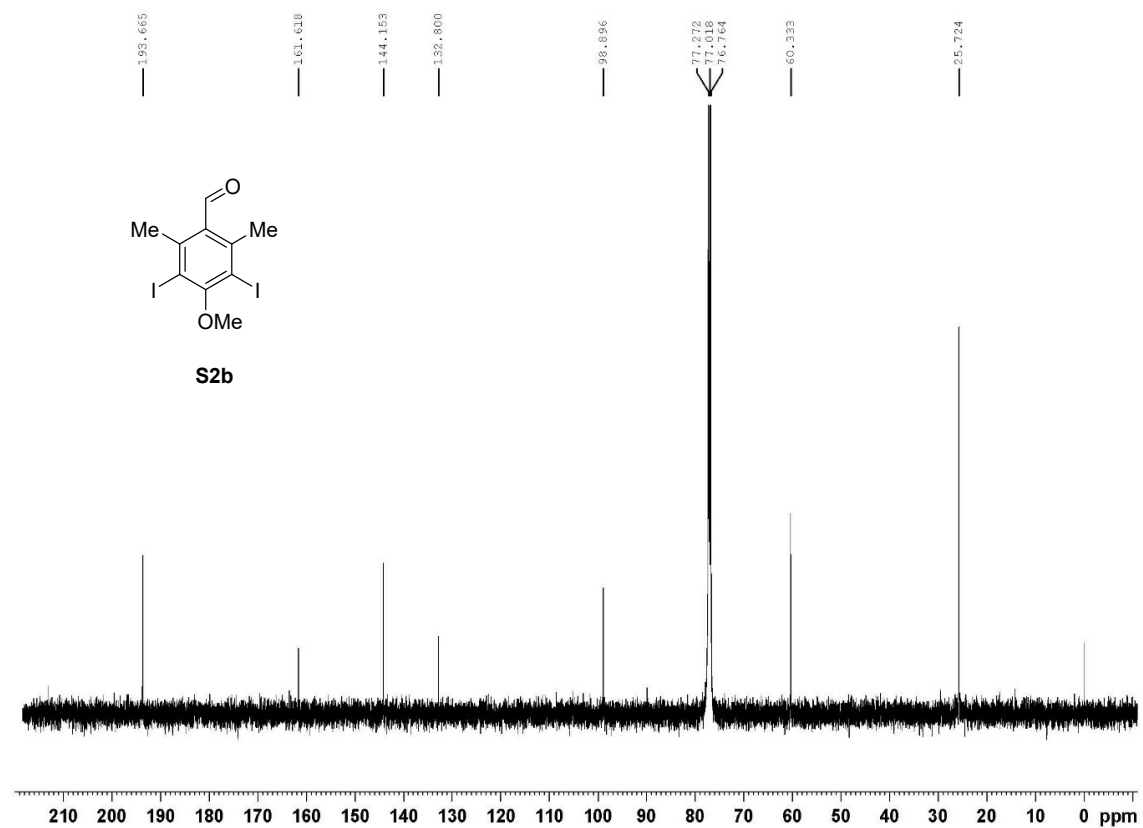
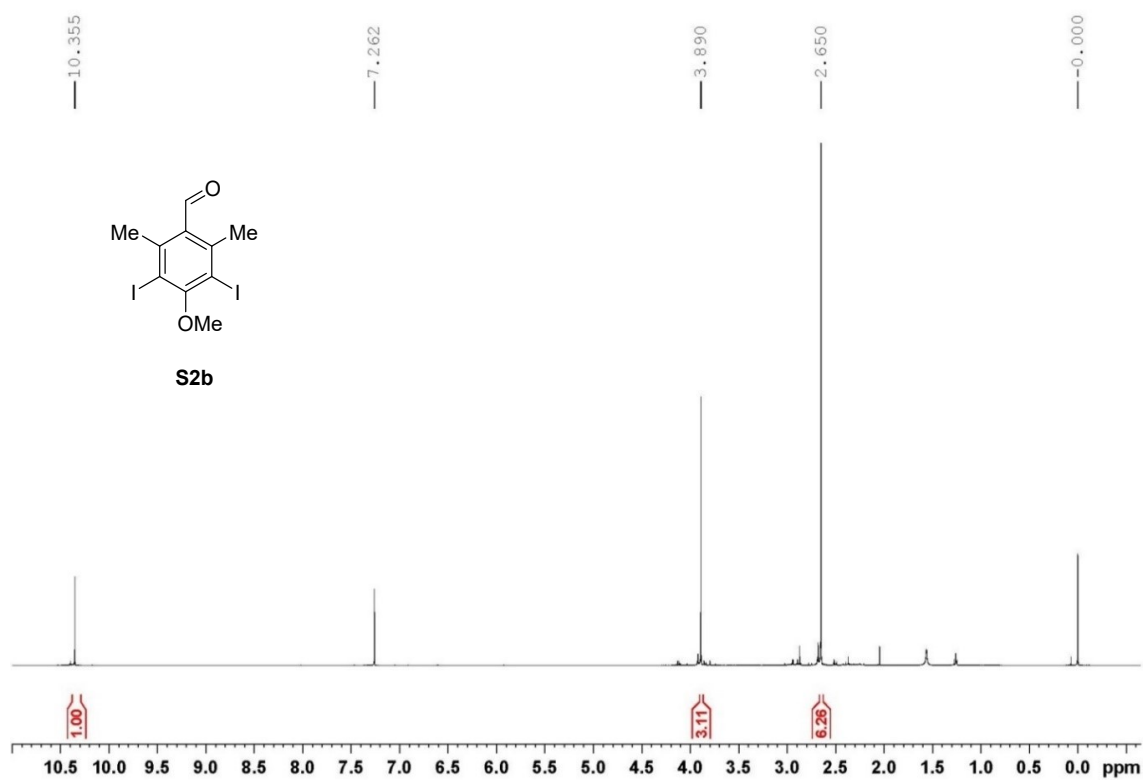
^[e] Upconversion quantum yield (50% maximum) upon 532 nm cw laser excitation at power densities of 1500 mW cm⁻¹. For details, see Figure 6e of the main paper.

6 NMR spectra

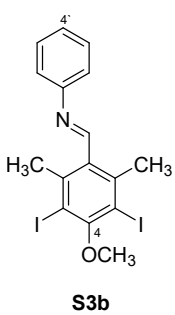
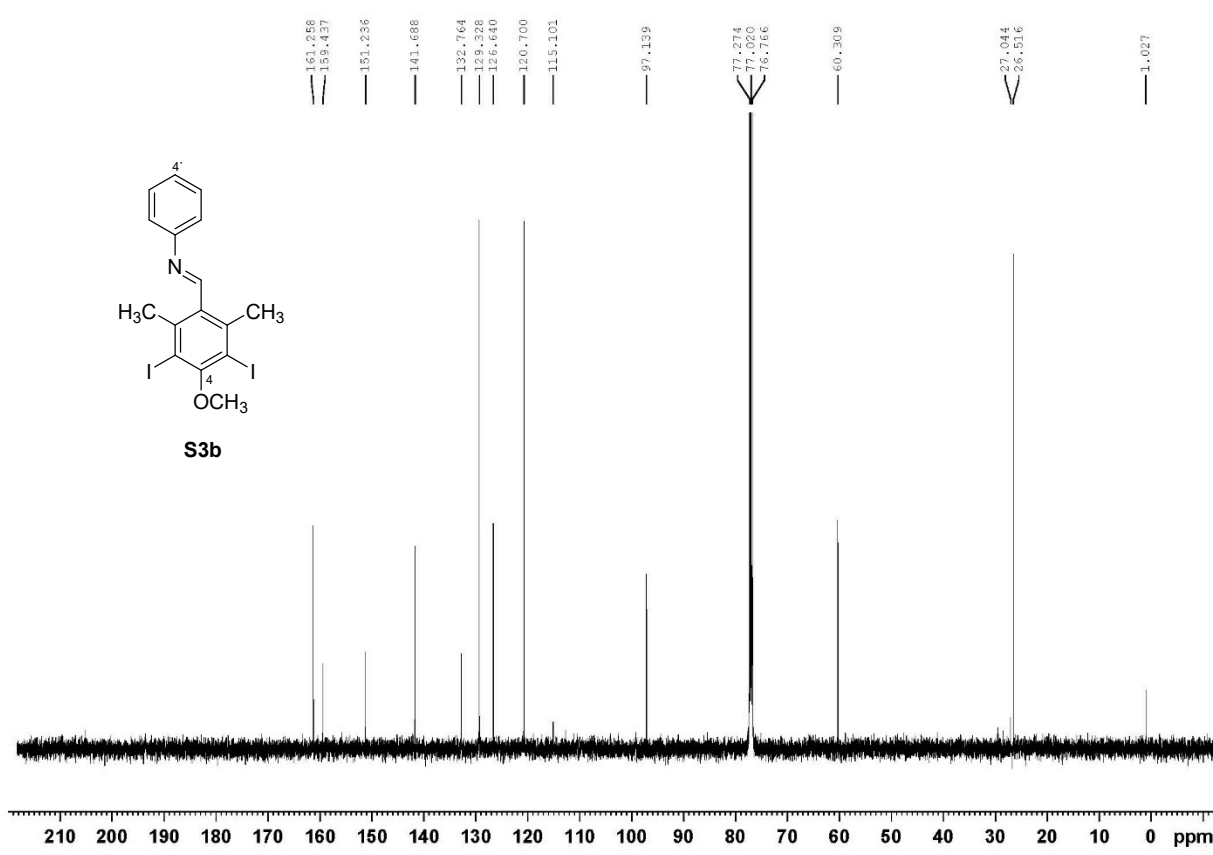
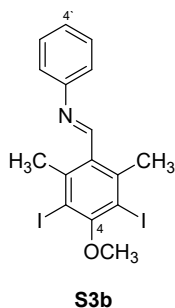
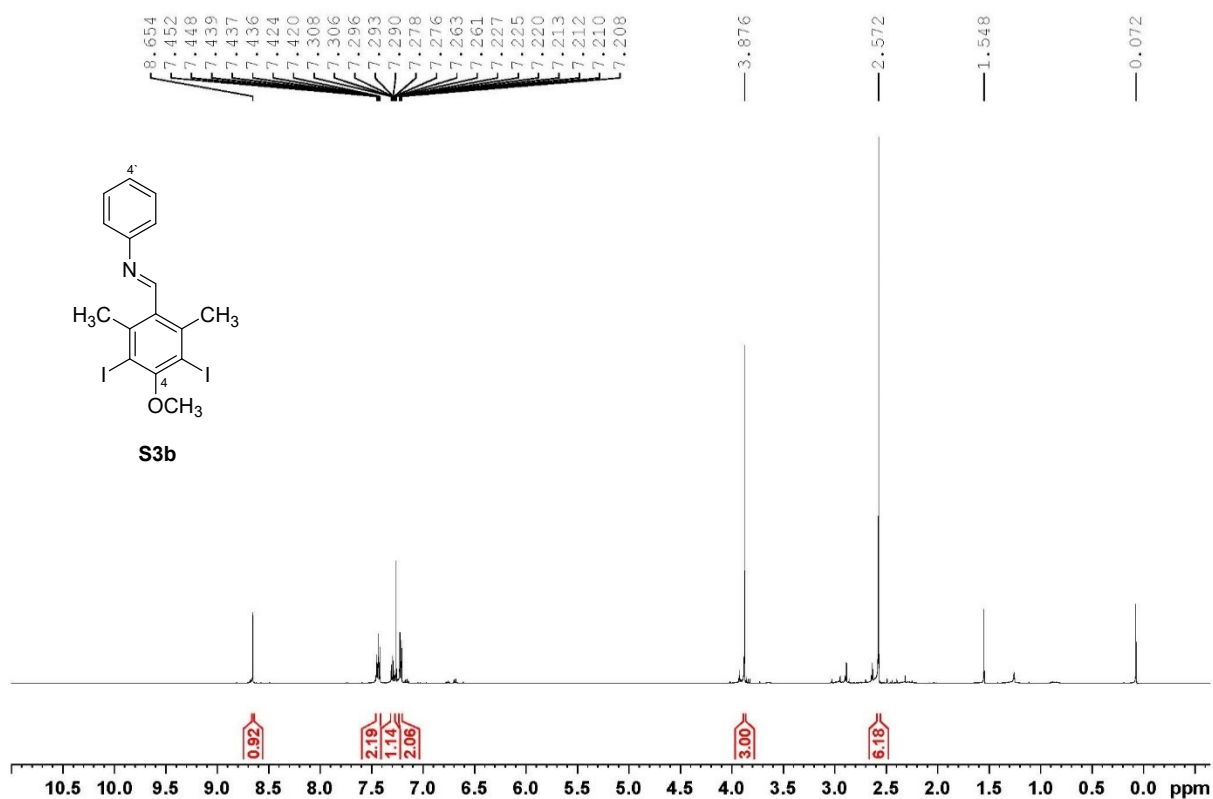
4-Hydroxy-3,5-diiodo-2,6-dimethylbenzaldehyde (S1a):

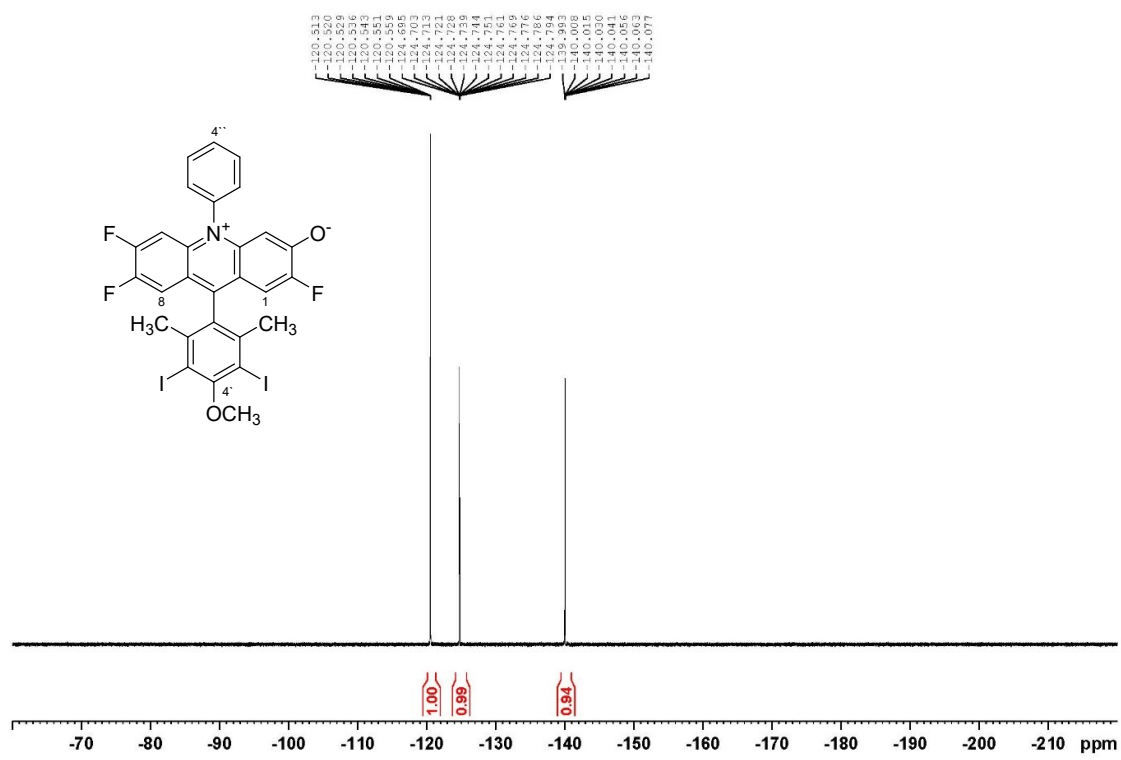


3,5-Diiodo-4-methoxy-2,6-dimethylbenzaldehyde (S2a):

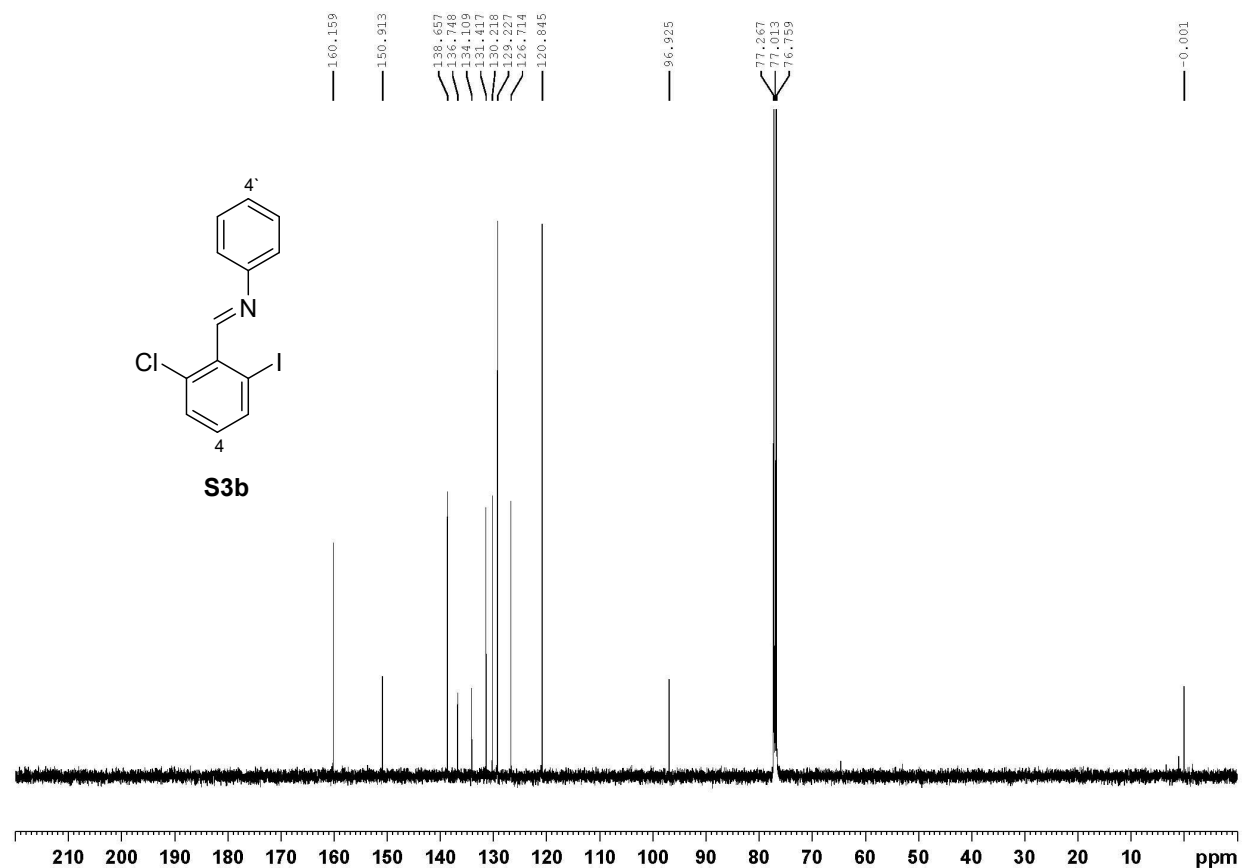
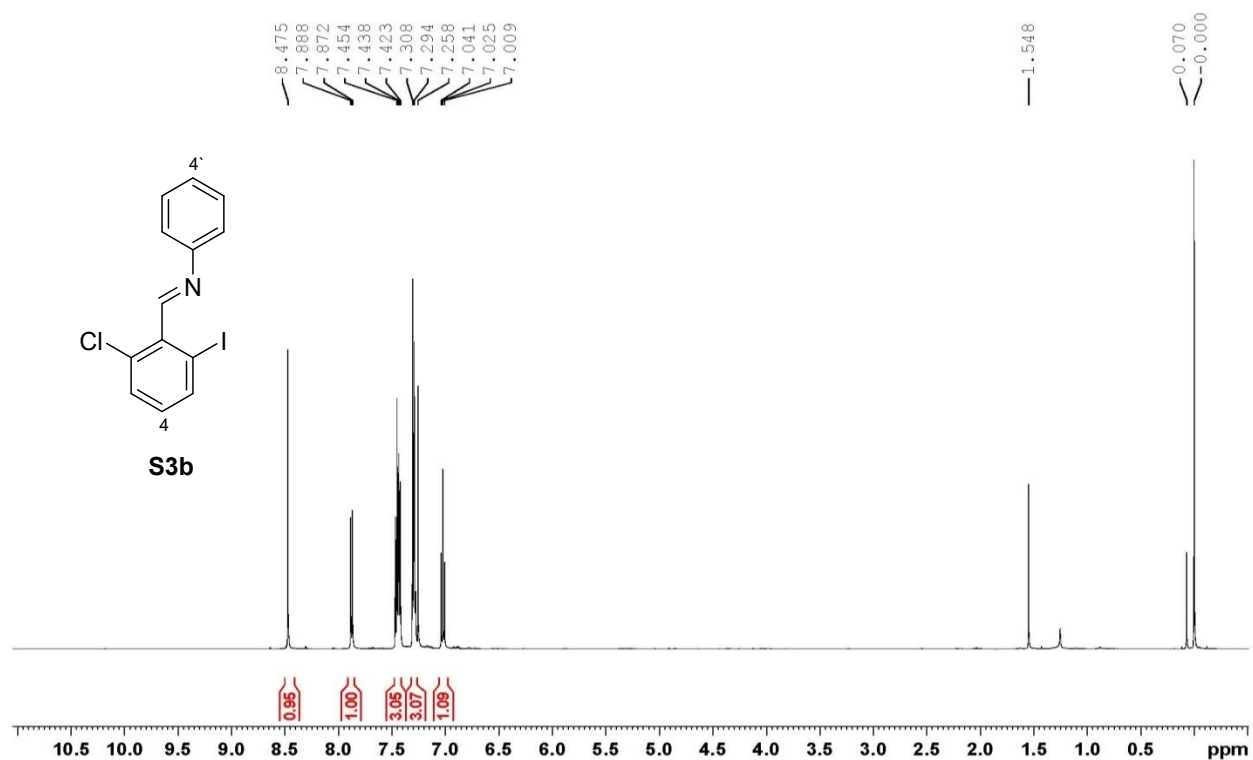


1-(3,5-Diiodo-4-methoxy-2,6-dimethylphenyl)-N-phenylmethanimine (S3a):

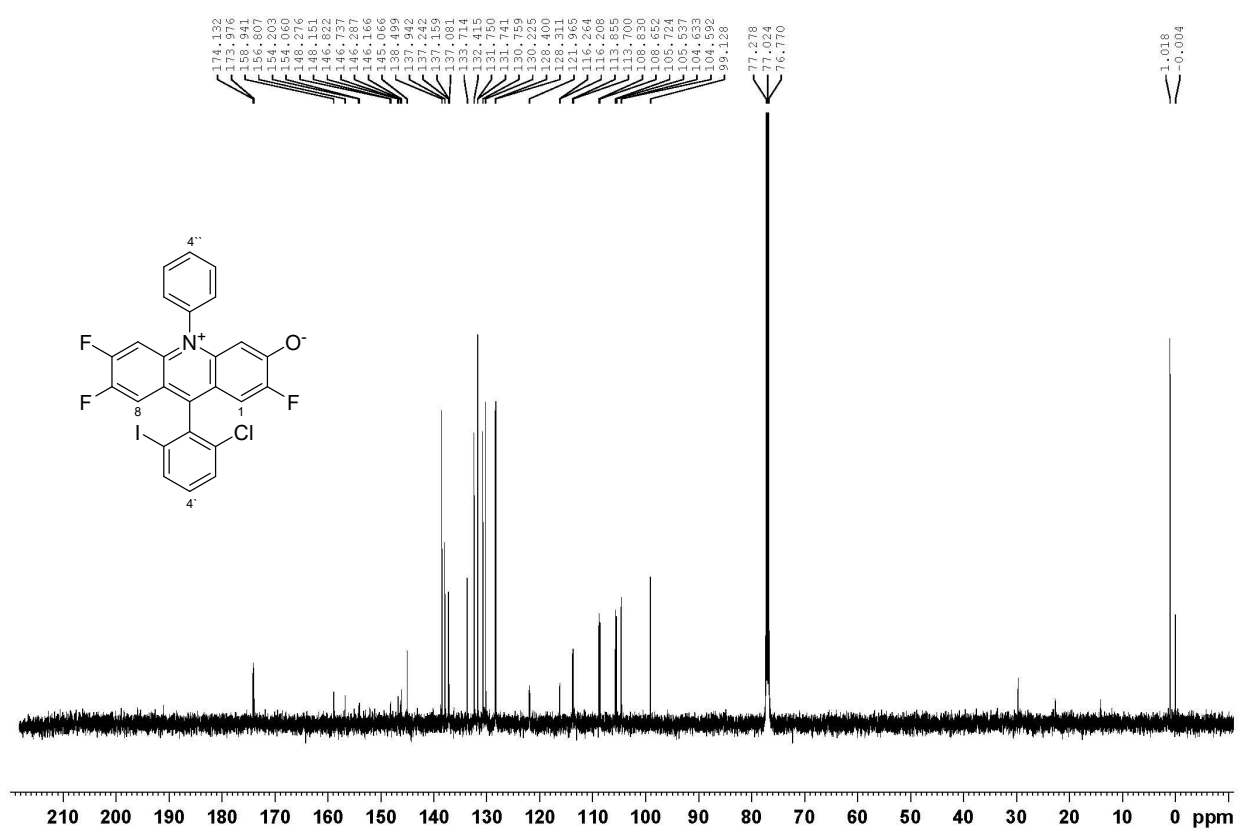
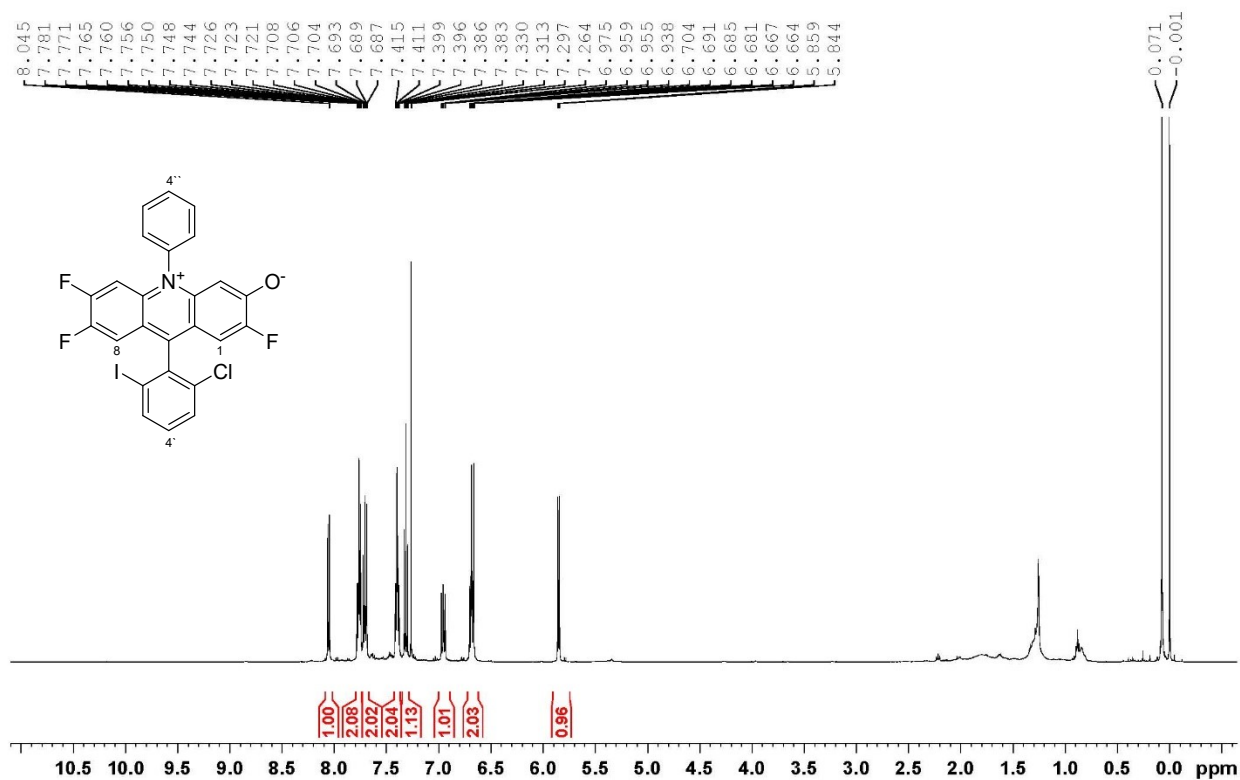


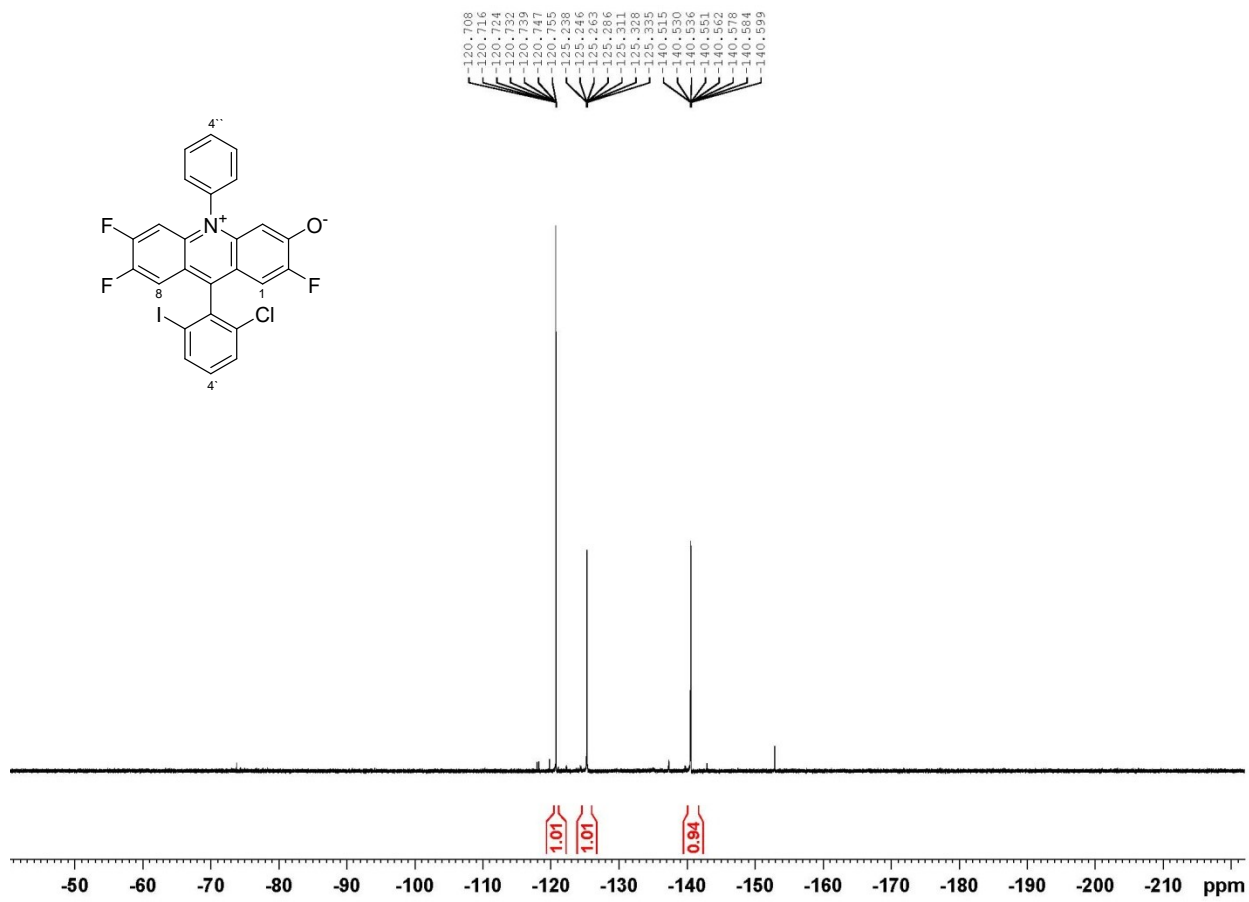


1-(2-Chloro-6-iodophenyl)-N-phenylmethanimine (S3b):

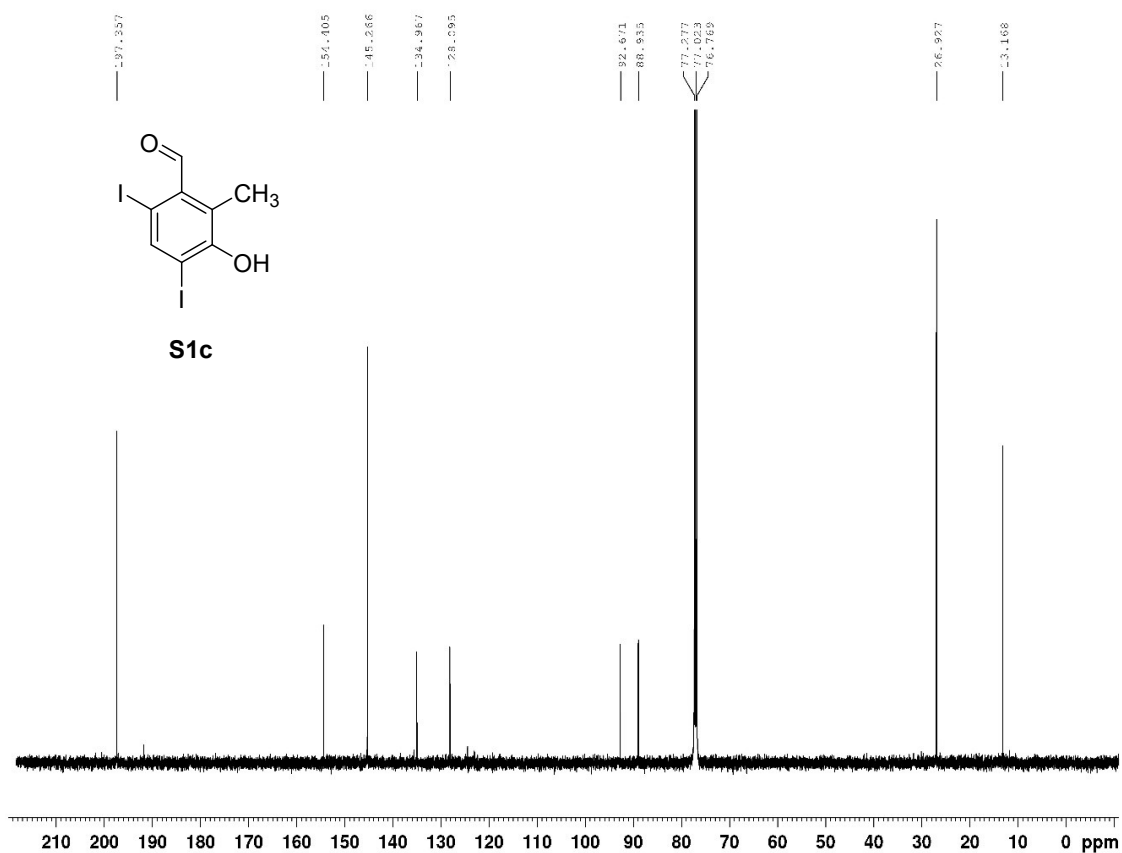
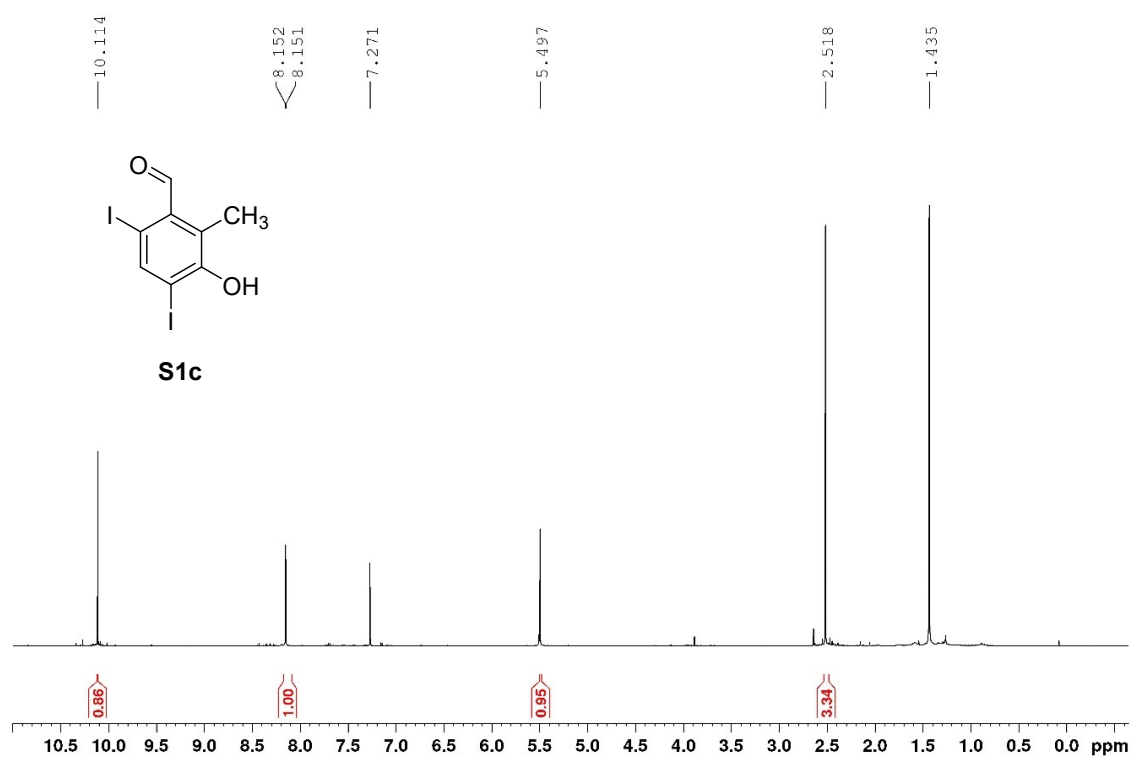


9-(2-Chloro-6-iodophenyl)-2,6,7-trifluoro-10-phenylacridin-10-ium-3-olate (PS(III)):

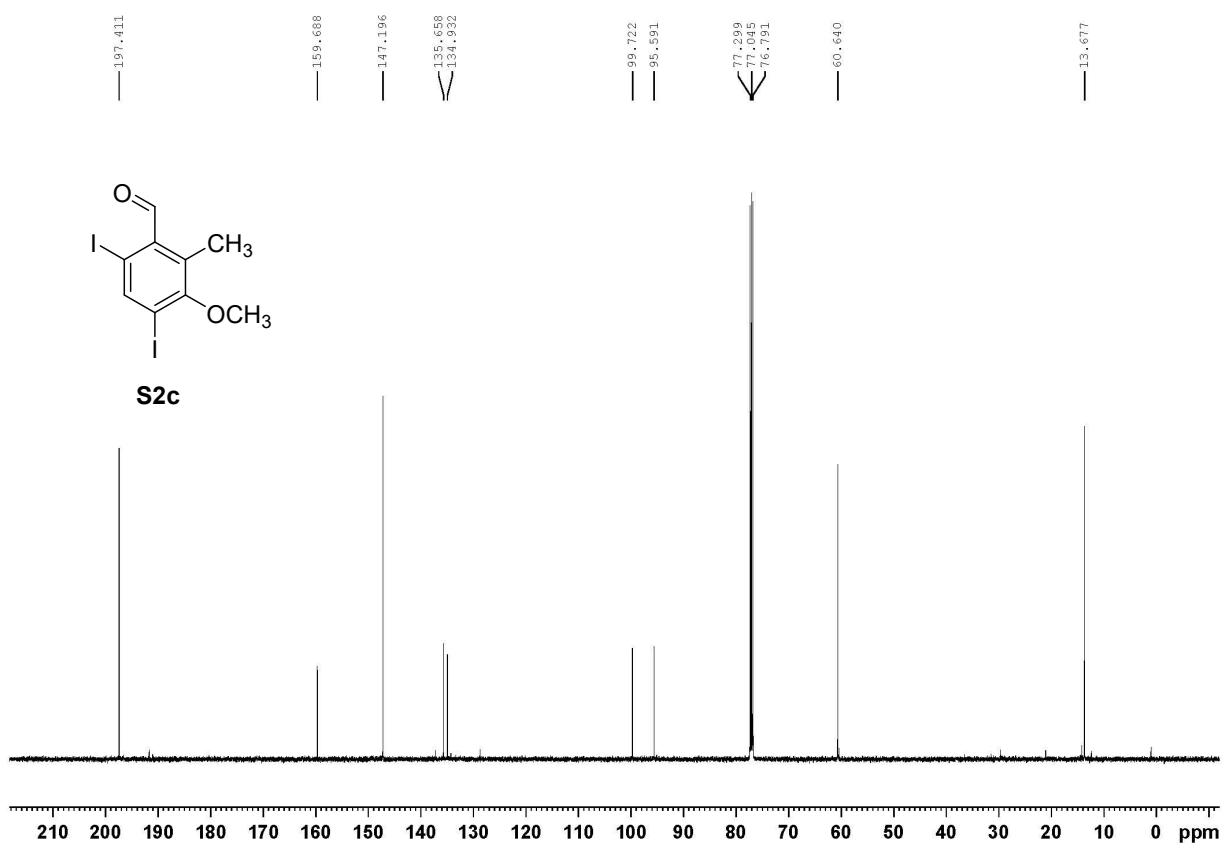
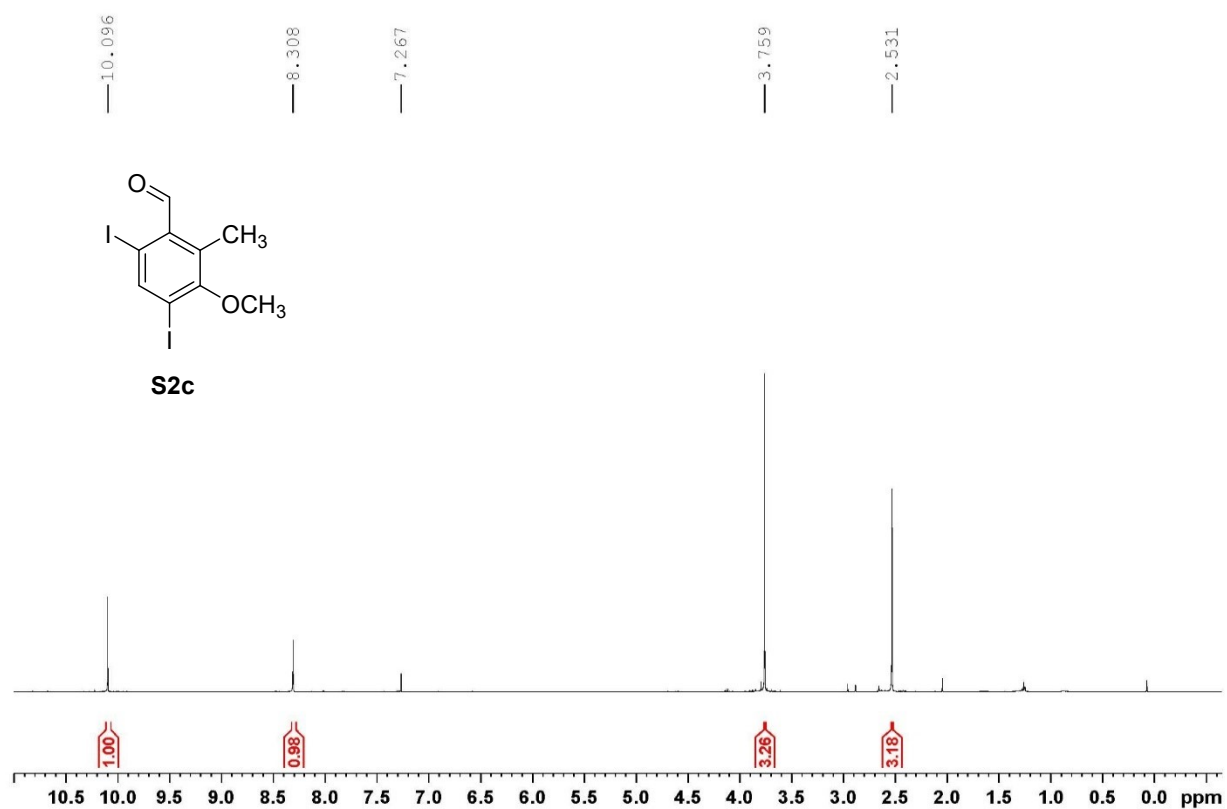




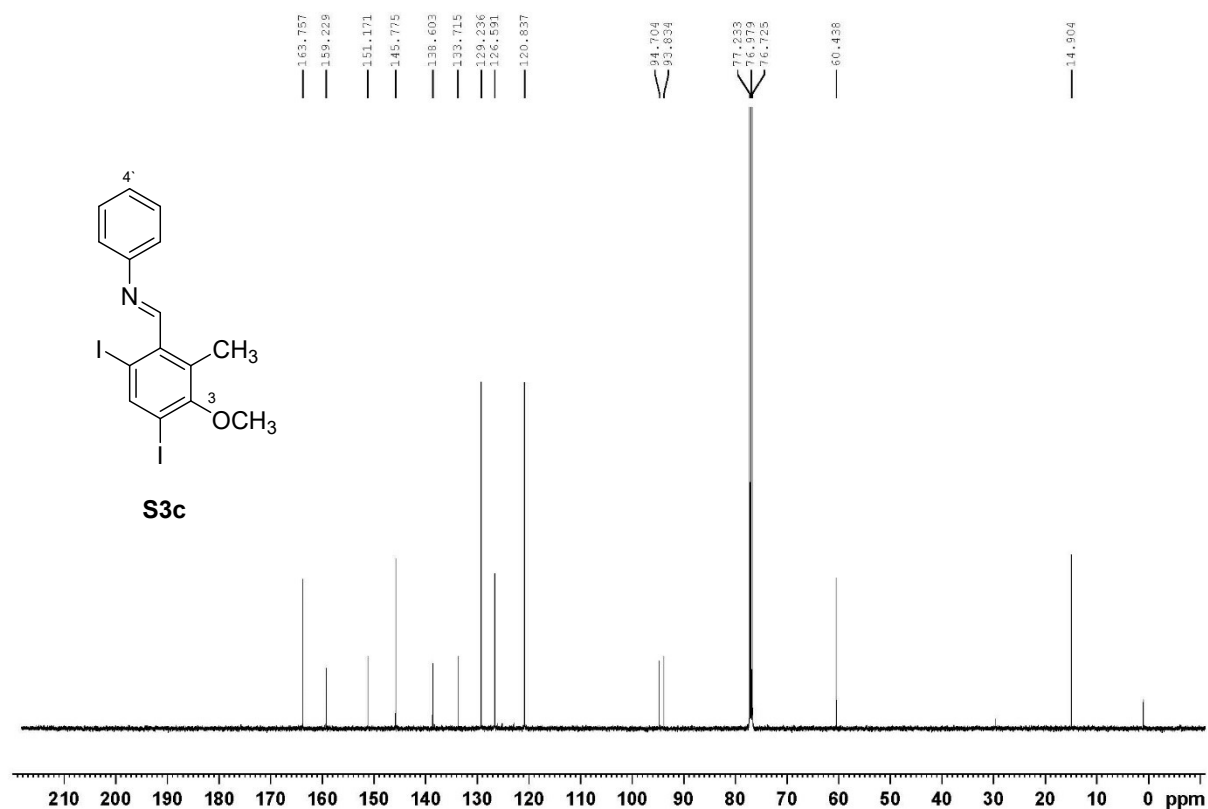
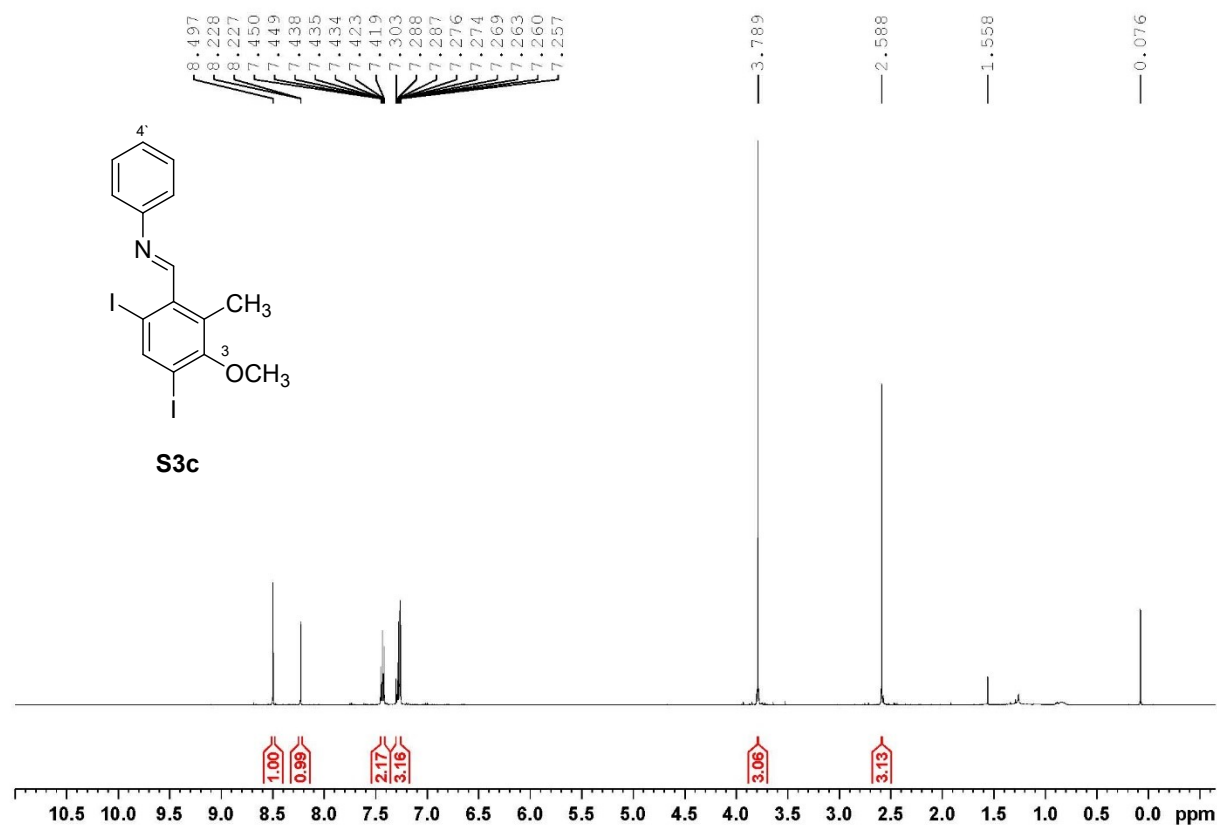
3-Hydroxy-4,6-diiodo-2-methylbenzaldehyde (S1c):



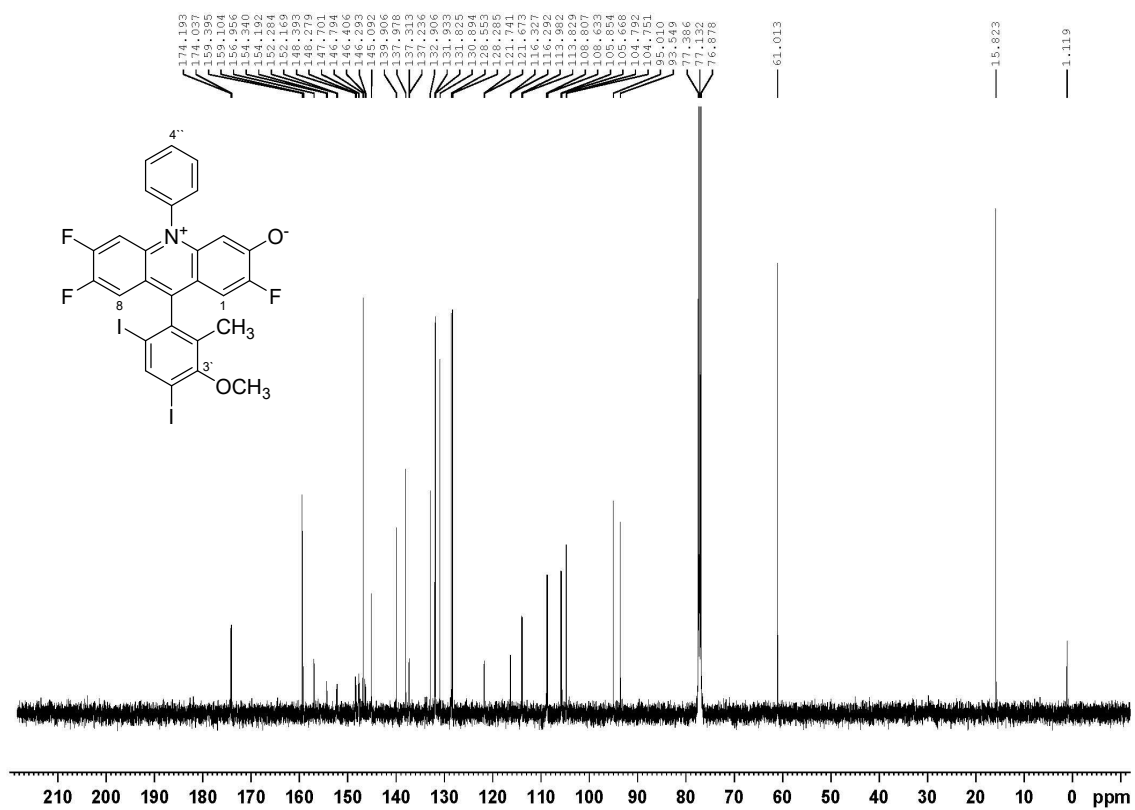
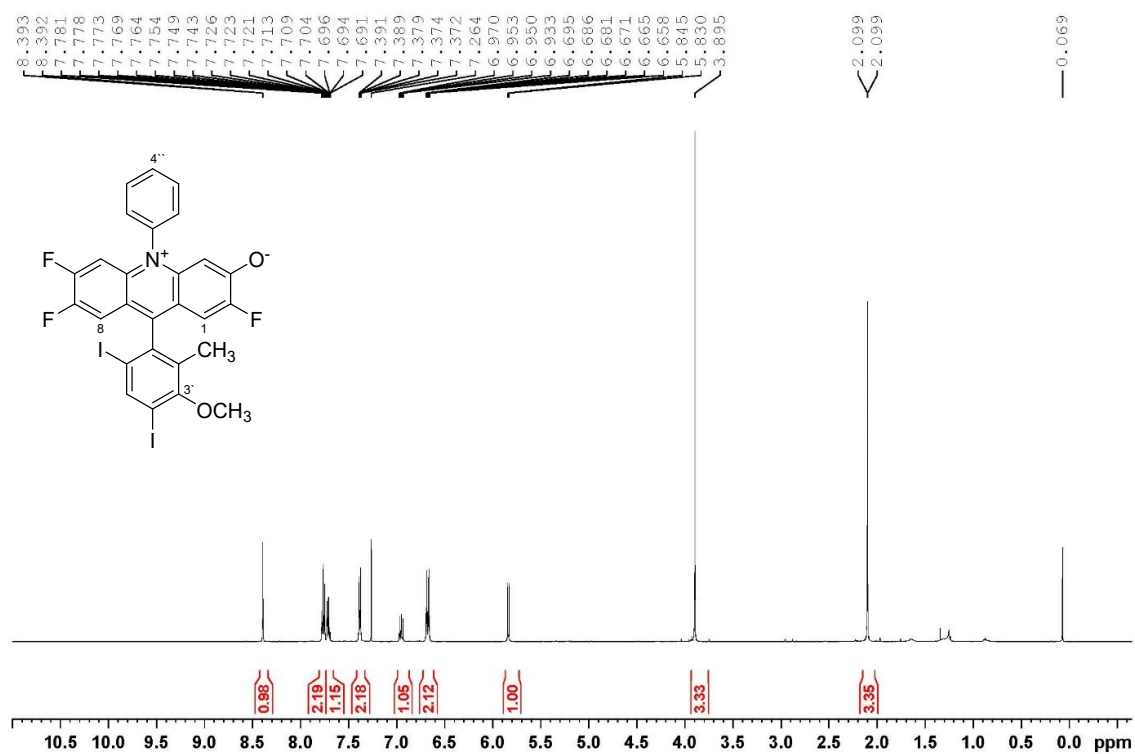
4,6-Diiodo-3-methoxy-2-methylbenzaldehyde (S2c):

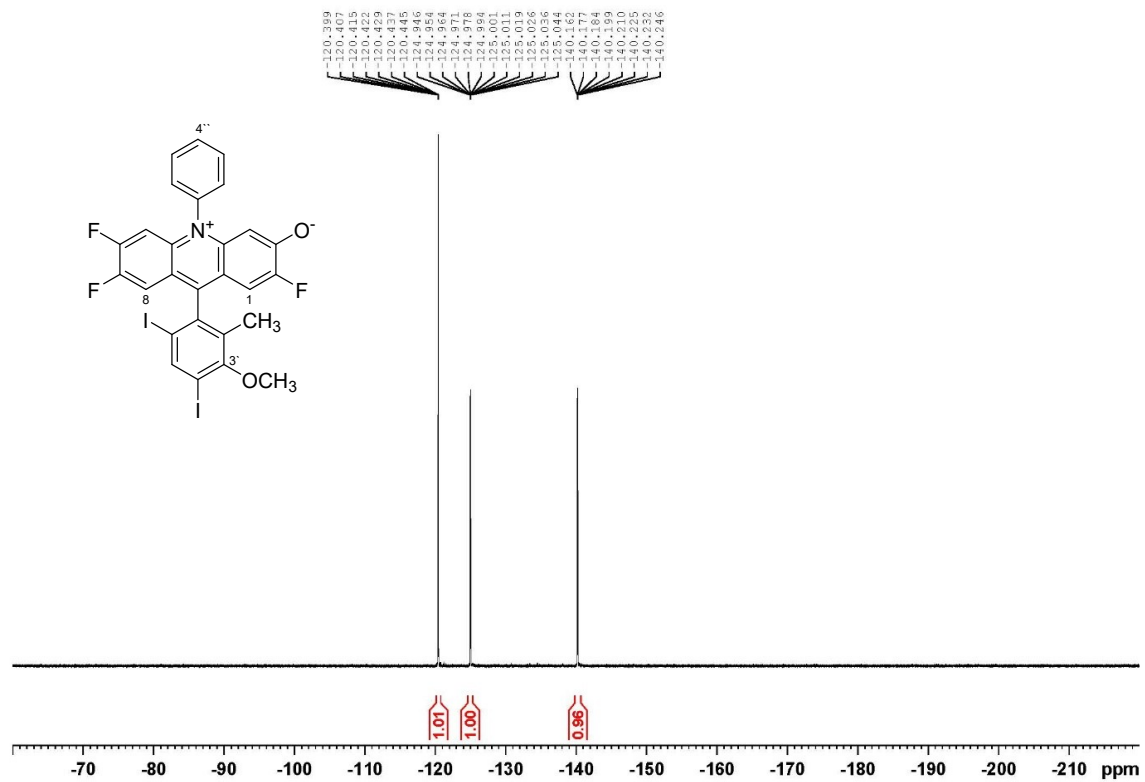


1-(4,6-Diiodo-3-methoxy-2-methylphenyl)-N-phenylmethanimine (S3c):



9-(4,6-Diiodo-3-methoxy-2-methylphenyl)-2,6,7-trifluoro-10-phenylacridin-10-ium-3-olate (PS(IV)):





7 References

1. V. Hutskalova and C. Sparr, *Org. Lett.*, 2021, **23**, 5143-5147.
2. H. Hodgson and W. Smith, *J. Chem. Soc.*, 1931, 76–78.
3. Y. Imai, Y. Nakano, T. Kawai and J. Yuasa, *Angew. Chem. Int. Ed.*, 2018, **57**, 8973-8978.
4. R. H. Compton, K. T. V. Grattan and T. Morrow, *J. Photochem.*, 1980, **14**, 61-66.
5. M. B. Ledger and A. G. Salmon, *J. Chem. Soc., Faraday Trans. 2*, 1976, **72**, 883-886.
6. P. Müller and K. Brettel, *Photochem. Photobiol. Sci.*, 2012, **11**, 632-636.
7. C. Kerzig and O. S. Wenger, *Chem. Sci.*, 2018, **9**, 6670-6678.
8. M. Montalti, A. Credi, L. Prodi and T. M. Gandolfi, *Handbook of Photochemistry*, CRC/Taylor & Francis: Boca Raton, FL, 3 edn., 2006.
9. J. K. McCusker, *Science*, 2019, **363**, 484–488.
10. L. Schmid, C. Kerzig, A. Prescimone and O. S. Wenger, *JACS Au*, 2021, **1**, 819-832.
11. L. Schmid, F. Glaser, R. Schaer and O. S. Wenger, *J. Am. Chem. Soc.*, 2022, **144**, 963-976.
12. J. A. Kübler, B. Pfund and O. S. Wenger, *JACS Au*, 2022, **2**, 2367-2380.
13. D. Rehm and A. Weller, *Isr. J. Chem.*, 1970, **8**, 259-271.
14. A. Chatterjee and B. König, *Angew. Chem. Int. Ed.*, 2019, **58**, 14289-14294.
15. I. Ghosh, R. S. Shaikh and B. König, *Angew. Chem. Int. Ed.*, 2017, **56**, 8544-8549.
16. M. S. Coles, G. Quach, J. E. Beves and E. G. Moore, *Angew. Chem. Int. Ed.*, 2020, **59**, 9522-9526.
17. M. Marchini, G. Bergamini, P. G. Cozzi, P. Ceroni and V. Balzani, *Angew. Chem. Int. Ed.*, 2017, **56**, 12820-12821.
18. F. Glaser, C. Kerzig and O. S. Wenger, *Chem. Sci.*, 2021, **12**, 9922-9933.
19. S. Neumann, O. S. Wenger and C. Kerzig, *Chem. Eur. J.*, 2021, **27**, 4115-4123.
20. G. J. Kavarnos and N. J. Turro, *Chem. Rev.*, 1987, **86**, 401–449.

21. K. A. McLauchlan and U. E. Steiner, *Mol. Phys.*, 1991, **73**, 241-263.
22. M. Goez, in *Annual Reports on NMR Spectroscopy*, Elsevier, 2009, pp. 77-147.
23. B. N. DiMarco, L. Troian-Gautier, R. N. Sampaio and G. J. Meyer, *Chem. Sci.*, 2018, **9**, 940-949.
24. T. J. B. Zähringer, M.-S. Bertrams and C. Kerzig, *J. Mater. Chem. C*, 2022, **10**, 4568-4573.
25. T. J. B. Zähringer, J. A. Moghtader, M. S. Bertrams, B. Roy, M. Uji, N. Yanai and C. Kerzig, *Angew. Chem. Int. Ed.*, 2023, **62**, e202215340.
26. N. Harada, Y. Sasaki, M. Hosoyamada, N. Kimizuka and N. Yanai, *Angew. Chem. Int. Ed.*, 2021, **60**, 142-147.
27. B. Pfund, D. M. Steffen, M. R. Schreier, M.-S. Bertrams, C. Ye, K. Börjesson, O. S. Wenger and C. Kerzig, *J. Am. Chem. Soc.*, 2020, **142**, 10468-10476.
28. S. M. Bachilo and R. B. Weisman, *J. Phys. Chem. A*, 2000, **104**, 7711-7714.
29. A. Haefele, J. Blumhoff, R. S. Khnayzer and F. N. Castellano, *J. Phys. Chem. Lett.*, 2012, **3**, 299-303.
30. H. C. Chen, C. Y. Hung, K. H. Wang, H. L. Chen, W. S. Fann, F. C. Chien, P. Chen, T. J. Chow, C. P. Hsu and S. S. Sun, *Chem. Commun.*, 2009, **27**, 4064-4066.
31. T. N. Singh-Rachford; and F. N. Castellano, *J. Phys. Chem. A*, 2009, **113**, 5912-5917.
32. M. Majek, U. Faltermeier, B. Dick, R. Perez-Ruiz and A. Jacobi von Wangelin, *Chem. Eur. J.*, 2015, **21**, 15496-15501.
33. W. Wu, H. Guo, W. Wu, S. Ji and J. Zhao, *J. Org. Chem.*, 2011, **76**, 7056-7064.
34. A. Olesund, J. Johnsson, F. Edhborg, S. Ghasemi, K. Moth-Poulsen and B. Albinsson, *J. Am. Chem. Soc.*, 2022, **144**, 3706-3716.
35. C. E. McCusker and F. N. Castellano, *Inorg. Chem.*, 2015, **54**, 6035-6042.
36. J. Saltiel, G. R. March, W. K. Smothers, S. A. Stout and J. L. Charlton, *J. Am. Chem. Soc.*, 1981, **103**, 7159-7164.